STRUCTURAL AND FUNCTIONAL ANALYSIS OF IMMUNITY-ASSOCIATED GTPASES

Dissertation zur Erlangung des akademischen Grades des Doktors der Naturwissenschaften (Dr. rer. nat.)

eingereicht im Fachbereich Biologie, Chemie, Pharmazie der Freien Universität Berlin

vorgelegt von
DAVID SCHWEFEL
aus Heidelberg

2010

Die vorliegende Arbeit wurde von Juli 2007 bis Oktober 2010 am Max-Delbrück-Centrum für Molekulare Medizin unter der Anleitung von
JUN.-PROF. DR. OLIVER DAUMKE
angefertigt.

1. Gutachter: PROF. DR. UDO HEINEMANN
2. Gutachter: JUN.-PROF. DR. OLIVER DAUMKE

Disputation am 17. Februar 2011

CONTENTS

LIST OF FIGURES

LIST OF TABLES

1 INTRODUCTION

1.1 GUANIN NUCLEOTIDE BINDING AND HYDROLYZING PROTEINS

Nucleotide triphosphate binding and hydrolyzing proteins are important in almost all facets of life. Among them, the mononucleotide-binding fold (P-loop NTPase fold) is the most prevalent one, representing 10-18% of all gene products in cellular organisms [1]. Structurally, the fold is characterized by a central β-sheet surrounded by α-helices on both sides. One of at least seven monophyletic protein lineages within the P-loop NTPases is the Guanosintriphosphatase (GTPase) superclass. Sometimes, these proteins are also termed guanine nucleotide binding proteins (GNBPs, G proteins). Since long time it is appreciated that GTPases function in a variety of fundamental cellular processes such as protein synthesis, hormone signaling, vision, cell proliferation and intracellular trafficking [2]. Astonishingly, the variety of these functions is mediated by an almost universally conserved molecular mechanism, which is detailed below.

1.1.1 *The G domain switch*

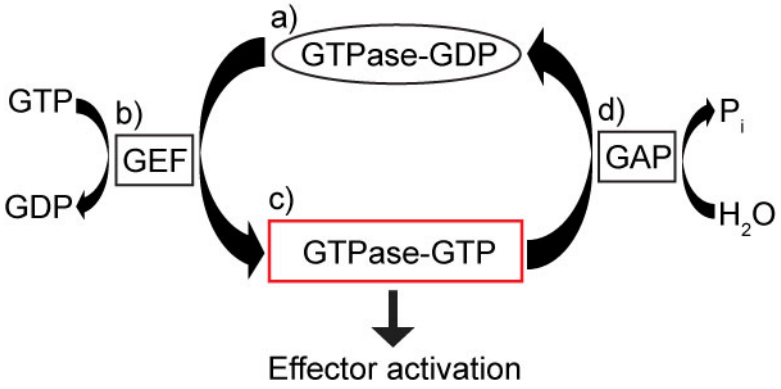

Figure 1: Schematic view of the G domain switch mechanism of small GTPases. The GDP-bound OFF-state is indicated as black ellipse, the GTP-bound ON-state as red rectangle. The events **a**-**d** are described in the text. GEF - guanine nucleotide exchange factor, GAP - GTPase-activating protein.

Apart from the large membrane-active mechanochemical GTPases and the motor ATPases (see the myosin/kinesin and dynamin protein families in 1.1.3), most other GTPases, e.g. the group of small GTPases, act as regulatory switches which cycle between ON and OFF states [3]. The interconversion between their functional states is determined by nucleotide binding and hydrolysis. For these processes, the presence of divalent magnesium ions is crucial. If GDP-bound, the guanine nucleotide binding domain (G domain) of the GTPase is in the OFF-state (Figure 1 **a**). Upon exchange of GDP against GTP, the G domain switches to the ON-

state. The release of GDP is intrinsically very slow, therefore this process can be accelerated by binding of auxiliary proteins termed guanine nucleotide exchange factors (GEFs) (Figure 1 **b**). In the GTP-bound ON-state, the G domain has the highest binding affinity towards effector molecules and can in turn activate them and initiate signaling (Figure 1 **c**). Return to the OFF-state is regulated by GTP hydrolysis. A second class of auxiliary proteins, termed GTPase-activating proteins (GAPs), accelerates the intrinsically slow GTP hydrolysis reaction (Figure 1 **d**).

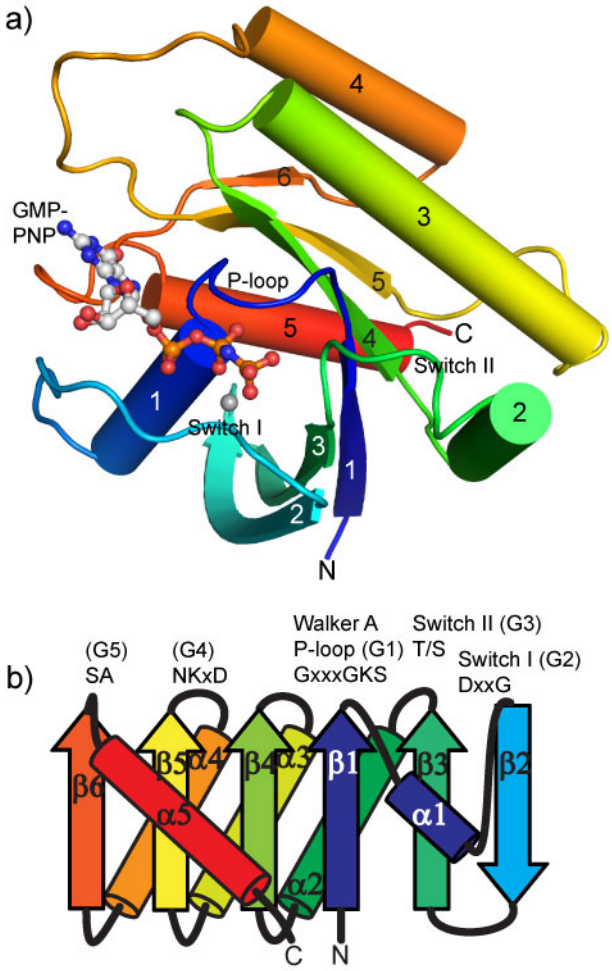

Figure 2: Schematic representations of the G domain fold. **a** Cartoon representation of the H-ras p21 G domain, bound to the non-hydrolyzable GTP analog GMP-PNP. The structure was determined by X-ray crystallography (PDB 5P21) [4]. β-strands are shown as flat arrows and α-helices as cylinders. Secondary structure elements are colored in a gradient according to their position within the primary structure, starting with dark blue at the amino-(N-)terminus and ending with red at the carboxy-(C-)terminus. The nucleotide analog is shown in ball-and-stick representation and colored according to atom types. Carbon atoms are colored white, nitrogen blue, oxygen red and phosphorous orange. The magnesium ion is shown as grey sphere. **b** Topology of the G domain fold. Secondary structure elements are shown and colored as in **a**. Conserved motifs and their amino acid residues are indicated.

How does the G domain switch work on the molecular level? To answer this question, the architecture of the G domain has to be considered. It will be presented

here using the example of the H-ras protein. Although it was not the first G protein, whose three-dimensional structure was revealed (which was EF-Tu in 1977 [5]), it raised great attention because mutations that lock Ras in the ON-state were often found in malignant tumors [6]. Therefore, Ras became one of the best studied small G proteins [7]. The G domain of Ras consists of 166 amino acid residues and folds into a central, curved six-stranded β-sheet, surrounded on both sides by five α-helices (Figure 2). The G domain provides an efficient platform for nucleotide binding by appropriate spatial arrangement of five loops on top of the sheet. These loops contain the highly conserved sequence motifs G1-G5 (Figure 2 **b**). The loop regions between helix α1 and strand β2 as well as between strand β3 and helix α2 are especially important for the conformational switch mechanism and are called switch I and II, respectively (Figure 2 **a**). Switch I contains the G2 motif, and the G3 motif is located just at the beginning of switch II [8].

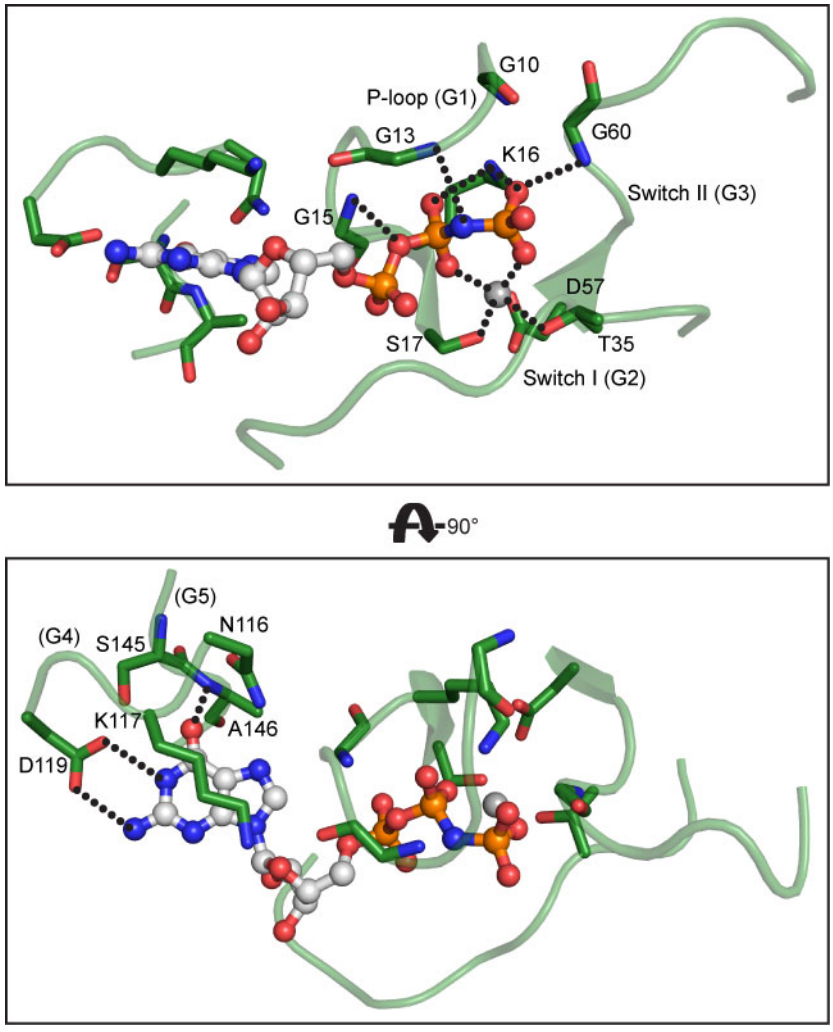

Figure 3: Detailed view of the H-Ras p21 nucleotide-binding site (see also Figure 2). Loops involved in GMP-PNP-binding are shown as green tubes, and selected amino acid residues are represented as sticks with carbon atoms colored green, nitrogen blue and oxygen red. The nucleotide analog is shown as in Figure 2. Protein-GMP-PNP interactions are indicated as dotted lines and further described in the text.

The sequence motifs G1-G3 are involved in contacts to the phosphate moieties of the nucleotide, whereas amino acid residues within G4 and G5 interact with the guanine base (Figure 3). The G1 motif, also called Walker A motif or phosphate-binding loop (P-loop) consists of the consensus sequence GxxxxGK[S/T], in the case of H-ras p21, the sequence reads G^{10}AGGVGKS^{17}. It wraps around the triphosphate, where Gly13 and Gly15 provide hydrogen bonds to the β-phosphate and the basic residue Lys16 intracts electrostatically with the β- and γ-phosphates (Figure 3, upper panel). Ser17 is involved in coordination of the magnesium ion, just as the invariant threonine residue of the G2 motif within the switch I region (Thr35 of H-ras). The tetragonal-bipyramidal magnesium coordination is completed by oxygens of the β- and γ-phosphates (Figure 3, upper panel) and two water molecules (not shown). Furthermore, the main chain nitrogen of Thr35 forms a hydrogen bond to an oxygen of the γ-phosphate (not shown). The G3 motif is located just before the switch II region and has the consensus sequence DxxG (H-ras D^{57}TAG^{60}). The aspartate is only indirectly involved in magnesium coordination via positioning of a water molecule, and the conserved glycine is hydrogen-bonded to the γ-phosphate (Figure 3, upper panel). The G4 motif is especially important for the specificity of the G domain towards guanosine nucleotides. It contains the consensus sequence NKxD (H-ras N^{116}KCD^{119}). The asparagine residue is not involved in nucleotide binding, but the lysine stacks on top of the purine ring. The aspartate forms a bifurcated hydrogen bond to the exocyclic amino group, which is not present in adenine nucleotides, and to an endocyclic nitrogen of the guanine base (Figure 3, lower panel). The G5 motif (H-Ras S^{145}AK^{147}) further contributes to the GTP specificity by positioning Asp119 via a hydrogen bond from Ser145 (not shown) and a hydrogen bond between the main chain nitrogen of Ala146 and the exocyclic oxygen of the GTP molecule (Figure 3, lower panel).

The structural framework for GTPase conformational switching is now assembled. The molecular switch can be described as a loaded spring mechanism [3]. In the ON-state, the above-mentioned conserved threonine in switch I (G2 motif) and the glycine residue in switch II (G3 motif) interact with the γ-phosphate of the nucleotide. Stabilized in this way by the γ-phosphate, the switch regions of all small G proteins adopt a remarkably similar, rigid conformation, allowing for recruitment and, in some cases, allosteric activation of effector proteins. Indeed, in known structures of active GTPase-effector complexes, one or both switch regions are involved in the binding interface (Figure 4).

Upon nucleotide hydrolysis and release of inorganic phosphate (see also Figure 5), the above-mentioned switch-γ-phosphate interactions are broken and therefore the switch regions relax into a new conformation which represents the GDP-bound OFF-state. In this relaxed state, the conformational variability of the switch regions within all small GTPases is very high, and the affinity towards effector proteins is reduced, leading to dissociation of the G protein-effector complex. In general, the magnitude of the conformational change varies within different small G proteins, but is in almost all cases restricted to the switch regions [3].

The mechanism of GTPase-catalyzed GTP hydrolyis is still controversially discussed [13, 14]. It is generally accepted, that a water molecule acts as nucleophile and attacks the γ-phosphate in-line (Figure 5 **a**, [15]). However, the nature of

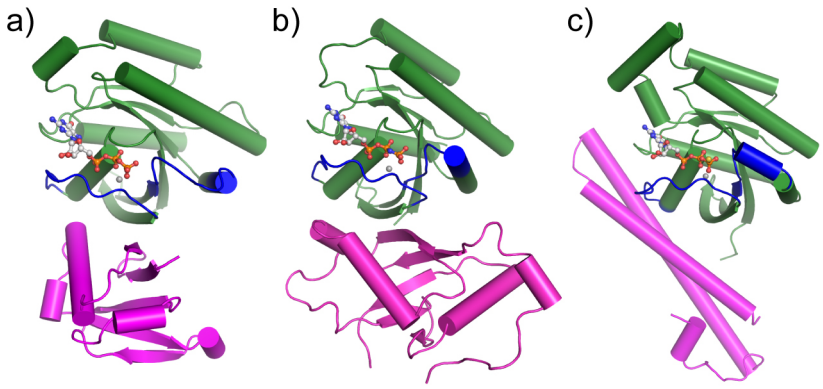

Figure 4: Examples of effector binding by small G proteins. **a** Cartoon representation of Rap1A (colored green) bound to the Ras-binding domain (RBD) of c-Raf1 (colored magenta) (PDB 1C1Y, [9]). Switch regions are colored blue. Here, only switch I is involved in c-Raf RBD binding. **b** Cartoon representation of Ras (green) bound to PI3K-γ (magenta) (PDB 1HE8, [10]). Switch regions are colored blue. Here, switch I is involved in effector binding in a similar way as in **a**, but switch II provides an additional salt bridge to the effector (not shown). **c** Cartoon representation of RhoA (green) complexed with the effector domain of PKN/PRK1 (magenta) (PDB 1CXZ, [11]). Switch regions are colored blue. Here, only switch I participates in effector binding, but in a completely different way as in **a**.

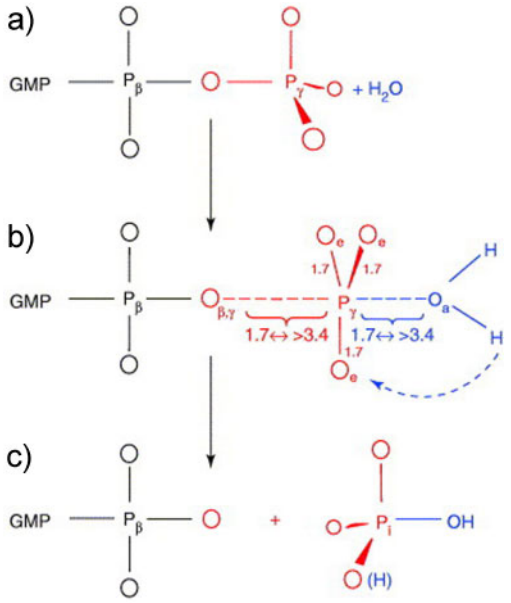

Figure 5: Mechanistic principle of phosphoryl transfer in GTPases. **a** Ground state of the reaction. **b** Transition state of the reaction, where bond lengths for a fully dissociative or fully associative state are given (see text). **c** Reaction products. Figure was taken from [12].

the transition state is a matter of debate. In a dissociative transition state, which involves a metaphosphate-like PO_3^{2-} state, bond-breaking of the β-γ-phosphate anhydride linkage has already occurred when the nucleophile approaches. In this case, bond lengths between γ-phosphate and $O_{\beta,\gamma}$ as well as the oxygen of

the approaching nucleophile would be around 3.4 Å (Figure 5 **b**). On the other side of the spectrum, in a fully associative transition state, bond-making to the nucleophile has already proceeded before bond-breaking of the anhydride linkage, and the above-mentioned bond lengths would be shorter, around 1.7 Å (Figure 5 **b**). In solution, a fully dissociative transition state of GTP hydrolysis has been demonstrated [16]. The nature of the transition state in the protein environment, however, is still elusive. Most probably, the hydrolysis mechanism is not fully conserved within GTPases, especially when it comes to the multitude of GAP mechanisms (see below) [12, 17].

The actual GTP hydrolysis reaction is intrinsically very slow within small G proteins, they are inefficient enzymes. As mentioned above, auxiliary GAPs bind to the G protein and accelerate the hydrolysis rate by several orders of magnitude [18]. Paradigm for GAP-stimulated GTP hydrolysis is the Ras-RasGAP system, which has been studied extensively [19]. RasGAP increases the GTPase rate of Ras from 0.03 min^{-1} to 324 min^{-1} [20]. The mode of action of RasGAP is threefold: (i) a positively charged arginine residue of RasGAP at the binding interface inserts into the active site and neutralizes the developing negative charge in the transition state of GTP hydrolysis. This residue is also called the arginine finger of the GAP. (ii) A main chain hydrogen bond from the arginine finger of the RasGAP to Gln61 of Ras stabilizes this residue. Gln61, also called the catalytic glutamine, which is located just downstream of the G3 motif, is thought to be important for GTP hydrolysis by positioning a water molecule which in turn acts as nucleophile and attacks the γ-phosphate [21] (see also Figure 5). Therefore, correct orientation of the catalytic glutamine is important for the hydrolysis reaction of Ras. (iii) Occlusion of the active site by RasGAP shields the reaction volume from solvent molecules.

The arginine finger mechanism is also conserved in other G protein-GAP systems (Figure 6). The G_α subunit of heterotrimeric G proteins contains a stimulatory arginine residue as well, but in this case it is provided by the large helical extension of the G domain and not from a separate GAP. GAPs for these proteins stimulate GTP hydrolysis by stabilizing the switch regions [22]. TBC-domain proteins which act as GAPs for Rab GTPases accelerate the GTPase reaction by inserting both the arginine finger and the catalytic glutamine in the active site. The putative catalytic glutamine of Rab itself is involved in GAP binding and not in catalysis [23]. The RanGAP system neither inserts an arginine nor a glutamine in the Ran substrate-binding pocket. The function of RanGAP is solely the stabilization of Ran's own catalytic glutamine residue [24]. A further exception is the mechanism of GTPase stimulation in the Rap1 GTPase. Here, the GAP provides a catalytic asparagine residue to position the attacking water molecule, because the G3-glutamine is missing in the Rap1 active site [25, 26]. In other G proteins as MnmE or dynamin, a positively charged ion, coordinated by the P-loop, switch I and the GTP-phosphates, can take the position of the guanidinium group of the arginine finger and counteract the negative charge of the transition state [27, 28].

The release of the reaction product is also intrinsically slow in small G proteins with a half-life of hours for the GDP-bound species. The equilibrium dissociation constant (K_d) of Ras towards GDP is in the picomolar range [29]. Auxiliary proteins, the GEFs, catalyze nucleotide-release by modifying the active site in such a way that the affinity for nucleotide is drastically reduced, thus allowing for nucleotide

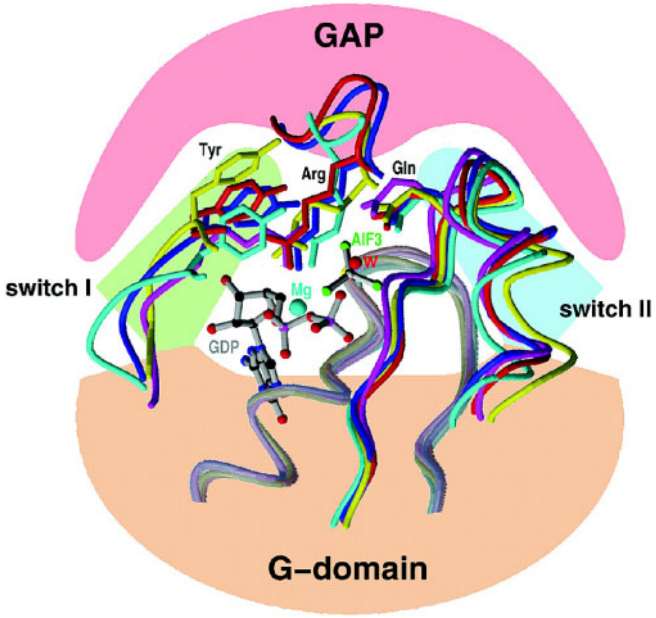

Figure 6: Conserved mechanism of GTPase-activation for Ras, Rho, Rac and $G_{i\alpha}$. Only the P-loop, switch I and switch II of the GTPase is shown in cartoon representation, as well as the GAP loops which provide the arginine fingers. The remainder of the proteins is indicated schematically. Ras-RasGAP is colored light green, Rho-RhoGAP red, Rac-ExoS cyan and $G_{i\alpha}$ magenta. All structures have been solved in the presence of GDP, magnesium and aluminium fluoride, which is a mimic of the transition state during GTP hydrolysis (indicated as AlF_3). The catalytic water is indicated as W. The arginine fingers and catalytic glutamines are indicated as Arg and Gln, respectively. Figure was taken from [3].

rebinding. Since the GTP concentration in the cell is fourfold higher than the GDP concentration (as measured in hepatocytes [30]), GEF-catalyzed nucleotide release and rebinding will result in a higher proportion of GTP-bound protein [18]. In principle, GEF binding induces structural changes in the P-loop and switch regions by embracing them in such a way, that the bound phosphate moiety of the nucleotide and the magnesium ion are pushed out of the active site (Figure 7).

1.1.2 *GTPase classification*

The GTPase superclass has been systematically classified, taking into account the huge amount of sequence and structural data which was gained in the last decades [31]. GTPases share, besides the typical Walker A motif (P-loop, G1 motif), a specific form of the Walker B motif including a conserved glycine residue (G3 motif) and the G4 motif which ensures specificity towards the guanosine base. Based on these and further shared sequence and structural motifs, the GTPase superclass can be subdivided into two large classes, the translation factor-related (TRAFAC) and the signal recognition/MinD/BioD (SIMIBI) class. Selected family members belonging to either class and their respective topologies are shown in Figure 8. In the following paragraphs, certain TRAFAC (1.1.3) and SIMIBI (1.1.4) superfamilies will be introduced in detail.

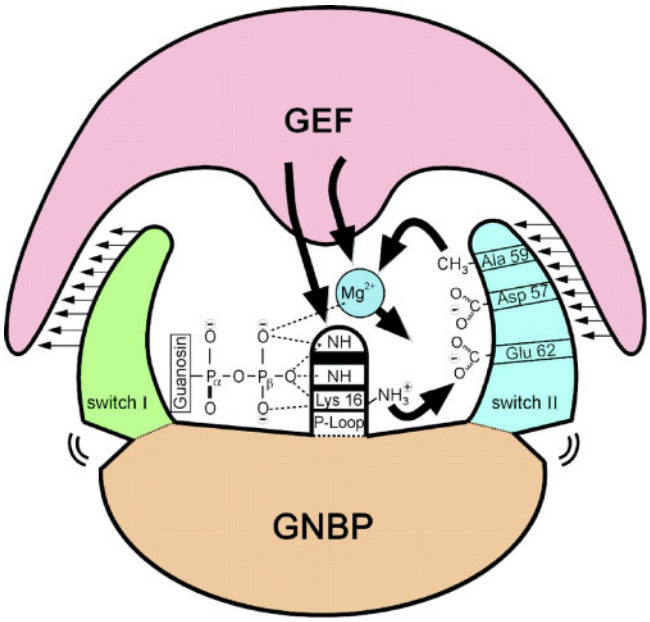

Figure 7: Mechanistic principles of nucleotide exchange mediated by GEFs. The Mg ion is pushed out from the active site either by elements of the GEF or by residues in switch II, which is in turn pulled towards the nucleotide-binding site. The conformation of the P-loop is disturbed as well by GEF binding, leading to loss of interaction with the phosphates. Figure was taken from [3].

1.1.3 *TRAFAC class*

1.1.3.1 *The translation factor superfamily*

This superfamily consists of the classical translation factors and the Bms1 family. The translation factors are conserved in all kingdoms of life and are involved in the initiation, elongation and termination steps during protein synthesis at the ribosome (Figure 8, [32]). Recently, the structures of Elongation factor-(EF-)Tu and EF-G in complex with the ribosome have been solved, providing important insight in the molecular mechanism of tRNA decoding and translocation [33, 34].

The Bms1 GTPase family is conserved in eukaryotes and has a distinct D to E amino acid substitution in the G3 motif. The prototype member, yeast Bms1p, has been implied in ribosome biogenesis. Interestingly, it has been proposed that the C-terminal domain of the protein acts as GAP (see also 1.1.1) for the N-terminal G domain [35].

1.1.3.2 *The OBG-HflX superfamily*

The OBG and HflX families are almost universally conserved and contain a characteristic F residue in the switch I region. OBG GTPases additionally feature a specific G-rich stretch of amino acids directly downstream of the G1 motif. They may be involved in ribosome assembly [36]. Crystal structure analysis of *Bacillus subtilis* OBG showed that a large N-terminal G-rich sequence stretch forms a unique type II helical extension [37].

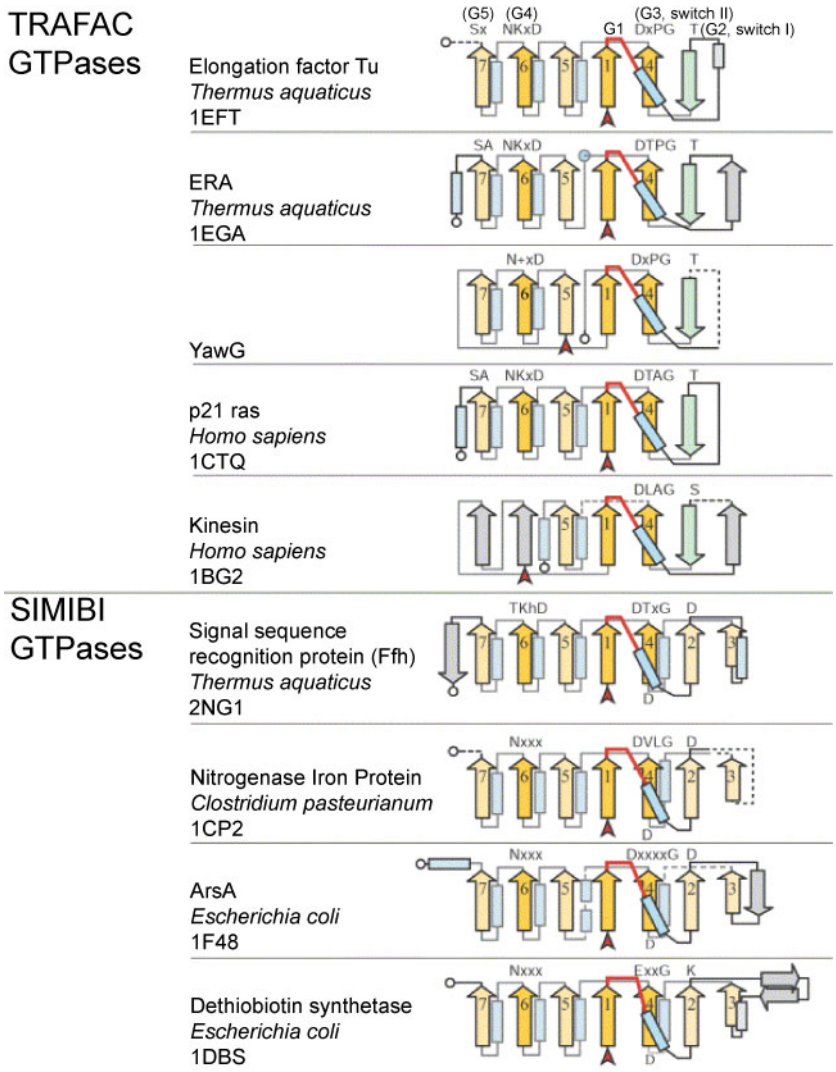

Figure 8: Topology diagrams of selected P-loop GTPAses. β-strands are indicated as arrows and numbered. Orange strands show strands 1, 4 and 6 which contain parts of the G1 (red line), G3 (DxPG) and G4 (NKxD) motif, respectively. The characteristic antiparallel strand from the TRAFAC class is shown in green. Strands presumably absent in the ancestral GTPase are colored gray. α-helices are shown as blue boxes. The N-terminus is indicated as red arrowhead, the C-terminus as black ring. Broken lines show secondary structure elements omitted for clarity. Highly conserved amino acids and the respective sequence motifs are indicated (x - any amino acid, h - hydrophobic). Figure was modified after [31].

The HflX family is widespread but not totally conserved, and its physiological function is not entirely clear, probably it is also related to ribosome assembly. The crystal structure of HflX from *Sulfolobus solfataricus* was solved recently, revealing an N-terminal domain which folds against the G1 motif and the switch II region of the C-terminal G domain. Biochemical analysis showed that the N-terminal domain slows the GTPase reaction down, probably acting as guanin-nucleotide dissociation inhibitor (GDI) [38, 39].

1.1.3.3 *The TrmE-Era-EngA-Septin-like superfamily*

This heterogenous superfamily was assembled based upon sequence similarities in between the G1 and G3 motifs, which separate it from the remaining GTPases. Only selected subfamilies will be discussed here. The Era GTPases (Figure 8) are conserved in bacteria and eukaryotes and are involved in chromosomal segregation and RNA binding [40]. The structure of *Escherichia coli* Era reveals a C-terminal K homology (KH) domain, which drastically changes its position relative to the G domain upon GTP hydrolysis. Switch I and II regions are involved in the KH-G domain contact. The KH domain recognizes part of the 16S rRNA, but RNA binding does not induce major conformational changes in the protein. A function for Era as rRNA chaperone was proposed [41].

EngA proteins as well are present in bacteria and eukaryotes and have the unique feature of two G domains arranged in tandem, separated by an acidic linker and followed by a C-terminal KH domain. They have been implied in ribosome assembly and stabilization as well. Mutagenesis and biochemical analysis of a *Thermotoga maritima* EngA homolog demonstrated that the two G domains have distinct catalytic mechanisms. The structure showed that the G domains are not in direct contact with each other, but that each of them binds via a different interface to the KH domain [42].

The septin-like family contains septins, paraseptins and other septin-related GTPases (see also Figure 14). Septins are only found in eukaryotes, whereas the other subfamilies are wider but more sporadic distributed, extending also to prokaryotic lineages. All members typically contain a divergent version of the guanine recognition motif (G4) at the end of the core strand β5 and an additional helix at the C-terminus of the GTPase domain. Septins in the budding yeast have been shown to assemble in rings along the bud neck and to function as scaffold that organizes the assembly of binding partners. In vertebrates, septins are involved in cell division, cytoskeletal dynamics and secretion [43]. Structural analysis showed that septins form linear, hetero-oligomeric filaments via two distinct interfaces [44, 45].

The paraseptin family features , amongst others, a conserved branch called the Aig1-Toc34/Toc159 group. The Toc34/Toc159-like GTPases are mainly found in plants and function as integral components of the chloroplast protein import machinery [46]. Several crystal structures of Toc34 have been solved, and a dimeric arrangement of the G domains was found. It was suggested, that one protomer within the dimer acts as GAP for the other protomer [47], but more recent studies call this result into question [48].

The Aig1 subgroup is found in viruses, bacteria and eukaryotes. The Aig1 protein was first identified in *Arabidopsis thaliana*, where it was shown to be up-regulated in response to infection of the plant with a *Pseudomonas syringae* strain. [49]. Interestingly, Aig1-like proteins also occur in the protozoan parasite *Entamoeba histolytica*, and it has been demonstrated that they are stronger expressed in pathogenic strains when compared to non-pathogenic ones [50]. This hints at a function of Aig1 proteins in virulence of pathogens as well as in defense mechanisms of the host organism. The GIMAP GTPases, which are subject of the present work, are included in the Aig1 subgroup as well (see Figure 14). They are suggested to function in the adaptive immune system, the main line of defense

against pathogens in jawed vertebrates. Detailed information on the GIMAP family is given in section 1.3.

1.1.3.4 *The Ras-like superfamily*

The large Ras-like GTPase family together with smaller families of related proteins form the Ras-like superfamily. Even if there are some prokaryotic members, the superfamily is predominantly eukaryotic. Ras-like GTPases consist of the Ras/Rab, Rac/Rho/Cdc42, trimeric/Arf/Sar1 and MglA GTPases. Structural and functional aspects of the Ras protein as prototypic member are provided in detail in 1.1.1. Rab GTPases are implied in vesicular trafficking. A multitude of Rab structures is known by now in various functional states [51]. Rho GTPases function in the organization of the actin cytoskeleton, which is important for many processes such as cell morphogenesis, migration, division and adhesion [52]. Heterotrimeric G proteins relay signals from G protein coupled receptors (GPCRs) at the plasma membrane to the cell interior. The G_α subunit contains the GTPase activity and has a large helical insertion upstream of the G2 motif. GPCR-induced GDP to GTP exchange in G_α leads to dissociation of the $G_{\beta\gamma}$ subunits and signaling initiation via binding and activation of downstream effectors [53]. The molecular mechanism of G_α activation by GPCRs is still not understood completely [54]. Arf proteins are involved in membrane trafficking and cytoskeleton organization. In contrast to other Ras-like GTPases, which are lipid-modified at the C-terminus to ensure proper membrane localization, the Arf GTPases contain a N-terminal myristoylated amphipatic helix which is exposed upon GTP-binding and inserts into the membrane [55]. Furthermore, the N-terminal helix of Arf-like Sar1p has been shown to induce membrane curvature [56].

1.1.3.5 *The myosin-kinesin superfamily*

This superfamily contains the two major families of eukaryotic motor ATPases. Kinesin mediates the movement of chromosomes, vesicles and organelles along microtubules, whereas myosin mediates movement along actin filaments. Members of this superfamily lost β-strands 6 and 7, which are replaced by additional N-terminal strands (Figure 8). Furthermore, both families lack the G4 motif and therefore lost their specificity towards GTP. The kinesin heavy chain contains both the nucleotide-binding and microtubulus-binding elements. In the cell, the heavy chain dimerizes and builds up a tetramer together with two light chains [57]. Myosin contains ATP- and actin-binding regions in its N-terminal head domain and dimerizes via a C-terminal coiled-coil stretch [58].

1.1.3.6 *The dynamin/Fzo/YbpR family*

This family consists mainly of the classical dynamins and dynamin-related membrane-active GTPases. These proteins are also called large GTPases, since the G domain is enlarged compared to Ras-like GTPases due to several insertions. Furthermore, they contain additional domains downstream of the G domain which are responsible for self-association, lipid binding and recruitment of interaction partners. They are further distinguished from other GTPases by their low nucleotide binding affinities and their tendency to oligomerize either by themselves or on a lipid

template, leading to stimulation of the GTPase reaction. Several family members induce membrane deformation *in vitro* and *in vivo*, but such activity was also described for some of the Arf-related GTPases (see 1.1.3.4, [59]). Dynamin itself is important for vesicle scission from the membrane during clathrin-mediated endocytosis. Other dynamins and dynamin-related proteins are involved in a variety of membrane budding processes such as phagocytosis or caveolae scission, as well as in organelle fusion and fission events [60]. A recent electron-microscopic study of a bacterial dynamin-like protein provided first insights into the spectacular conformational changes the protein undergoes upon membrane binding and into the mechanism which causes the extreme lipid bilayer deformation [61].

1.1.4 *SIMIBI class*

The SIMIBI class class of GTPases differs from the TRAFAC class in several aspects [31]. The part of the β-sheet upstream of the G3 motif forms two parallel β-strands, whereas the corresponding part in TRAFAC GTPases is arranged in an antiparallel manner (Figure 8). There are several differences on the sequence level as well. Within the G1 motif, there is an additional conserved glycine residue, leading to the consensus sequence GxxGxGK[S/T]. Furthermore, the SIMIBI GTPases contain a conserved aspartate residue in the switch I region instead of the invariant threonine of the TRAFAC members. An additional conserved aspartate residue is found at the beginning of strand β4, but it is not involved in nucleotide binding. Finally, the G4 specificity motif is not as conserved as in the TRAFAC class, and consequently, many SIMIBI members lost GTP specificity.

The SIMIBI class consists of the MinD/Mrp-Etk superfamily, the BioD-FTHFS superfamily and the Signal-recognition-associated GTPase family. Prototypic members of selected SIMIBI families will be described here. Paradigm of the SIMIBI class are the signal recognition particle GTPase (SRP54/Ffh in bacteria) and the signal recognition particle receptor (SR/FtsY in bacteria), whose α-subunit contains GTPase activity. The proteins are universally conserved and mediate co-translational targeting of proteins destined for membrane-insertion or secretion [62]. SRP54 and the SR form hetero-dimers with pseudo-twofold symmetry, where the substrate binding sites are situated at the dimer interface in such a way, that the 3'-OH of one GTP interacts with the γ-phosphate of the opposite GTP. This arrangement, building up a composite active site, is important for the reciprocal stimulation of GTP-hydrolytic activity and subsequent dissociation of the dimer [63].

MinD is a cell-division inhibiting ATPase, which is conserved in bacteria, archaea and also present in chloroplasts, but not in mitochondria. Its structure has been determined in the ADP- and AMP-PNP-bound states, but no significant structural differences were found. Conserved residues around the ATP-binding site have been shown to be important for the recruitment of binding partners *in vivo*. In contrast to other SIMIBI GTPAses which form dimers, such as the above-mentioned SRP-SR system, the MinD crystal structure is monomeric [64].

1.2 LYMPHOCYTE DEVELOPMENT AND MAINTENANCE

1.2.1 *The adaptive immune system*

The mammalian adaptive immune system arose approximately 500 million years ago and is present in all jawed vertebrates (gnathostomata) [65]. It allows for highly specific defense against invading pathogens like bacteria, viruses, fungi and parasites, and it additionally provides long-lasting immunological memory (for a thorough description, which is beyond the scope of this introduction, see e.g. [66]). The constituents steps towards the emergence of an adaptive immune system are (i) the appearance of lymphocytes, (ii) acquisition of antigen-binding receptor diversification, (iii) structural basis of recognition specificity, (iv) evolution of mechanisms for receptor selection and (v) regulatory processes that provoke and attenuate immune responses [67]. Especially point (i) will be elaborated in this introduction, since the G protein family which is subject of the present work plays a role in this process (see below).

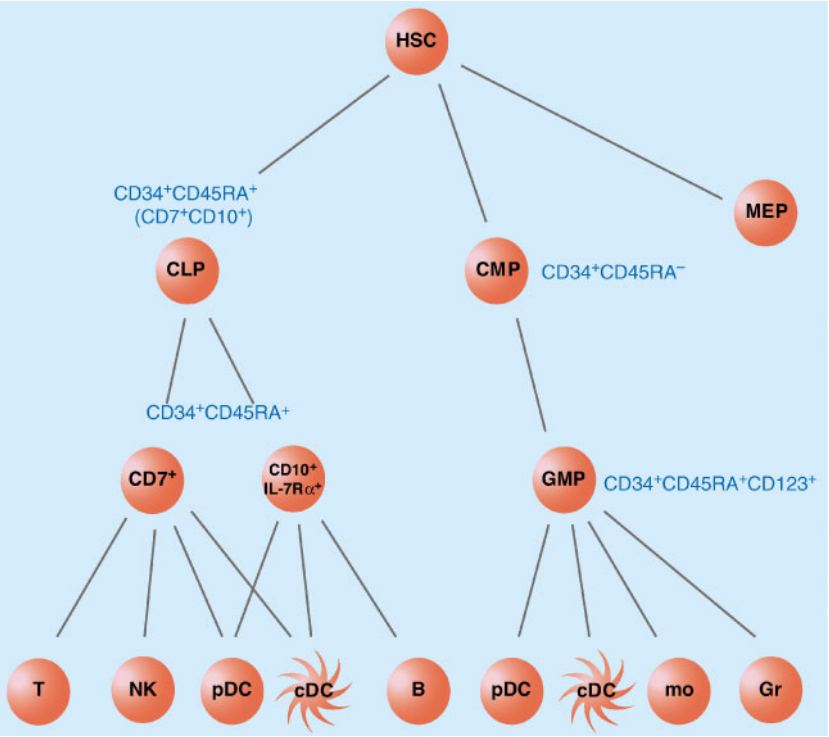

Figure 9: Human lymphoid progenitors. Model for the development of common lymphocyte progenitor (CLP), common myeloid progenitor (CMP), megakaryocyte/erythrocyte progenitor (MEP) and granulocyte/monocyte precursor (GMP) from hematopoietic stem cells (HSC). Further differentiation is shown into T cells (T), natural killer cells (NK), plasmacytoid dendritic cells (pDC), conventional dendritic cells (cDC), B cells (B), monocytes (mo) and granulocytes (Gr). Surface markers are indicated. Figure was modified after [68].

Key players of the adaptive immune system are lymphocytes, specialized cells that mature in the central or primary lymphoid organs. The so called **B** lymphocytes develop in the **B**one marrow, whereas the **T** lymphocytes ripen in the

Thymus. Both lineages are derived from a common hematopoietic stem cell precursor which resides in the bone marrow (Figure 9). Mature lymphocytes recirculate between the blood stream and the peripheral or secondary lymphoid organs, which are the lymph nodes, the spleen and mucosal-associated lymphoid tissues. The function of secondary lymphoid organs is twofold: foreign antigens trapped by specialized cells are accumulated there, in order to display them to lymphocytes. Furthermore, sustaining signals are transmitted to circulating lymphocytes which did not encounter their antigen yet, in order to keep them alive and maintain a suitable lymphocyte cell number.

The central principle of the adaptive immunity is the clonal selection of lymphocytes. This hypothesis was already formulated in the late 1950s by Burnet [69]. It contains four central postulates, the first one stating that each lymphocyte bears a single type of receptor with unique specificity. Secondly, that the interaction between a foreign molecule and and a lymphocyte receptor capable of binding this molecule with high affinity leads to lymphocyte activation. Thirdly, that the differentiated effector cells derived from an activated lymphocyte will bear receptors of identical specificity. And last, that lymphocytes bearing receptors specific for ubiquitous self molecules are deleted at an early stage in lymphoid cell development and therefore absent from the repertoire of mature lymphocytes. Strikingly, at the time of formulation of this hypothesis, neither antigen receptors nor the function of lymphocytes themselves were known. The mechanisms of how adaptive immunity is achieved were clarified later bit by bit and some parts are even today not fully understood.

Nevertheless, nowadays it is proven that a diverse repertoire of B and T cell receptors is generated by somatic recombination events in their respective genes during lymphocyte development [70, 71]. Self-reactive lymphocyte receptors are eliminated by initiation of apoptosis ([72] and see below). Therefore, the immune system is not restricted to a genetically determined limited set of antigen receptors, but can create an almost infinite diversity of binding specificity, enabling it to cope with continuously evolving pathogens.

If a mature T lymphocyte encounters its antigen in secondary lymphoid tissues and is able to bind it with high affinity, and if it receives additional co-stimulatory signals, it becomes activated. The activated T cell will start to divide, a process called clonal expansion. The resulting pool of activated T cells with identical T cell receptor specificity will further differentiate into effector cells. Differentiation can lead to cytotoxic effector T cells, which kill infected cells (cell-mediated immunity), to T helper cells, which can activate B cells and thereby stimulate antibody production (humoral immunity), or to long-living memory T cells. The other effector T cells are short-lived and will undergo apoptosis if the antigen is cleared.

1.2.2 *B lymphocyte development and maintenance*

B cells mature in a certain microenvironment in the bone marrow [73] and undergo several maturation stages which are schematically depicted in Figure 10. The B cell precursors are spatiotemporally organized by reticular cells secreting the chemokine CXCL12 and later by interleukin-7-(IL-7)-producing stromal cells

(Figure 10). Notably, very early B cell precursors still have T lineage potential [74]. The transcription factors E2A, early B cell factor (EBF) and Pax5 are important in the first developmental stage, which is the commitment of a stem cell to a pre-pro-B cell [75].

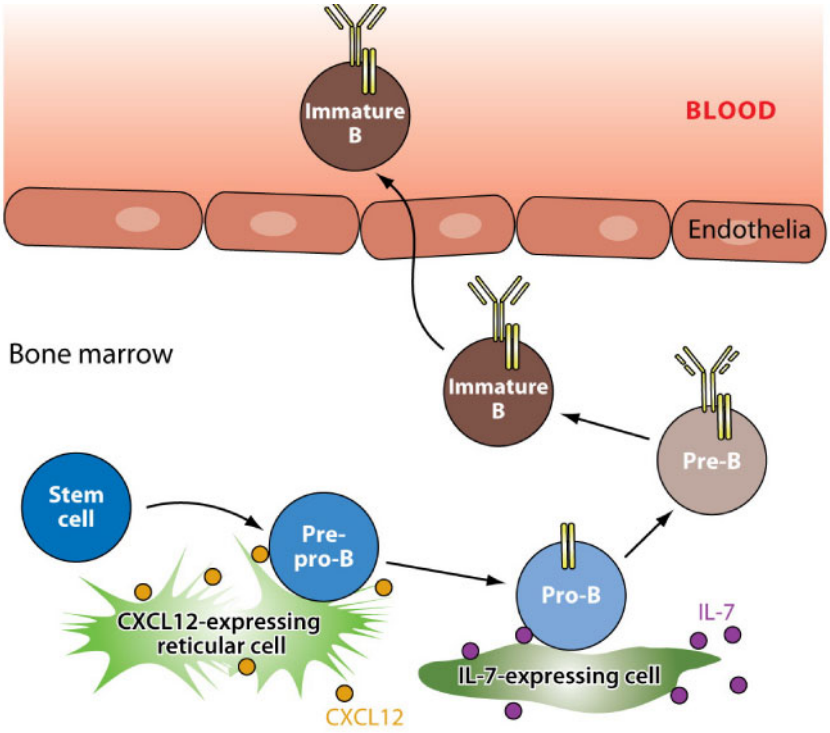

Figure 10: Proposed model for the B cell developmental stages in their specific microenvironment. Key events at the single stages are described in the text. Expression of a pre-B cell receptor is indicated at the pre-B cell stage, with the surrogate light chain shown as split bar, since it is composed of two proteins, λ5 and V_{preB}. From the immature B cell stage on, the cell expresses a fully functional BCR. Figure was taken from [76].

Somatic recombination events in the B cell receptor gene are initiated in the pro-B cell stage, dependent on high expression levels of the *rag1* and *rag2* genes (Recombination-activating genes), on IL-7 and on Pax5 [76]. To be more specific, certain gene segments, called variable (V), diversity (D) and joining (J) segments within the immunoglobulin heavy chain (IgH) locus, are recombined to generate variation in the receptor structure [67]. Therefore, the process is called VDJ-recombination.

If the IgH rearrangement was productive, the cell proceeds to the pre-B cell stage and expresses a pre-B cell receptor (pre-BCR), consisting of the rearranged heavy chain and a surrogate light chain. In a first checkpoint, the functionality of the pre-BCR is probed. If pre-BCRs are crosslinked by binding to the surface of stromal cells, pre-BCR signaling is initiated, resulting in cell proliferation and subsequent down-regulation of the surrogate light chain and *rag1/2* genes [77]. Furthermore, the IL-7 responsiveness of the pre-B cells ceases and they move away from IL-7 expressing stromal cells [76].

When the pre-B cells stop dividing, somatic recombination of the Ig light chain is initiated. In the case of the light chain, only V and J segments are rearranged, therefore the process is called VJ-recombination. Productive rearrangement of this locus is essential for expression of a fully functional BCR on the cell surface, for cell survival and for progress to the developmental stage of an immature B cell. In a second checkpoint, the BCR will be probed for strong crosslinking by self-antigens [77]. If this is the case, the cell will die by apoptosis (clonal deletion). Alternatively, a process called receptor editing can change the BCR specificity from self to non-self via further somatic gene rearrangement in the Ig light chain [78]. In addition, immature B cells with lower avidity to self-antigen can become unresponsive (anergic), but still survive.

Immature B cells then leave the bone marrow and migrate via the blood stream to the secondary lymphoid organs, the first one being the spleen. Further differentiation into and homeostasis of mature B cells is dependent on BCR signaling and B cell activating factor belonging to the TNF family (BAFF-)mediated environmental survival signals [76]. BAFF is expressed on the surface of follicular dendritic cells, which cluster in the center of follicular zones within spleen, lymph nodes and other secondary lymphoid tissues [79].

1.2.3 *T lymphocyte development and maintenance*

T cells arise from hematopoietic stem cells (Figure 9) which originate in the bone marrow and migrate to the thymus, where further maturation takes place. The thymus as primary lymphoid organ is located in the midline of the body just above the heart and can be histologically divided into a central medulla and the peripheral cortex. Crosstalk between architectural stromal cells and the migrating developing T lymphocytes (also called thymocytes) is crucial for spatiotemporal organization of an adequate microenvironment during thymocyte development (Figure 11, [80]).

The lymphoid progenitor cells enter the thymus via vasculature located near the cortico-medullary junction. Homing of the progenitors is mediated by PSGL1 which interacts with P-selectin expressed by the thymic endothelium (Figure 11 **a**). T cell developmental stages are coarsely subdivided according to expression of the cell surface glycoproteins cluster of differentiation (CD) 4 and CD8, which act as co-receptors. Early stage thymocytes neither express CD4 nor CD8 and are therefore called $CD4^{-}CD8^{-}$ double negative (DN). Interactions of these T cell precursors with the thymic stroma triggers T lineage commitment and involves Notch1 signaling, activated by the Notch1 ligand Delta-like 4 expressed on stromal cells [81].

DN thymocytes relocate towards the outer cortex of the thymus guided by chemokine signaling (Figure 11 **b**). On their way, rearrangement of the T cell receptor (TCR) β chain is initiated, in a similar VDJ-recombination process as in developing B cells (see 1.2.2). In a first checkpoint, called β-selection, in-frame rearrangement of the TCRβ chain is verified. Signaling through a pre-TCR, composed of the rearranged β chain, CD3 chains and pre-Tα ensures survival of the cell, whereas a non-functional TCRβ chain leads to elimination of the cell by apoptosis. Thymocytes which pass β-selection undergo a proliferative burst, initiate CD4 and

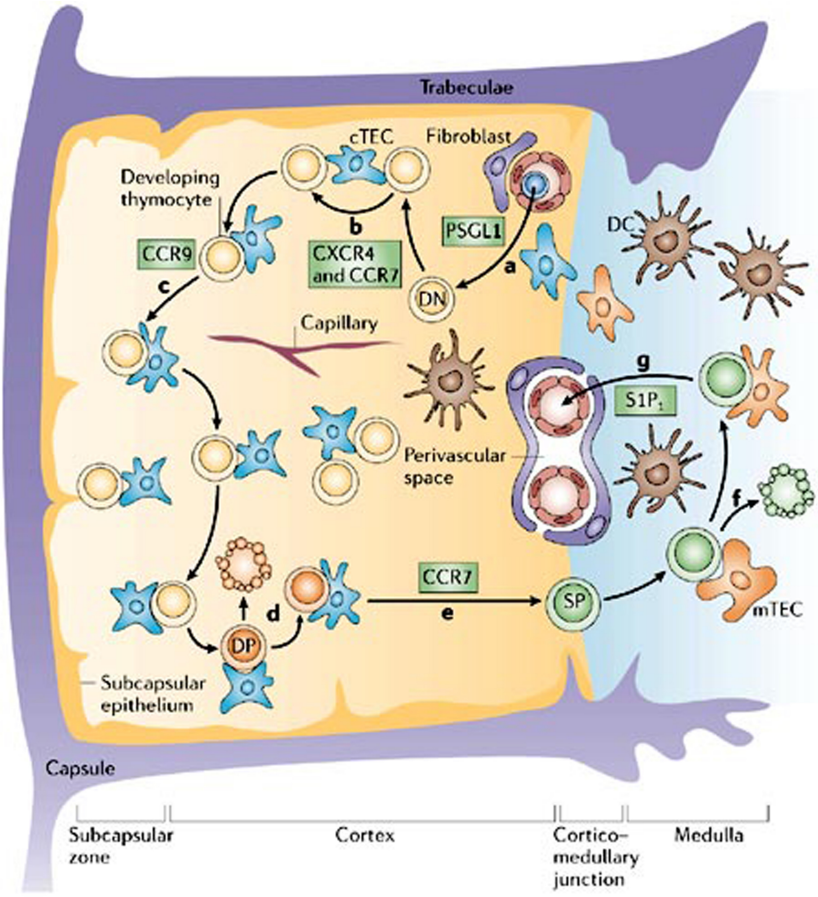

Figure 11: Proposed model for the T cell developmental stages in their specific microenvironment. Key events **a-g** are described in the text. Chemokine and other receptors involved in thymocyte homing are shown in green boxes. DN - $CD4^-CD8^-$ double negative thymocytes, DP - $CD4^+CD8^+$ double positive thymocytes, SP - $CD4^+CD8^-$ or $CD4^-CD8^+$ single positive thymocytes, CXCR4 - CXC-chemokine receptor 4, CCR7/9 - CC-chemokine receptor 7/9, $S1P_1$ - sphingosine-1-phosphate receptor 1, cTEC - cortical thymic epithelial cell, DC - dendritic cell, mTEC - medullary thymic epithelial cell, PSGL1 - platelet-selectin glycoprotein ligand 1. Figure was taken from [80].

CD8 expression and proceed to the $CD4^+CD8^+$ double positive (DP) stage [82]. The thymic subcapsular region might regulate the rate of DP thymocyte production via additional transforming growth factor-β (TGFβ) expression (Figure 11 **c**).

Analogous to the Ig light chain, the TCRα locus does not contain a D segment. Immediately after successful pre-TCR signaling, VJ-recombination of the TCRα chain is initiated, and is finished when the dividing DP cells become quiescent. Productive TCRα rearrangement leads to surface expression of an intact TCRαβ complex. These thymocytes interact through their TCR with self peptide-major histocompatibility complex (pMHC) assemblies which are surface-presented by cortical thymic epithelial cells (cTECs) and dendritic cells. If this interaction is of low avidity, the DP thymocytes receive survival signals and further differentiate. This process, called positive selection, ensures the ability of the TCR to bind pMHC and therefore enriches functional TCRs, but avoids autoreactivity [83]. DP

thymocytes which fail to interact with pMHC at all will die by neglect within few days. In contrast, TCR binding to pMHC with too high avidity leads to induction of cell death by apoptosis, probably mediated by the apoptotic effectors Bim and Nur-77 [72, 84]. This so-called negative selection further contributes to the elimination of self-reactive TCRs [85]. Altogether, only 3-5% of all DP thymocytes survive these checkpoints in the thymic cortex (Figure 11 **d**).

Positively selected DP thymocytes migrate from the cortex to the medulla, mediated by chemotaxis involving the chemokine receptor CCR7 which is expressed on DP cells, and its ligands CCL19 and CCL21, which are produced by medullary TECs (Figure 11 **e**). Furthermore, the DP cells are induced to differentiate into CD4 or CD8 single positive (SP) thymocytes. Thymocytes that bind MHC class II (i.e. MHC molecules that bind and present peptides derived from extracellular proteins) differentiate into the CD4 lineage and become T helper cells. MHC class I-restricted thymocytes (i.e. thymocytes binding MHC molecules that present intracellular antigens) differentiate into the CD8 lineage and become cytotoxic T cells. CD4 commitment requires the transcription factor GATA-3 and ThPOK, whereas CD8 commitment requires STAT5 signaling and the transcription factor Runx3 [82].

SP lineage commitment is further accompanied by deletion of self-reactive thymocytes which overcame the above-mentioned checkpoints (Figure 11 **f**). This process is important for generating central tolerance of T cells to tissue-specific self-antigens. Medullary TECs express tissue-specific antigens promiscuosly, and in this way the maturating thymocytes are able to scan a multitude of these antigens within the thymus [86]. Tissue-specific antigen expression by mTECs is dependent on the transcription factor autoimmune regulator (AIRE), and AIRE deficiency leads to severe autoimmune disorder in mice and humans [87].

In addition, regulatory T (T_{reg}) cells are generated in the thymic medulla, which express the surface markers CD4 and CD25. T_{reg} production is dependent on the transcription factor forkhead box P3 (FOXP3). Mutations in the *foxp3* gene lead to severe autoimmune conditions, since T_{reg} cells contribute to self-tolerance by their ability to suppress activation of the adaptive immune system [88].

Emigration of mature SP thymocytes is mediated by SP-specific expression of the sphingosine-1-phosphate receptor 1 ($S1P_1$). S1P concentration is higher in serum than in most tissues, therefore SP thymocytes are attracted to the perivascular space and subsequently enter the blood stream or the lymph (Figure 11 **g**). The thymic emigrants, called naive T cells, recirculate between blood, lymph and secondary lymphoid organs. For their survival, they are dependent on continuous TCR signaling, provided by interaction of the TCR with self-peptide-MHC complexes as well as on IL-7 signaling via the JAK/STAT5 pathway [89].

1.3 GTPASES OF IMMUNITY-ASSOCIATED PROTEINS

1.3.1 *General features*

GTPases of immunity-associated proteins (GIMAPs) belong to a conserved clade of guanine-nucleotide binding (G) proteins found in plants [49], animals [90] and other eukaryotes. They are also present in certain bacteria, certain picor-

naviruses and herpesviruses (Aravind, L., personal communication). Due to historical reasons, the nomenclature of this protein family is confusing to some extent. The GIMAP naming convention was introduced in reference [91]. An alternative nomenclature exists, referring to these proteins as immunity-associated nucleotide binding proteins (IANs, [92]). Besides that, some family members have additional synonyms. An overview is given in Table 1. For consistency, the GIMAP nomenclature is used throughout this work.

GIMAP #	IAN #	SYNONYMS
GIMAP1 (Q8WWP7)	IAN2	iap38 [93], imap38 [94],
GIMAP2 (Q9UG22)	IAN12	imap2 [95, 96]
GIMAP3-*ps* [1]	IAN4	
GIMAP4 (Q9NUV9)	IAN1	imap4 [96]
GIMAP5 (Q96F15)	IAN5	IAN4 [97, 98, 99], IAN4L1 [100], Irod [101]
GIMAP6 (Q6P9H5)	IAN6	IAN2 [102]
GIMAP7 (Q8NHV1)	IAN7	
GIMAP8 (Q8ND71)	IAN9, 10, 11 [103]	
GIMAP9 [2]	IAN3	

Table 1: GIMAP nomenclature. The Uniprot accessions in parentheses refer to the human orthologs.

[1] Pseudogene in humans.
[2] Not present in the human genome.

Gimap genes are organized in chromosomal clusters, encoded on human chromosome 7, mouse chromosome 6 and rat chromosome 4, respectively. Within these three species, the clusters are similarly arranged (Figure 12). In humans, there are only seven *Gimap* genes, because the human *gimap3* ortholog is a pseudogene and *gimap9* is not present in the human genome [91].

The present work is focused on human GIMAPs. The encoded proteins have a molecular mass of 33-38 kDa and are comprised of an amino-(N-)terminal G domain containing a GIMAP-specific signature motif, the conserved box, followed by distinct carboxy-(C-)terminal extensions of 60-130 amino acids length. The 75 kDa GIMAP8 alone differs in being composed of three consecutive GIMAP-specific G domains. Human GIMAP1, GIMAP2 and GIMAP5 have one or two additional hydrophobic helical segments at their C-termini predicted to form transmembrane (TM) spanning helices (Figure 13).

Sequence analysis indicated that GIMAPs belong to the TRAFAC class of GTPases. Within the TRAFAC class, GIMAPs, together with the plant-specific Toc (translocon at the outer envelope membrane of chloroplasts) proteins, comprise a distinctive clade, called the paraseptins, which is closest to the septins (Figure 14, see also the paragraph concerning paraseptins in 1.1.3.3).

In the following paragraphs, the current state of knowledge regarding the individual GIMAP family members will be presented.

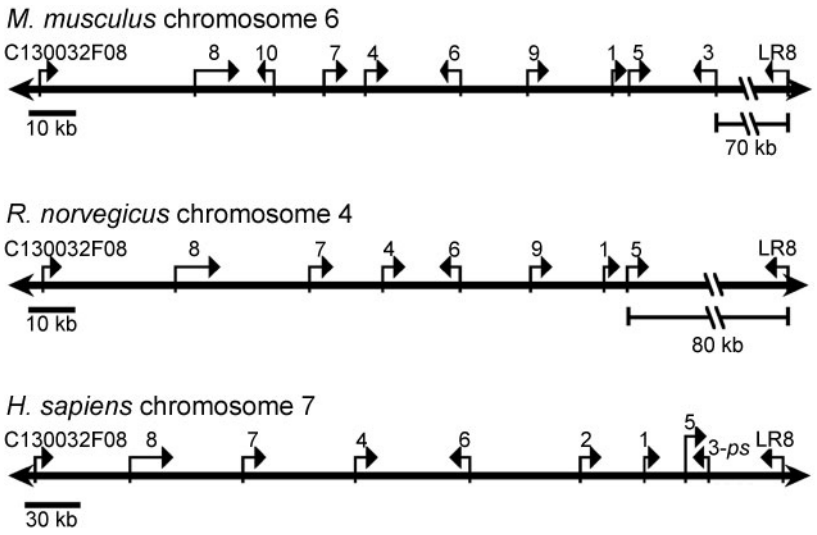

Figure 12: GIMAP chromosomal organization. Corresponding *gimap* nomenclature is indicated above the schemes. Figure was modified after [104].

1.3.2 *GIMAP1*

GIMAP1 was first described in mice, where its expression in spleen cells was reported to be induced by infection with *Plasmodium chabaudi*, a rodent malaria parasite [93]. However, a more recent study was not able to reproduce these results and showed that GIMAP1 is constitutively expressed in all lymphocyte lineages [105].

Human GIMAP1 is composed of 306 amino acids with a molecular weight of 34 kDa. It contains one predicted helical membrane anchor at the C-terminus (amino acid position 273-292, Figure 13). Furthermore, GIMAP1 did not exhibit any GTP-binding. However, it is important to note that the initial GTP-loading state of the recombinant protein was not analyzed before subjecting it to the binding assay. In tissue array hybridization experiments, human GIMAP1 was found mainly in spleen and lymph node tissues, to a lesser extent in heart and lung tissues. Within a human cell line, the protein localized to the endoplasmic reticulum [96].

Quantitative RT-PCR showed up-regulation of GIMAP1 on the mRNA level in T lymphocyte development during the transition from the $CD4^{-}CD8^{-}$ DN to the $CD4^{+}CD8^{+}$ DP stage in mice and rats [104, 103], hinting at a role of GIMAP1 in thymocyte maturation. Quantitative proteomics revealed that GIMAP1 is down-regulated during the differentiation of activated T lymphocytes into T helper 2 cells [106]. This finding suggests that GIMAP1 expression is repressed by the IL-4/STAT6 signaling pathway which drives the development of a T helper cell 2 phenotype [107].

Strikingly, conditional knockout of GIMAP1 in mouse lymphoid tissues resulted in a massive loss of peripheral B and T cells (>90% in spleen and lymph nodes), highlighting the central function of GIMAP1 in regulation of lymphocyte survival in the B and T cell lineage [108].

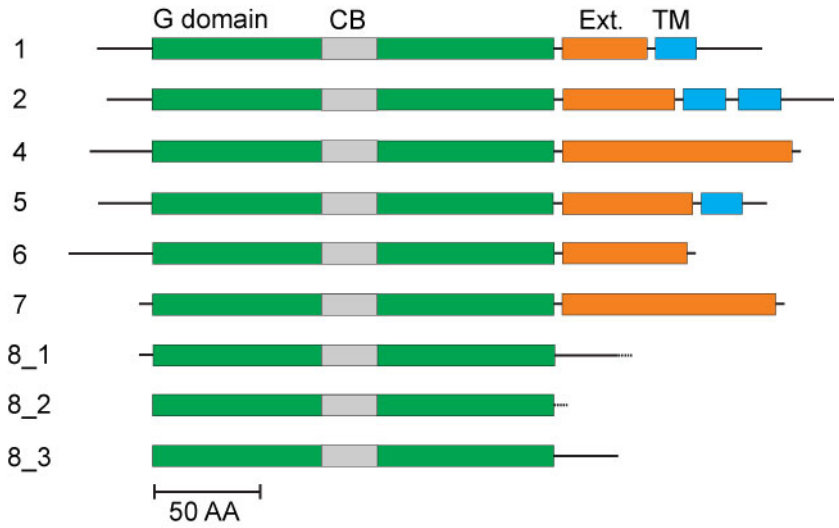

Figure 13: Human GIMAP domain organization. GIMAP nomenclature is indicated on the left. The three G domains of GIMAP8 are individually aligned. CB - GIMAP-specific conserved box, Ext. - C-terminal extension, TM - predicted transmembrane segment

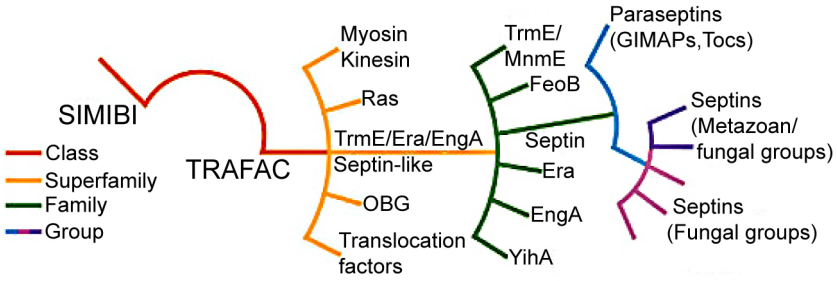

Figure 14: Positioning of the paraseptin clade in the P-loop NTPase superclass. Figure was modified after [43].

1.3.3 *GIMAP2*

GIMAP2 is only present in the human genome and not found in mice and rats [91]. The protein comprises 337 amino acids and has a molecular weight of 38 kDa. Two helical transmembrane segments are predicted at the C-terminus, encompassing amino acids 271-291 and 297-317 (Figure 13). Up to now, no functional data regarding GIMAP2 are available.

1.3.4 *GIMAP3*

GIMAP3 is expressed in mice, but its ortholog is a pseudogene in humans and not present in the rat genome [91]. However, phylogenetic analysis shows that GIMAP3 is closely related to GIMAP5 (Figure 15). It was discovered in murine 32D hematopoietic precursor cells expressing the BCR/ABL oncoprotein. It consists of 301 amino acids with a molecular weight of 34 kDa. A predicted C-terminal helical membrane anchor encompasses amino acids 280-300 (Figure 13). It possesses

GTP-binding activity [109]. Mouse GIMAP3 mRNA is almost exclusively found in spleen and lymph nodes [104]. GIMAP3 was shown to reside at the mitochondrial outer membrane, and the predicted membrane anchor was necessary for this subcellular localization [109].

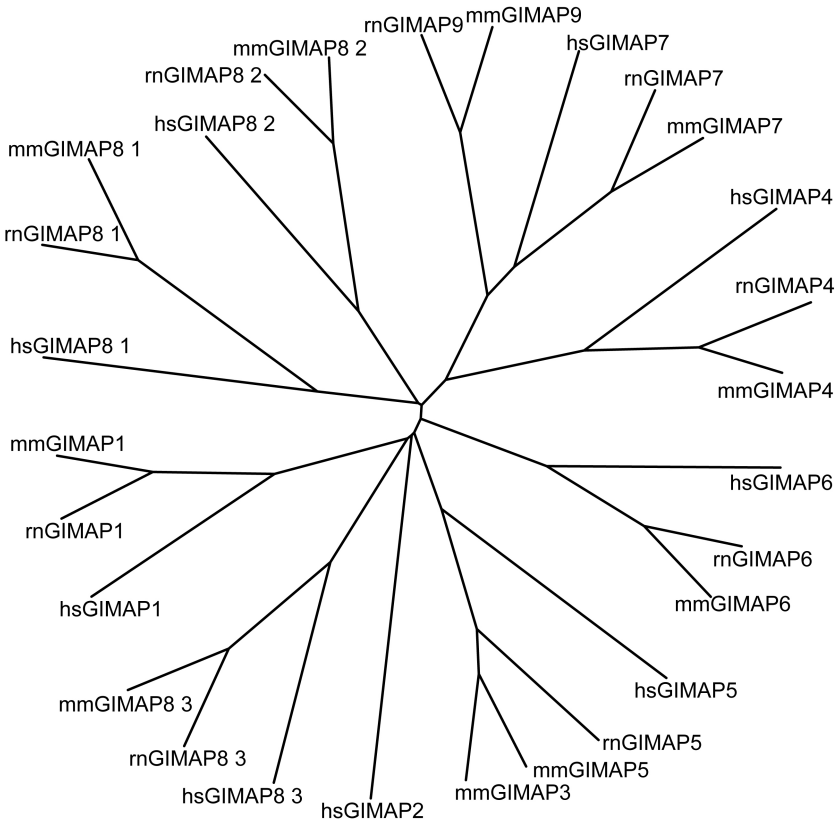

Figure 15: Unrooted phylogenetic tree showing the relations between human, mouse and rat GIMAPs. The graph was calculated using the clustalW sequence alignment [110] and quicktree [111] programs.

Quantitative RT-PCR experiments with purified thymocyte subsets showed a drastic up-regulation of GIMAP3 during the maturation of $CD4^+CD8^+$ DP to $CD4^+CD8^-$ and $CD4^-CD8^+$ SP thymocytes. shRNA-mediated knockdown of GIMAP3 in immature thymocytes in fetal thymus organ culture resulted in significantly reduced generation of mature $CD4^+CD8^-$ SP and $CD4^-CD8^+$ SP T cells. Furthermore, co-immunoprecipitation studies showed an association of over-expressed and endogenous GIMAP3 with the anti- and proapoptotic proteins Bcl-2, Bcl-xL and Bax. These results suggest that GIMAP3, together with other GIMAPs (see below), relays T cell receptor signals and controls survival or death of immature thymocytes at the stage of positive selection, possibly via interaction with Bcl-2 family members [104].

1.3.5 *GIMAP4*

GIMAP4 was initially identified by a mRNA differential display technique, where it was shown to be induced during positive selection of mouse thymocytes [90].

It contains 328 amino acids and has a molecular weight of 38 kDa (Figure 13). The last 100 amino acids exhibit a high propensity to form a coiled coil motif. Biochemical analysis proved GMP-PNP- and GDP-binding activity of the protein with equilibrium dissociation constants of 0.5 µM and 6 µM, respectively. GIMAP4 also showed GTP hydrolytic activity [102].

In mouse tissues, GIMAP4 mRNA is expressed in the spleen, lung, kidney and to a lesser extend in heart and skeletal muscle [90]. In humans, it can be found in the spleen as well and in the digestive tract [102]. In both species, the protein is present in all lymphocyte lineages [90, 102, 112]. Microscopy and subcellular fractionation experiments proved a cytoplasmic localization of rat and mouse GIMAP4 [112, 113].

Several studies support a role of GIMAP4 in thymocyte development. Besides the above-mentioned differential display experiment, another report using the same technique showed induction of GIMAP4 in the $CD4^-CD8^-$ DN developmental stage, when thymocyte β-selection takes place. Additionally, up-regulation of GIMAP4 at the protein level in SP thymocytes was reported [112]. RT-PCR results corroborate this finding [104]. In rats as well, GIMAP4 protein expression is detectable in the $CD4^-CD8^-$ DN thymocyte subset, vanishes completely during the transition to the $CD4^+CD8^+$ DP stage and is again drastically induced in the SP subsets [113]. Furthermore, over-expression of GIMAP4 in mouse $CD4^-CD8^-$ DN thymocytes in fetal thymus organ culture lead to increased apoptosis at the $CD4^+CD8^+$ DP stage and to disturbance of further thymocyte development. In the same study, specific interaction of GIMAP4 with the pro-apoptotic Bax protein was demonstrated by co-IP experiments [104]. Two independent microarray studies showed up-regulation of GIMAP4 in thymocytes undergoing negative selection [114, 115]. Taken together, these results hint at a role of GIMAP4 in apoptosis regulation during selection checkpoints in thymocyte maturation.

However, GIMAP4 knockout mice exhibit normal T cell development, selection and maintenance. But interestingly, upon induction of apoptosis in $GIMAP4^{-/-}$ T cells, the number of apoptotic cells is 2-4x higher compared to wild type T cells, concomitant with a reduction of the number of dead T cells. Therefore, apoptosis takes longer time in T cells lacking GIMAP4. This implies that the function of GIMAP4 in wild type T cells is acceleration of apoptosis. Further analysis of apoptotic processes in the knockout cells suggests that GIMAP4 acts in the execution of apoptosis and not in its induction phase [112].

GIMAP4 deficiency in thymocytes and lymphocytes of the inbred BN laboratory rat strain was discovered recently. Apparently, an AT insertion in the *gimap4* gene leads to a premature stop codon and to truncation of the last 21 amino acids of the translated protein. By an unknown mechanism, this in turn results in 95% reduction of the GIMAP4 protein level, while the mRNA level remains unchanged. The stability of the truncated protein seems to be unchanged as analyzed by pulse-chase experiments. Furthermore, the truncated protein still shows cytosolic localization. Importantly, T cells purified from BN rats recapitulate the delayed apoptosis phenotype of GIMAP4 knockout mice, albeit the effect is somewhat milder. This could be explained by the fact that the BN rat is a hypomorph for GIMAP4 and not a total knockout [113].

GIMAP4 could play a role not only in lymphocyte development, but also in the activation of peripheral B and T cells, since down-regulation of GIMAP4 on the protein, but not on the mRNA level was found upon *in vitro* stimulation of isolated human lymphocytes [102].

Furthermore, similar to GIMAP1 (see 1.3.2), GIMAP4 is down-regulated during the differentiation of activated T cells in T helper 2 cells as shown by quantitative proteomics [106], indicating repression of GIMAP4 by the IL-4/STAT6 pathway. However, another proteomic study demonstrated GIMAP4 induction by IL-7 [116]. A recent publication stated that GIMAP4 expression is under control of factor PHF11, a transcriptional co-activator of NF-κB [117]. Therefore, the *gimap4* gene expression seems to be regulated by multiple mechanisms.

1.3.6 *GIMAP5*

GIMAP5 in humans contains 307 amino acids and has a molecular weight of 35 kDa. The sequence stretch encompassing residues 235-265 is predicted to form a coiled coil motif. Furthermore, the predominantly hydrophobic amino acids 285-305 at the C-terminus are predicted to form a helical membrane anchor (Figure 13). Further biochemical data on GIMAP5 are not available up to now.

Human tissue arrays proved high levels of GIMAP5 mRNA expression in spleen, lymph nodes, lung and placenta. Lower levels of GIMAP5 mRNA could also be detected in kidney, liver and muscle tissues [91, 101]. In mice, GIMAP5 is present in B as well as in T cells. Several subcellular localization experiments were conducted, which lead to diverse results, including ER localization in a human cell line [101], mitochondrial localization of human GIMAP5 [118] and mitochondrial localization of rat GIMAP5 [98]. Probably the most trustworthy report using monoclonal antibodies to stain endogenous GIMAP5 in a human T cell line revealed a lysosomal localization of the protein [119]. Furthermore, within thymocyte subsets, the expression level of GIMAP5 increases during maturation into the SP stage [104].

Insights into the importance of GIMAP5 for T lymphocyte maintenance originated from a certain laboratory rat strain, the biobreeding diabetes-prone (BBDP) rat, which was already described in the late 1970s and which develops spontaneous type 1 diabetes [120]. These rats also show a severe reduction in the number of peripheral T cells (lymphopenia) [121]. Furthermore, while thymocyte development appears to be normal, peripheral T cells from the BBDP rat have an up to 3x increased apoptosis rate [98, 122, 123]. These apoptosis-prone peripheral T cells additionally show a partially activated phenotype [97].

More than 20 years later, a single nucleotide deletion in the *gimap5* gene was reported in BBDP rats, which leads to a frameshift in the codon for amino acid 85 and to a change of 19 amino acids downstream until a premature stop codon occurs [95]. Follow-up studies proved that complementation with an intact *gimap5* gene rescues lymphopenia in BBDP rats [124]. However, transplantation of GIMAP5$^{-/-}$ bone marrow in non-lymphopenic, non-diabetic animals did not recapitulate the BBDP rat phenotype [125]. This suggests that GIMAP5 deficiency in lymphocyte precursors alone is not sufficient for development of lymphopenia, but also GIMAP5 deficiency in the lymphocyte environment must contribute to the

phenotype. Contrary to this finding, siRNA-mediated knock-down of GIMAP5 in a human T cell line has been shown to induce apoptosis [98]. Furthermore, additional genetic factors account for type 1 diabetes pathogenesis in the BBDP rat [126]. Nevertheless, excessive numbers of effector T cells with an altered T cell receptor repertoire, caused by the GIMAP5 mutation, seem to increase the susceptibility of the BBDP rat to autoimmune diabetes, according to a recent report [127]. Interestingly, backcrossing of the BBDP GIMAP5 truncated variant in the PVG-RT1^{u} rat strain also lead to lymphopenia, but not to the development of diabetes. Instead, the rats developed autoimmune intestinal inflammation, similar to human eosinophilic gastroenteritis [128].

Furthermore, the expression of almost the whole GIMAP family is turned down in regulatory T cells of patients suffering from type 1 diabetes [129]. The role of GIMAP5 in human diseases is further underpinned by the observation that single nucleotide polymorphisms in GIMAP5 are associated with IA2-autoantibodies in type 1 diabetes patients and systemic lupus erythematosus [130, 131, 132].

Importantly, a recently generated GIMAP5 knockout mouse recapitulated the lymphopenic phenotype of the BBDP rat. The knockout mice do not develop diabetes, but die after approximately 15 weeks, probably due to liver failure. Apparently, the final stages of thymocyte development as well as the survival of thymic emigrants are defective. Additionally, NK and NKT cell differentiation is completely blocked. Furthermore, transfer of GIMAP5$^{-/-}$ bone marrow in an wild type environment did not rescue the GIMAP5$^{-/-}$ T cell population, indicating an intrinsic T cell defect, contrary to the above-mentioned findings from the BBDP rat [133].

Another GIMAP5-deficient mouse strain was generated in a forward genetic screen aimed at identifying determinants for NK and CD4^{-}CD8^{+} SP T cell development. These so called *sphinx* mice contain a G38C mutation in the P-loop of GIMAP5, which renders the protein unstable, thus mimicking a GIMAP5 knock out mouse. *Sphinx* mice suffer from lymphopenia, hepatic extramedullary hematopoiesis, weight loss and intestinal inflammation. Transplantation experiments demonstrated a cell-intrinsic function of GIMAP5. Interestingly, hematopoietic stem cells from *sphinx* mice are unable to reconstitute the B cell compartment of irradiated recipients, and *sphinx* B cells cannot generate antigen-specific IgG or IgM responses, even if canonical B cell receptor signalling pathways are intact. Furthermore, *sphinx* B cells arrest in the S phase of the cell cyle. Therefore, the yet unidentified pathway in which GIMAP5 acts could link B cell responses to cell cycle progression [134].

The same report which connects GIMAP1 and GIMAP3 to the intrinsic apoptotic pathway in mouse thymocytes (see 1.3.4, 1.3.5) also claimed a function of GIMAP5 in the generation of CD4^{+}CD8^{+} DP thymocytes and a specific interaction of GIMAP5 with the pro- and anti-apoptotic proteins Bax, Bcl-2 and Bcl-xL [104]. This contradicts the above-mentioned *in vivo* experiments, which at most detect disturbances at the very late stages of thymocyte development if GIMAP5 is knocked out. Furthermore, co-localization of GIMAP5 and Bcl-2 could not be confirmed in a rat cell line [135].

Other authors found that GIMAP5 is transcriptionally controlled by Notch [136]. It was also reported that loss of GIMAP5 in the BBDP rat induces ER stress-

induced apoptotic signaling through the C/EBP-homologous protein (CHOP) [137]. Therefore, the mechanism of GIMAP5 apoptosis protection in lymphocytes is yet unclear, despite the multitude of studies dealing with this GIMAP family member.

1.3.7 *GIMAP6*

Human GIMAP6, the smallest member of the GIMAP family, has 292 amino acids and a molecular weight of 33 kDa (Figure 13). No biochemical analysis of the protein has been conducted so far. Its mRNA is highly expressed in mouse spleen, lymph node and lung tissues, and it is present in mouse B and T cells [104]. Its expression increases slightly during the maturation of thymocytes into the SP stage in mice [104], whereas its expression is highest in the DP thymocyte subset in rats [103].

In a microarray study, GIMAP6 was found to be strongly downregulated in non-small cell lung cancer tissue samples from 6 patients, when compared to the surrounding non-tumor tissue [138].

1.3.8 *GIMAP7*

Human GIMAP7 consists of 300 amino acids with a molecular weight of 34.5 kDa (Figure 13). As in GIMAP4, approximately the last 100 amino acids are predicted to form a coiled-coil region. There are no biochemical data available for the protein. In mice, its mRNA is detectable in thymus, spleen, lymph node and lung tissue, and it is expressed in B and T cells [104]. In rats, it is most strongly expressed in peripheral T cells. In mice and rats, its expression in thymocytes is low and unchanged over all developmental stages [104, 103]. Experiments addressing the function of GIMAP7 in lymphocytes have not been conducted so far.

1.3.9 *GIMAP8*

GIMAP8 is an exceptional member of the GIMAP family, since it contains three G domains in a single protein chain (Figure 13). Up to now, no other protein containing three G domains is known. It was first discovered in mice and contains 688 amino acids with a molecular weight of 77 kDa [139]. There are no biochemical data available for GIMAP8. In a multiple mouse tissue northern blot, GIMAP8 mRNA was shown to be expressed mainly in the thymus and to a lesser extent in the heart [139]. Another report found GIMAP8 mRNA in RT-PCR experiments in mouse lymph node, spleen, thymus and lung tissues, within splenic cells, it was expressed in T and B cells [104]. In rats, GIMAP8 is strongly expressed on the protein level in the thymus, much lesser in the spleen and within lymph node cells only in T cells, not in B cells [103]. The subcellular localization of GIMAP8 was reported to be at the ER, Golgi apparatus and at the mitochondria, although in a not very convincing experiment using over-expressed protein in the CHO cell line [139].

Within thymocyte subsets in rats, GIMAP8 expression increased significantly in the $CD4^+CD8^+$ DP stage, whereas it is lower in mature SP lymphocytes [103]. In mice, the opposite was shown, with low and unchanging levels of GIMAP8 mRNA in thymocytes and higher expression in splenic SP T cells [104]. Furthermore, mouse GIMAP8 expression seems to be repressed upon infection with the rodent malaria parasite *Plasmodium chabaudi* and seems to exert an anti-apoptotic effect when over-expressed in a fibroblast cell line [139].

1.3.10 *GIMAP9*

The *gimap9* gene is only present in mice and rats [91]. However, phylogenetic analysis shows that it is a close relative to GIMAP7, which is also present in humans (Figure 15). In mice, GIMAP9 mRNA is expressed in spleen and lymph node and within splenic cells, it is present in T and B cells; furthermore, its expression increases in the positively selected thymocyte SP subsets [104].

1.4 SCOPE OF THE PRESENT WORK

GIMAPs are a heterogenous family of GTPases with the unifying characteristic that they occur mainly in tissues and cells of the adaptive immune system. Numerous studies, especially a number of animal models, suggest a role of GIMAP family proteins in life and death decisions in developing and recirculating lymphocytes (see above). However, even these results propose opposing roles of different family members, i.e. anti-apoptotic function of GIMAP1 and GIMAP5 as well as a pro-apoptotic effect of GIMAP4. Furthermore, on the biochemical and structural level, GIMAPs are barely or not at all characterized.

Therefore, the aim of the present doctoral thesis was a solid investigation of the basic biochemical and structural features of at least one representative GIMAP family member. Based on these findings, mutational and cell-based studies should further clarify the molecular mode of action of GIMAPs in lymphocytes. The work should create the molecular basis for further *in vivo* studies of GIMAPs in the immune system.

2 MATERIALS AND METHODS

2.1 MATERIALS

2.1.1 *Instruments*

The instruments used in this study are listed in Appendix A, Table 13.

2.1.2 *Chemicals*

Chemicals from the following companies have been used: Roth (Karlsruhe, D), Calbiochem (Darmstadt, D), Jena Bioscience (Jena, D), GE Healthcare (Piscataway, USA), Sigma-Aldrich (Steinheim, D), and Avanti (Alabaster, USA).

2.1.3 *Enzymes*

Enzymes used in this study are listed in Appendix A, Table 14.

2.1.4 *Kits*

Kits used in this study are listed in Appendix A, Table 15.

2.1.5 *Bacteria strains*

- *E.coli* TG1 K12, genotype *supE, hsdΔ 5, thi, Δ(lac-proAB), F'[traD36, proAB$^+$, lac^q, lacZΔ M15]* (Promega, Mannheim, D)
- *E.coli* BL21 (DE3) Rosetta, genotype *F$^-$ ompT hsdsSB (rB$^-$ mB$^-$) gal dcm (DE3) pRARE (CmR)* (Novagen, Darmstadt, D) with *pRARE* containing the tRNA genes *argU, argW, ileX, glyT, leuW, proL, metT, thrT, tyrU and thrU*

2.1.6 *Plasmids*

- pGex6P1 (Amp^R, GE healthcare, Piscataway, USA)
- pSKB-LNB (Kan^R, O. Daumke, MDC Berlin)
- pEGFP-C3-MCS (Kan^R, based on pEGFP-C3, Clontech, Mountain View, USA; MCS exchanged against MCS from pGex-6P-1, O. Daumke, MDC Berlin)
- pmCherry-C (Kan^R, based on pEGFP-C1, Clontech, Mountain View, USA; *EGFP* gene exchanged against *mCherry* gene, AG Lewin, MDC Berlin)

2.1.7 *Cell lines*

- HeLa cells (Human cervix carcinoma cell line) [140]

were a generous gift from Marion Papst, MDC Berlin

- Jurkat cells (Human T cell leukemia cell line) [141]

were a generous gift from the group of Stephan Mathas, MDC Berlin

2.1.8 *Media and buffers*

Media used in the present work and their composition/ordering numbers are listed in Appendix A, Table 16. Buffers and their composition are shown in Appendix A, Table 17.

2.1.9 *cDNA clones*

A list of cDNA clones used in this work can be found in Appendix A, Table 18.

2.2 MOLECULAR BIOLOGY METHODS

2.2.1 *Polymerase chain reaction*

Amplification of DNA fragments were conducted using *Pfu* polymerase according to standard procedures [142].

2.2.2 *Restriction digest*

DNA restriction digests were performed using enzymes from New England Biolabs, Frankfurt am Main, D, according to the manufacturer's protocol.

2.2.3 *Agarose gel electrophoresis*

1% agarose gels were prepared and run according to standard procedures [142].

2.2.4 *DNA purification*

DNA bands were cut out of the agarose gel and purified using the QIAquick Gel Extraction Kit, Qiagen, Hilden, D according to the manufacturer's protocol.

2.2.5 *Ligation*

Plasmids and inserts were quantified by measuring the absorption at 260 nm. 10 ng plasmid was ligated with a sixfold molar excess of insert using T4 DNA Ligase from New England Biolabs, Frankfurt am Main, D, according to the manufacturer's protocol.

2.2.6 *Preparation of chemically competent* E. coli

Chemically competent *E. coli* cells were prepared according to [143].

2.2.7 *Transformation of chemically competent* E. coli

Plasmids were transformed using the heat shock method according to standard protocols [142]. For plasmid maintenance and amplification, the *E.coli* TG1 strain was used. For protein expression, the *E.coli* BL21 (DE3) Rosetta strain was employed.

2.2.8 *Preparation of* E. coli *cryo stocks*

For long-term storage of bacteria, cryo stocks were prepared by mixing 1 ml of a 5 ml LB overnight bacteria culture with 0.5 ml sterile glycerol. Cryo stocks were stored at -80°C.

2.2.9 *Site-directed mutagenesis*

Site-directed mutagenesis was performed using the QuickChange kit according to the manufacturer's protocol.

2.2.10 *Survey of prepared constructs*

A survey of the constructs used in the present study can be found in the Appendix A, Table 19.

2.3 BACTERIA AND BIOCHEMICAL METHODS

2.3.1 *Antibiotics*

Ampicillin was used at a final concentration of 100 µg/ml. Chloramphenicol was used at a final concentration of 34 µg/ml. Kanamycin was used at a final concentration of 10 µg/ml in liquid cultures and at 50 µg/ml in agar plates.

2.3.2 *Protein over-expression test in* E. coli

To test for over-expression of the desired construct, a 5 ml overnight LB *E.coli* BL21 (DE3) Rosetta culture supplemented with the respective antibiotics, grown at 37°C, carrying the respective expression plasmid, was induced with 40 µM IPTG and grown for further 2 h. A 1 ml sample was taken and centrifuged for 5 min at 13200 rpm. The pellet was resuspended in 400 µl 1x SDS sample buffer, boiled for 10 min at 95°C and 5 µl were loaded on a NuPAGE Novex 4-12% Bis-Tris gel.

2.3.3 *Protein solubility test*

To test the solubility of the over-expressed protein, 1 l TB modified medium supplemented with the respective antibiotics was inoculated 1:100 with an overnight *E.coli* BL21 (DE3) Rosetta culture in LB medium. Cells were grown under shaking to an OD_{600} of 0.5 at 37°C. Bacteria cultures were cooled to 18°C, protein expression was induced by addition of 40 µM IPTG and cultures were grown for another 20 h. Bacteria were collected by centrifugation at 5000 rpm for 7 min and pellets were resuspended in 30 ml lysis buffer per pellet from 1 l bacteria culture. The bacteria suspension was passed at least two times through a microfluidizer to disrupt the cells. The lysate was centrifuged at 35.000x g and 4°C for 35 min in a Optima L-100 K ultracentrifuge using a type 35 rotor. The supernatant was filtered through a 0.2 µm filter and applied on a 1 ml GSTrap HP chromatography column equilibrated with 5 column volumes (CV) buffer I. The column was washed with 30 CV buffer I. Bound protein was eluted with 5 ml elution buffer. Samples taken at every step of the test purification were analyzed using SDS-PAGE (see 2.3.12).

2.3.4 *Large scale protein over-expression in* E. coli

10 l TB modified medium supplemented with the respective antibiotics were 1:100 inoculated with an overnight *E.coli* BL21 (DE3) Rosetta culture in LB medium containing the expression constructs. Cells were grown under shaking to an OD_{600} of 0.5 at 37°C. Bacteria cultures were cooled to 18°C, protein expression was induced by addition of 40 µM IPTG and cultures were grown for another 20 h. Bacteria were collected by centrifugation at 5000 rpm for 7 min and pellets were resuspended in 30 ml lysis buffer per pellet from 1 l bacteria culture. The cell suspension was stored at -40°C.

2.3.5 *Over-expression of selenomethionine-(SeMet-)derivatized protein*

To produce SeMet-labeled protein, M9 minimal medium supplemented with the respective antibiotics was inoculated with an overnight LB culture of the respective expression clone in a 1:100 dilution. Cells were grown to an OD_{600} of 0.5 at 37°C. Then, an amino acid supplement (L-lysine, L-phenylalanine, L-threonine to a final concentration of 100 mg/l, L-isoleucine, L-leucine, L-valine and L-SeMet to a final concentration of 50 mg/l, respectively) was added to inhibit endogenous methionine biosynthesis and start SeMet incorporation [144]. 15 min after addition, the bacteria culture was cooled to 18°C. Protein expression was induced by the addition of 40 µM IPTG. Further growth and harvesting of the cells was conducted in the same way as for the native protein.

2.3.6 E. coli *cell lysis and preparation of the cytosolic fraction*

The bacteria suspension was thawed on ice and stirred thoroughly. The suspension was passed at least two times through a microfluidizer to disrupt the cells. The lysate was centrifuged at 35.000x g and 4°C for 35 min in a Optima L-100 K

ultracentrifuge using a type 35 rotor. The supernatant was filtered through a 0.2 µm filter.

2.3.7 *Affinity chromatography and GST-tag cleavage*

All chromatographic procedures were conducted at 4°C. The filtered supernatant was applied on a chromatography column loaded with 15 ml GSH Sepharose beads equilibrated with 5 CV of buffer I. The column was washed with buffer I until E_{280} reached baseline. Afterwards, the column was washed with 3 CV buffer II to remove protein bound Mg^{2+} and nucleotide. In GIMAP7 preparations, the buffer II wash step was omitted, because the affinity of GIMAP7 towards nucleotides was much lower than in the case of GIMAP2 and GIMAP5. Instead, an additional wash step with buffer I containing 1% CHAPS was conducted. The column was washed again with 3 CV buffer I to remove EDTA or CHAPS. GSH Sepharose beads were resuspended in 1 CV buffer I and transferred to a Falcon tube. 1 mg GST-PreScission protease was added to cleave the amino-terminal GST-tag. Five amino acids, Gly-Pro-Leu-Gly-Ser, remained as cloning artifact at the N-terminus after proteolytic cleavage. The suspension was incubated for 15 min on a roller and for further 20 h at 4°C without agitation. The column was re-packed and cleaved GIMAP2 collected by eluting with buffer I until E_{280} reached baseline.

2.3.8 *Size-exclusion chromatography (SEC)*

After concentrating the elution fraction from 2.3.7 to 2 ml, the protein was centrifuged for 5 min at 13200 rpm. The supernatant was applied on a Superdex 75 SEC column for GIMAP2 and GIMAP5 preparations or on a Superdex 200 SEC column for GIMAP7 preparations at aflow rate of 1 ml/min. The columns were equilibrated with 2 CV SEC buffer. The peak fractions containing the protein of interest were pooled and concentrated to approximately 35 mg/ml. For analytical size-exclusion chromatography, Superdex 75 10/300 GL (all GIMAP2 and GIMAP5 constructs) or Superdex 200 10/300 GL (all GIMAP7 constructs) columns were used. Protein sample with a volume of 0.25 ml at a concentration of 0.1 mg/ml in SEC buffer was injected, and the columns were operated at a flow rate of 0.75 ml/min.

2.3.9 *Protein concentration*

Protein solutions were concentrated using Amicon centrifugal filter devices with a 10 kDa cutoff according to the manufacturer's protocol.

2.3.10 *Protein concentration determination*

Total protein content in lysates or mixed protein solutions were determined using the Bradford assay [145]. For purified proteins, concentration was determined by measuring E_{280} and using calculated extinction coefficients [146].

2.3.11 *Protein storage*

Pooled, concentrated peak fractions from SEC were divided into 25 µl aliquots and flash-cooled by plunging them into liquid N_2. Aliquots were stored at -80°C.

2.3.12 *Sodium dodecyl sulfate polyacrylamide gel electrophoresis (SDS-PAGE)*

NuPAGE Novex 4-12% Bis-Tris gels were used in the Xcell Sure Lock system according to the manufacturer's protocol.

2.3.13 *Determination of protein-bound nucleotide*

Nucleotide-determination was carried out according to [147]. Protein samples were diluted with SEC buffer to a final concentration of 50 µM in a volume of 20 µl and applied on a high pressure liquid chromatography (HPLC) system equipped with a reversed-phase ODS-2 hypersil column equilibrated with HPLC buffer. Runs were conducted at a flow rate of 1.5 ml/min. Denatured proteins were adsorbed at a nucleosil 100 C18 pre-column. Nucleotide peaks were detected by measuring E_{254}. The column was calibrated using standard nucleotide solutions at a concentration of 50 µM in SEC buffer.

2.3.14 *Isothermal titration calorimetry (ITC)*

ITC experiments were carried out at 8°C in a VP-ITC in ITC buffer at a protein concentration of 25 µM for GIMAP2 and GIMAP5 or 50 µM for GIMAP7 in the cell. Nucleotide concentrations in the syringe were 0.33 mM in the case of GIMAP2 and GIMAP5 or 1 mM in the case of GIMAP7. Binding isotherms were fitted and equilibrium dissociation constants were calculated using the Microcal ORIGIN software.

2.3.15 *Nucleotide hydrolysis assays*

Single turnover GTPase rates of the indicated GIMAP7 constructs were determined in GTPase buffer at 20°C in 20 mM HEPES pH 7.5, 150 mM NaCl, 2.5 mM DTT, 5 mM KCl, 5 mM $MgCl_2$ in the presence of 50 µM protein and 50 µM GTP using a standard HPLC-based method (see 2.3.13). For multiple turnover assays, a saturating GTP concentration of 500 µM was used with increasing concentrations of GIMAP7 in the same buffer. Rates derived from a linear fit to the initial reaction rates (<40% GTP hydrolyzed) were plotted against the protein concentrations. For determination of the apparent K_d and k_{max}, a simple binding model was fitted to the data which describes the interaction of two GTP-bound GIMAP7 molecules inducing GTP hydrolysis [148].

2.3.16 *Sedimentation equilibrium analytical ultracentrifugation (AUC)*

Molecular mass studies of all GIMAP constructs in 10 mM HEPES, pH 7.5, 150 mM NaCl, 2 mM $MgCl_2$, 2.5 mM DTT and the indicated nucleotide concentrations were performed in an XL-A type analytical ultracentrifuge (Beckman) equipped with UV absorbance optics. Sedimentation equilibrium experiments were carried out using six-channel cells with 12 mm optical path length and the capacity to handle three solvent-solution pairs of about 70 µl liquid. Sedimentation equilibrium was reached after 2 h of overspeed at 24000 rpm followed by an equilibrium speed of 20000 rpm for about 30 h at 10°C. The radial absorbance in each compartment was recorded at three different wavelengths between 270 and 290 nm depending on the concentration used in the experiments. Molecular mass determinations employed the global fit of the three radial distributions using the programs POLYMOLE or POLYMOLA [149]. When proteins adopt a monomer-dimer equilibrium, the molecular mass, M, can be treated approximately as a weight average parameter (M_w). This value is a composite of the monomer molecular mass (M_m) and that of the dimer (M_d) and the partial concentrations of monomers, c_m, and dimers, c_d.

$$M_w = \frac{c_m M_m + c_d M_d}{c_m + c_d} \tag{2.1}$$

Therefore, the equilibrium constant, K_d, can be derived with

$$K_d = \frac{c_m^2}{c_d} \tag{2.2}$$

2.4 CRYSTALLOGRAPHIC AND COMPUTATIONAL METHODS

2.4.1 *Protein crystallization*

Before crystallization, proteins were diluted to 15 mg/ml in the case of GIMAP2 or to 10 mg/ml for GIMAP7 with SEC buffer. Magnesium chloride and nucleotides in highest purity, if applicable, were added to a final concentration of 2 mM. We observed that GIMAP2, even in its original buffer, showed heavy precipitation after one day incubation at room temperature. Consequently, all further GIMAP2 crystallization experiments were conducted at 4°C. Since commercial screens did not yield any initial crystallization condition, a variety of precipitants were tested for their compatibility with crystal formation of GIMAP2. These crystallization attempts were performed in hanging drop vapor-diffusion 24 well setups. The reservoir contained 0.5 ml solution and crystallization drops were composed of 1 µl protein + 1 µl reservoir solution.

Single crystals of nucleotide-free $GIMAP2^{1\text{-}260}$ grew in conditions containing 11% - 19% 2-propanol. After further refinement, the final crystals used for data collection were grown in 11% - 12% 2-propanol and 15% glycerol. Crystals grew to a size of approximately 200 µm x 50 µm x 50 µm and could be directly cryo-cooled. SeMet- derivatized crystals were prepared in the same way.

GDP-loaded GIMAP2$^{21\text{-}260}$ crystallized in 19% 2-propanol. Crystals (approx. 100 µm x 10 µm x 10 µm) were prepared for cryo-cooling by a brief transfer in a solution containing 10 mM HEPES pH 7.5, 150 mM NaCl, 2.5 mM DTT, 2 mM magnesium chloride, 2 mM GDP, 19% 2-propanol and 20% glycerol.

GDP-loaded GIMAP2$^{1\text{-}234}$ crystallized in 12.5% 2-propanol and 30% glycerol and could be cryo-cooled without addition of further cryoprotectant.

Crystals of GTP-loaded GIMAP2$^{1\text{-}234}$ could be obtained by performing an additive screen. The final crystallization condition contained 6% 2-propanol and 10 mM ATP. Single needles (approx. 100 µm x 10 µm x 10 µm) were cryo-cooled after a short transfer to a solution containing 10 mM HEPES pH 7.5, 150 mM NaCl, 2.5 mM DTT, 2 mM magnesium chloride, 2 mM GTP, 6% 2-propanol, 10 mM ATP and 25% glycerol. Notably, GIMAPs contain a canonical G-domain including the guanine specificity motif G4 and are not known to bind ATP.

GDP-loaded GIMAP5$^{1\text{-}276}$ initially formed microcrystals in 11% 2-propanol. After testing 48 ions as additives (from the Hampton PEG/ion screen) at a final concentration of 50 mM, clusters of small plates could be grown in 16% 2-propanol and 50 mM ammonium citrate. A single plate (50 µm x 50 µm x 5 µm) could be broken off and frozen after transfer to a solution containing 10 mM HEPES pH 7.5, 150 mM NaCl, 2.5 mM DTT, 2 mM magnesium chloride, 2 mM GDP, 16% 2-propanol, 50 mM ammonium citrate and 20% glycerol.

For crystallization of GIMAP7, GMPPNP and MgCl2 were added to a final concentration of 2 mM. Crystallization trials were performed using the hanging-drop vapour-diffusion method at 20°C. 1 µl of the protein solution was mixed with an equal volume of reservoir solution, with a reservoir volume of 0.5 ml. Similar to the GIMAP2 approach, several precipitants were tested, and promising conditions were further refined by varying the buffer substance and the pH-value. The final crystallization condition contained 19% PEG 3350 and 100 mM MOPS pH 6.5. Tangly crystal plates with dimension of 200 µm x 200 µm x 10 µm appeared after one day. Single plates were separated, transferred to a cryo-solution containing 10 mM HEPES (pH 7.5), 300 mM NaCl, 2.5 mM DTT, 2 mM MgCl2, 2 mM GMPPNP, 32% PEG 3350, 100 mM MOPS pH 6.5. All crystals were cryo-cooled by plunging in liquid nitrogen.

2.4.2 *Data collection*

Datasets of single crystals were recorded using the rotation method with a ϕ increment of 1° at a temperature of -173°C. Beamline 14.2, BESSY II, Berlin, Germany, was used with a MAR165 CCD detector, except for the GIMAP2$^{1\text{-}234}$•GTP needle and the GIMAP5$^{1\text{-}276}$•GDP and GIMAP7 plate-like crystals, for which a dataset was recorded at the microfocus setup at BESSY II beamline 14.1, which is equipped with a Rayonics MX 225 CCD detector. Initial indexing and determination of an optimal data collection strategy was done using Mosflm [150]. A fluorescence scan of SeMet-derivatized nucleotide-free GIMAP2$^{1\text{-}260}$ crystals was conducted using a Bruker AXS/Roentec X-ray fluorescence detector. Recorded intensities were integrated and scaled with the program XDS [151].

2.4.3 *Protein structure solution*

A short overview over the theoretical aspects of X-ray diffraction can be found in Appendix B. Here, the methodological details are described.

Initially, trials to solve the structure of nucleotide-free GIMAP2$^{1\text{-}260}$ by molecular replacement using the distantly related GTPase Toc34 from pea (PDB 1h65) as template failed. Therefore, SeMet-derivatized protein was prepared and crystallized in the absence of nucleotide. Using an X-ray fluorescence scan, the peak energy was determined as 12655.69 eV with f′ and f″ values of 5.14 and 7.58, respectively. The data set collected at the peak energy showed anomalous signal up to high resolution. SeMet-substituted crystals were isomorphous to the native crystals but diffracted X-rays to higher resolution. Consequently, a low energy remote data set was collected from a second derivatized crystal up to a resolution of 1.5 Å. A single anomalous dispersion (SAD) protocol was applied to solve the phase problem as implemented in the program autoSHARP [152]. Seven out of seven selenium sites were found using SHELXD [153]. 218 out of 260 amino acid residues were automatically placed by phenix.autobuild [154].

Structures of all the other GIMAP2 crystals described in this study were solved by molecular replacement using the structure of nucleotide-free GIMAP2$^{1\text{-}260}$ as template. The GIMAP7•GMPPNP structure was solved using GIMAP2$^{1\text{-}234}$•GTP as search model. All molecular replacement trials were conducted using the program Molrep [155].

2.4.4 *Atomic model building and refinement*

Atomic models were built and fitted into electron density maps using the program Coot [156]. GIMAP2 and GIMAP5 structures were refined using the program Refmac5 [157] via the CCP4 graphical interface [158]. Standard positional refinement has been applied , preceded by TLS (Translational, libration, screw rotation displacement) refinement [159]. 5% of the measured X-ray intensities were set aside from the refinement for cross-validation [160]. The GIMAP7 structure was refined using the program Phenix [154], where additionally non-crystallographic symmetry restraints were included.

2.4.5 *Protein structure validation and deposition*

All-atom contacts and geometry of the atomic models were evaluated using the Molprobity server [161]. Validated models were deposited in the Protein Data Bank (http://www.pdb.org), with the following accession numbers: nucleotide-free GIMAP2$^{1\text{-}260}$: 2xtp, GIMAP2$^{21\text{-}260}$•GDP: 2xto, GIMAP2$^{1\text{-}234}$•GDP: 2xtm and GIMAP2$^{1\text{-}234}$•GTP: 2xtn. The models of GIMAP5$^{1\text{-}276}$•GDP and GIMAP7•GMPPNP will be deposited when the manuscripts, which are currently in preparation, will be accepted.

2.5 CELL BIOLOGICAL METHODS

The cell biological work was done in cooperation with the group of Stephan Mathas, AG Dörken, MDC Berlin. Microscopy was performed in cooperation with the group of Burkhard Wiesner, FMP Berlin.

2.5.1 *Cell culture*

HeLa cells were cultivated in MEM supplemented with 10% fetal calf serum, 2 mM L-glutamine, 100 U/ml penicillin and 0.1 mg/ml streptomycin. Jurkat cells were cultivated in RPMI medium (Invitrogen) supplemented with 10% fetal calf serum, 2 mM L-glutamine, 100 U/ml penicillin and 0.1 mg/ml streptomycin. 37°C and 5% CO_2 were maintained in the incubator.

2.5.2 *Transfection of HeLa cells*

HeLa cells were grown on cover slips in 6-well plates and transfected at <70% confluency using the Roti-Fect reagent according to the manufacturer's protocol. 0.5 µg DNA was applied for each tranfection.

2.5.3 *Electroporation of Jurkat cells*

$5x10^6$ cells were washed with PBS, centrifuged at 1200 rpm for 5 min and resuspended in 0.5 ml OPTIMEM medium. Cells were transferred in a cuvette (see Table 13) and electroporated with 30 µg of the respective plasmid DNA using a Gene Pulser. An exponential electroporation protocol was chosen at 300 V and 500 µF. The cells were further incubated for 10 min at 37°C in the incubator. Afterwards, cells were diluted in 10 ml prewarmed medium.

2.5.4 *Microscopy*

48 hours after electroporation, cells were washed with PBS and, if applicable, stained with BODIPY 493/503 according to [162]. Hela cells grown on cover slips were mounted on a ZEISS LSM 510 microscope, covered with medium and inspected. Jurkat cells were resuspended in 25 µl RPMI medium, mounted on the microscope in between two cover slips and inspected. Excitation wavelengths and emission filters, respectively, were for BODIPY or EGFP 488 nm, BP505-530 and for mCherry 543 nm, LP560.

2.6 GTPASE HIGHER-ORDER RELATIONSHIP ANALYSIS

The GTPase higher-order relationship analysis was performed by L. Aravind, National Center for Biotechnology Information, National Library of Medicine, National Institutes of Health, Bethesda, MD 20849, USA.

Structure similarity searches were performed using the DALIlite program [163]. Pairwise structure alignments were built using both DALIlite and the MUSTANG

program [164]. The comparisons of sequence alignment-profiles of the different GTPase groups was performed using the HHpred program [165] after deriving hidden Markov models from each alignment with the HMMer3 package (http://hmmer.janelia.org/).

2.7 RNA PREPARATION AND RT-PCR ANALYSIS

RNA preparation and RT-PCR analysis was performed by Karl Köchert, AG Stephan Mathas, MDC Berlin.

Total RNA was prepared using the RNeasy kit (Qiagen). For reverse transcriptase-polymerase chain reaction (RT-PCR) analyses, first strand cDNA-synthesis was performed by use of the first-strand cDNA synthesis Kit (Roche, Germany) adding oligo-p(dT)15 primer according to the manufacturer's recommendation. Primers used for RT-PCR analyses were as follows: GAPDH sense 5' - ATGCTGGCGCTGAGTAC - 3', GAPDH antisense 5' - TGAGTCCTTCCACGATAC - 3'; GIMAP1 sense 5'- GGCTTCTTGTGGCCAACTT - 3', GIMAP1 antisense 5' - TCCTTCCTGGTGAAGACGAT - 3'; GIMAP2 sense: 5' - AGGAACACCAATGGACCAAA - 3', GIMAP2 antisense 5' - GAGCCACCATTGAGGTCTTC - 3'; GIMAP4 sense 5'- TTTCTCAACATCCTGGCTTAG - 3', GIMAP4 antisense 5' - GTGGCTTTGTGCTCTTCCTC - 3'; GIMAP5 sense 5' - ATCAGTTTCCAGCCAACACC - 3', GIMAP5 antisense 5' - TCAGCTTGGACTCAAACACG - 3'; GIMAP6 sense 5' - GCCTTGTCCTCCTTGTGTTC - 3', GIMAP6 antisense 5' - ACCACCTGCTGATCCTCATC - 3'; GIMAP7 sense 5' - CAAAAGCAACAGCTCAAGCA - 3', GIMAP7 antisense 5' - TGTGCTTCATGGCTGACTTC - 3'; GIMAP8 sense 5' - GAATGATGAGGCAGTGCTGA - 3', GIMAP8 antisense 5' - ATCCAGCATCTGGTTGAAGG - 3'. All PCR products were verified by sequencing.

3 RESULTS

3.1 BIOCHEMICAL CHARACTERIZATION OF GIMAPS

3.1.1 *Screening for soluble protein*

CONSTRUCT	CLONED	OVER-EXPRESSION	SOLUBLE
hsGIMAP1	+	+	-
hsGIMAP1 1-275	+	+	-
hsGIMAP2	+	-	-
hsGIMAP2 1-260	+	+	+
hsGIMAP4	+	-	-
hsGIMAP5	+	+	-
hsGIMAP5 1-276	+	+	+
hsGIMAP6	-	-	-
hsGIMAP7	+	+	+
hsGIMAP8	+	+	-

Table 2: Summary of recombinant protein over-expression and solubility. The amino acid residue range of truncated constructs is indicated.

To make biochemical and structural characterization of GIMAPs possible, the genes were PCR-amplified from cDNA (Table 18) and cloned via standard restriction enzyme cloning methods in the bacterial expression vector pGex6P1 (see 2.2). For family members containing predicted transmembrane segments, truncated versions were prepared lacking the hydrophobic C-terminal patches to increase solubility. GIMAP6 yielded no PCR product, even using an alternative template or different sets of primers. Resulting sequence-verified clones were transformed in the *E. coli* Rosetta DE(3) strain, allowing for IPTG-inducible expression of N-terminal GST-fusion proteins with a PreScission protease cleavage site in the linker region between GST and the protein of interest. Protein over-expression and solubility was checked in small scale as described in 2.3.2 and 2.3.3. GIMAP4 was not over-expressed upon IPTG induction. Full length GIMAP1, GIMAP2, GIMAP5 and GIMAP8 were not found in the soluble fraction of *E. coli* lysates, most probably due to nonspecific aggregation and subsequent sedimentation in the ultracentrifugation step. However, constructs corresponding to the cytoplasmic portions of GIMAP2 (amino acid residues 1-260, GIMAP2$^{1\text{-}260}$) and GIMAP5$^{1\text{-}276}$ were soluble and could be enriched using small-scale GSH-sepharose affinity chromatography. Furthermore, full length soluble GIMAP7 could be produced. The results are summarized in Table 2.

3.1.2 *Protein purification*

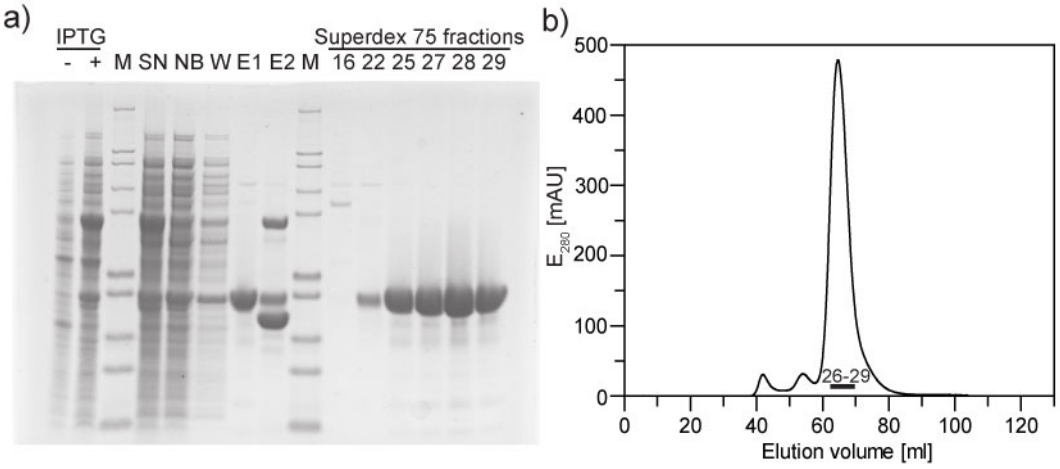

Figure 16: Typical GIMAP2 purification procedure. **a** 4-12% SDS PAGE of various samples taken during the purification. -/+ IPTG, whole-cell bacteria lysates before and after induction; M, molecular weight marker, bands correspond to 200 kDa, 116 kDa, 97 kDa, 66 kDa, 55 kDa, 36.5 kDa, 31 kDa, 21.5 kDa, 14 kDa, 6 kDa (from top to bottom); SN, supernatant of bacterial lysates after ultracentrifugation; NB, non-bound material after GSH-sepharose column; W, wash fraction of the same column; E1, eluate after protease cleavage containing the GIMAP construct; E2, GSH elution showing GST, the GST-tagged protease and some remaining GIMAP2 which bound unspecifically to the column. 16-29, fractions collected during size exclusion chromatography. **b** Superdex75 size-exclusion chromatogram. Fractions pooled and concentrated for further experiments are indicated.

Constructs which were found to be soluble in the pilot experiment described above were produced on larger scale for biochemical and structural studies. Proteins were purified in two steps using GSH-sepharose affinity chromatography, followed by size-exclusion chromatography (see 2.3.4 - 2.3.11). A typical purification procedure for C-terminally truncated GIMAP2$^{1\text{-}260}$ is shown in Figure 16 and for GIMAP7 in Figure 17. GIMAP5$^{1\text{-}276}$ was purified in the same way and behaved identically as GIMAP2$^{1\text{-}260}$. All three proteins could be purified almost to homogeneity.

3.1.3 *Nucleotide binding*

Homogenous nucleotide-loading of the protein sample is a prerequisite for all subsequent biochemical and structural experiments. Therefore, the nucleotide-loading state of the purified proteins was determined by HPLC measurements (see 2.3.13). Purified GIMAP2$^{1\text{-}260}$ appeared to be partially GTP-bound (Figure 18, blue trace), and the same was true for GIMAP5$^{1\text{-}276}$. An additional washing step with EDTA was applied to the column-immobilized proteins during purification in order to remove Mg ions and nucleotide (Figure 18, green trace). In contrast, purified GIMAP7 was nucleotide-free. These data suggest that the G domains of

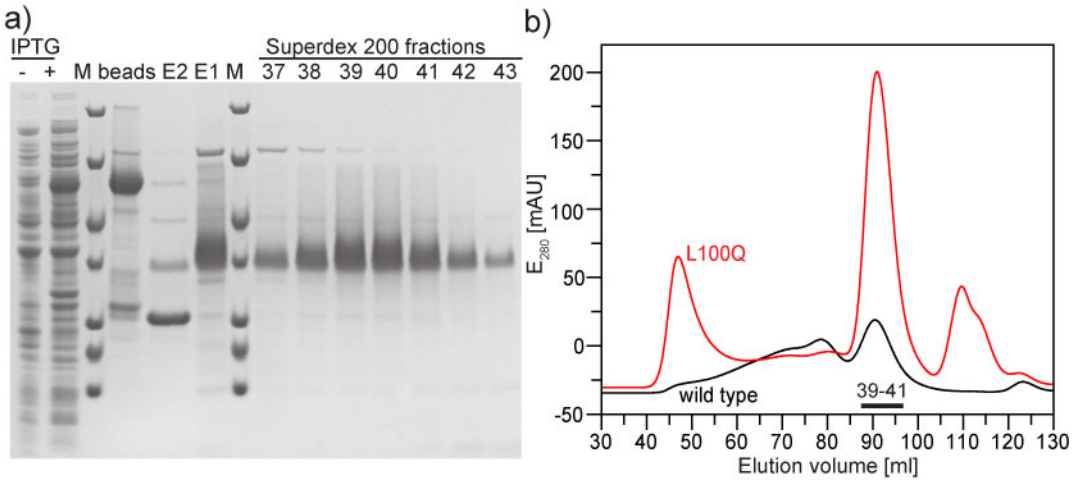

Figure 17: Typical GIMAP7 purification procedure. **a** 4-12% SDS PAGE of various samples taken during the purification. -/+ IPTG, whole-cell bacteria lysates before and after IPTG induction; M, molecular weight marker, bands correspond to 116 kDa, 66 kDa, 45 kDa, 35 kDa, 25 kDa, 18 kDa, 14 kDa (from top to bottom); beads, sample of the GSH-Sepharose beads after sample application and wash; E2, elution of GST and PreScission-protease; E1 - elution of cleaved GIMAP7; 37-43, fractions collected during size exclusion chromatography. **b** Superdex 200 size-exclusion chromatogram for GIMAP7 (black trace) and for the GIMAP7 L100Q variant (red trace, see also 3.1.3). Fractions pooled and concentrated for further experiments are indicated.

GIMAP2 and GIMAP5 have higher affinity towards GTP than GIMAP7, and that they are not able to hydrolyze GTP.

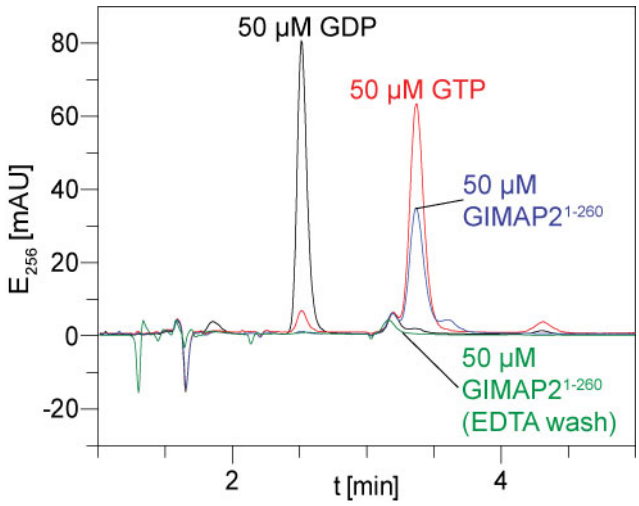

Figure 18: Copurification of GIMAP2$^{1\text{-}260}$ and GTP. 50 µM GIMAP2$^{1\text{-}260}$ (blue trace) was applied to HPLC analysis. A peak corresponding to the GTP standard was evident. An additional washing step of GIMAP2 on the GSH beads with a buffer containing 10 mM EDTA induced nucleotide release (green trace). Nucleotide standards are shown for comparison (50 µM GDP - black, 50 µM GTP - red).

In order to quantify the affinity of the purified proteins towards GDP and GTP, ITC experiments were performed (see 2.3.14). GIMAP2$^{1\text{-}260}$ bound GTP with

an equilibrium dissociation constant (K_d) of 40 nM and GDP with a K_d of 630 nM (Figure 19 **a**). Similar results were obtained for GIMAP5$^{1-276}$ binding to GTP, whereas GDP was bound with a slightly higher affinity of 170 nM (Figure 19 **b**).

For GIMAP7, protein yields were too low for ITC experiments to proceed (only 1 mg protein out of 20 l bacteria culture). To improve the solubility of this construct, we created a homology model of the G domain of GIMAP7, based on the GIMAP2 structure (see 3.2), and identified surface-exposed hydrophobic residues which might reduce the solubility. A surface-exposed leucine in the dimerization interface of the G domain was discovered (Leu100) which is replaced by a polar residue in most other GIMAPs (see also the multiple sequence alignment in Appendix C). In line with our expectations, the exchange of Leu100 to glutamine resulted in a significant increase in the protein yield (Figure 17). Elution volume in size exclusion chromatography was the same as for the wild type protein, as well as the kinetics of GTP hydrolysis (Figure 20). Therefore, ITC experiments and crystallization trials (see 3.4.1) were conducted using the GIMAP7 variant L100Q.

GIMAP7 L100Q bound with 250-fold lower affinity than GIMAP2 to a non-hydrolyzable GTP analogue, (GTP-γ-S; K_d=10 µM), and with an even lower affinity to GDP (K_d=32 µM) (Figure 19 **c**).

Taken together, the cytoplasmic portions of GIMAP2 and GIMAP5 bind nucleotides with high affinity in the nanomolar range, where the affinity for GTP is one order of magnitude higher than for GDP. GIMAP7 binds nucleotides generally with lower affinity in the micromolar range, where the affinity for GTP-γ-S is threefold higher than for GDP.

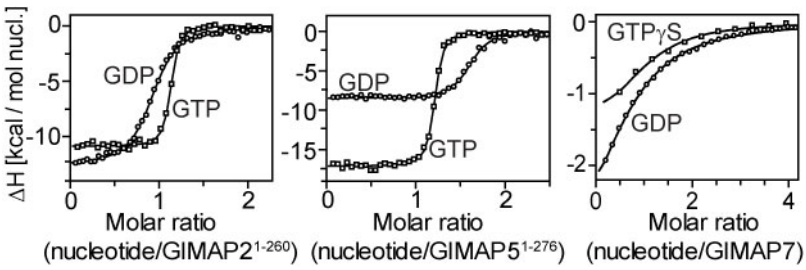

Figure 19: Nucleotide binding affinities of GIMAP2$^{1-260}$ (**a**), GIMAP5$^{1-276}$ (**b**) and GIMAP7 L100Q (**c**) as determined by ITC. Following values were obtained from the fittings: GIMAP2$^{1-260}$ GTP (□) - K_d=40 ± 7 nM (n=1.1), GIMAP2$^{1-260}$ GDP (○) - K_d=630 ± 40 nM (n=0.9). GIMAP5$^{1-276}$ GTP (□) - K_d=43 ± 5 nM (n=1.1), GIMAP5$^{1-276}$ GDP (○) - K_d=174 ± 20 nM (n=1.5). GIMAP7 L100Q GTP-γ-S (□) - K_d=10 ± 2 µM (n=0.9), GIMAP7 L100Q GDP(○) - K_d=32 ± 2 µM (n=0.8).

3.1.4 *GTP hydrolysis*

To check if the purified proteins show catalytic activity, single turnover assays monitoring one cycle of GTP hydrolysis were conducted (see 2.3.15). No GTPase activity was detected for the cytoplasmic domains GIMAP2 and GIMAP5, even at high protein concentration (50 µM) and long (24 h) incubations (Figure 20 **a**). However, GIMAP7 efficiently hydrolyzed GTP in this assay (Figure 20 **a**). In multiple-turnover assays (excess of GTP over protein), GIMAP7 showed a protein concentration dependent GTPase reaction with a k_{max} of 3.2 min^{-1} and an apparent

K_d of 1.2 µM indicating that the GTPase function is stimulated by association of GIMAP7 monomers in solution (Figure 20 **b**). Altogether, these results prove that at least the cytoplasmic domains of GIMAP2 and GIMAP5 are catalytically silent, whereas GIMAP7 is a GTPase.

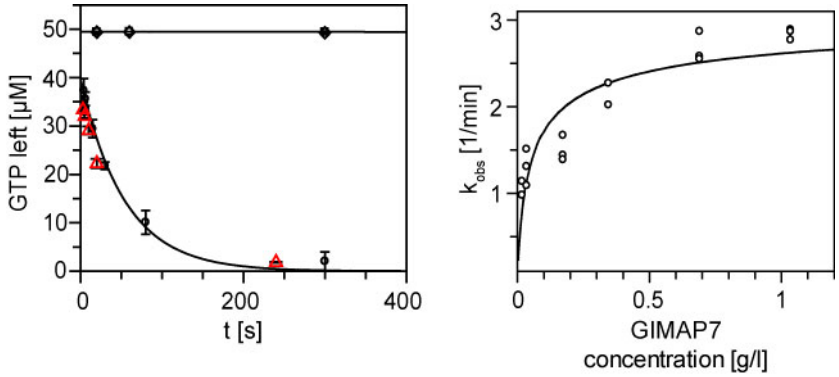

Figure 20: **a** Single turnover GTP hydrolysis of GIMAP2$^{1\text{-}260}$ (□), GIMAP5$^{1\text{-}276}$ (◊), GIMAP7 (○) and GIMAP7 L100Q (△) was measured by HPLC, using a nucleotide and protein concentration of 50 µM. Data points represent mean value ± standard deviation of three independent experiments. An exponential decay was fitted to the GIMAP7 data. **b** Initial observed rates of multiple turnover GTP hydrolysis reactions at 500 µM GTP (○) were determined for GIMAP7 at the indicated protein concentrations (at least 2 independent experiments). Data were fitted to a monomer-dimer equilibrium [148]. A k_{max} value of 3.2 ± 0.2 min^{-1} and a K_d value of 1.2 ± 0.4 µM was obtained from the fittings.

3.1.5 *Oligomeric state of the proteins*

To determine the self-assembly status of purified proteins in solution dependent on the nucleotide-loading state, GIMAP2$^{1\text{-}260}$ and GIMAP7 were subjected to sedimentation equilibrium analytical ultracentrifugation analysis. With this method, the apparent molecular weight of protein assemblies can be determined at different protein concentrations (see 2.3.16). In the presence of GDP, the cytoplasmic portion of GIMAP2 was shown to be monomeric even at high protein concentrations (Figure 21 **a**). Upon addition of GTP, the protein formed low-affinity dimers with a K_d of 260 µM (Figure 21 **a**). GIMAP7 showed dimerization already in the GDP-bound state with a K_d of 100 µM (Figure 21 **b**). Addition of the non-hydrolyzable GTP analog GMP-PNP lead to a tenfold decrease of the K_d value (Figure 21 **b**). Taken together, these results show a GTP-stimulated dimerization in both GIMAP2 and GIMAP7, albeit with different affinities.

3.2 STRUCTURES OF GIMAP2

3.2.1 *Structure determination of nucleotide-free GIMAP2*

To obtain insights into the atomic structure of GIMAP2, purified GIMAP2$^{1\text{-}260}$ was crystallized using 2-propanol as precipitant (see 2.4.1). Crystals appeared after 1 hour at 4°C and grew to their final size over night (Figure 22). X-ray data were

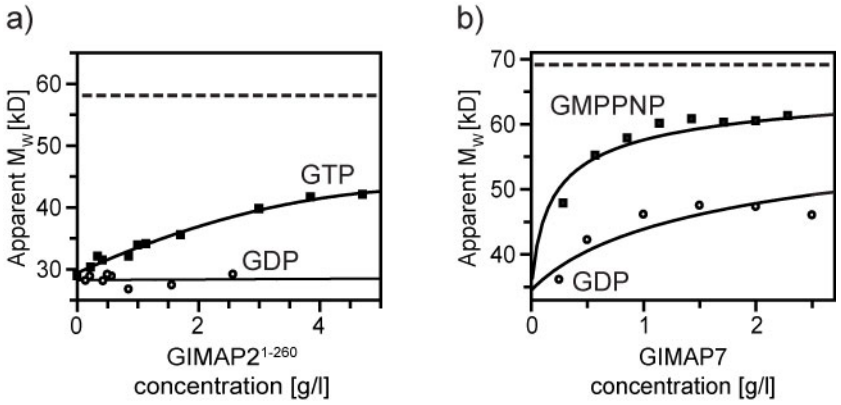

Figure 21: Oligomeric state of GIMAP2 and GIMAP7 in solution, dependent on the nucleotide-loading state. Equilibrium sedimentation analytical ultracentrifugation experiments were performed for $GIMAP2^{1-260}$ (**a**) and GIMAP7 (**b**) to determine apparent molecular weights at the indicated protein concentrations. For GIMAP2, 100 µM GTP (■) or 100 µM GDP (○) were present, whereas 200 µM GMPPNP (■) or 500 µM GDP (○) were used for GIMAP7 to saturate the protein. Monomer-dimer equilibria were fitted to GIMAP2 in the presence of GTP (K_d=250 ± 20 µM), and to GIMAP7 in the presence of GDP (K_d=110 ± 20 µM) and GMP-PNP (K_d=9 ± 1 µM). The dashed line indicates the molecular weight of the corresponding GIMAP dimers.

collected as described in 2.4.2. The selenomethionine-substituted crystals diffracted X-rays to a maximum resolution of 1.5 Å and belong to the orthorhombic space group $P2_12_12_1$ with cell dimensions a=57.4 Å, b=60.8 Å, c=72.0 Å, $\alpha=\beta=\gamma=90°$. Data collection statistics for the peak dataset and the low-energy remote dataset (see also 2.4.3) are given in Table 3.

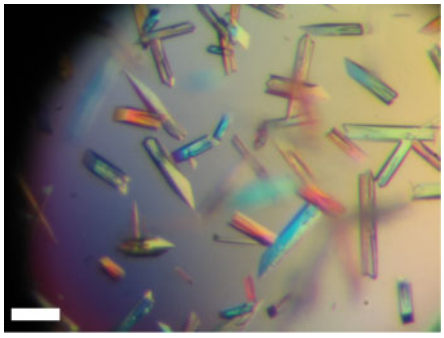

Figure 22: Crystals of selenomethionine-substituted $GIMAP2^{1-260}$. The white bar corresponds to 100 µm.

DATA COLLECTION	GIMAP2$^{1\text{-}260}$ PEAK	REMOTE
Beamline	BESSY 14.2	BESSY 14.2
Wavelength [Å]	0.9797	0.9849
Space group	$P2_12_12_1$	$P2_12_12_1$
Cell dimensions		
a [Å]	57.4	57.4
b [Å]	60.8	60.8
c [Å]	72.0	72.0
$\alpha=\beta=\gamma$	90	90
V_M[†]	2.15	2.15
Resolution [Å]	50 (1.80)[‡] - 1.75	50 (1.59) - 1.50
No. of observed reflections	183804 (11439)	179638 (28189)
No. of unique reflections	48628 (3489)	40986 (6487)
R_{meas} [%][§]	6.8 (50.0)	7.8 (59.7)
$I/\sigma(I)$	14.6 (3.2)	14.7 (3.6)
Completeness [%]	99.1 (95.9)	99.7 (99.1)
Overall B-factor (Wilson) [Å^2]	26.9	22.3
Anomalous phasing power	1.8	
Figure of merit (acentr./centr.)	0.435/0.133	

Table 3: Data collection statistics for crystals of selenomethionine-substituted GIMAP2$^{1\text{-}260}$.

[†] According to [166].
[‡] Numbers in parentheses apply for the highest resolution shell.
[§] According to [167].

Initial phases for nucleotide-free GIMAP2$^{1\text{-}260}$ were calculated using the peak data set and a preliminary atomic model was built (see 2.4.3). The model was manually completed and refined against the low energy remote high resolution data as described in 2.4.4. The final model includes amino acids 21-222 and 236-254 of GIMAP2. The model was validated and deposited in the Protein Data Bank (see 2.4.5). 99% of all residues are in the favored regions of the Ramachandran plot. Refinement statistics are given in Table 4.

REFINEMENT	GIMAP2$^{1\text{-}260}$
Resolution [Å]	50 - 1.5
No. of reflections used	38935
R_{work} † / R_{free} ‡	18.3/20.5
No. of atoms	
Protein	1764
Water	169
Average B-factors [Å^2]	
Protein	16.1
Water	24.3
R.m.s. deviation	
Bond lengths [Å]	0.010
Bond angles [°]	1.170

Table 4: Refinement statistics for GIMAP2$^{1\text{-}260}$.
† $R_{work} = \frac{\sum_{h,k,l}||F_{obs}(h,k,l)|-|F_{calc}(h,k,l)||}{\sum_{h,k,l}|F_{obs}(h,k,l)|}$.
‡ R_{free} was calculated with 5% of the data excluded from the refinement.

3.2.2 *Structure analysis of nucleotide-free GIMAP2*

The N-terminal 20 residues of GIMAP2 are disordered and not included in the model. Ser21 is right at the beginning of the first strand of a typical G domain fold containing a central β-sheet sandwiched by two layers of α-helices (Figure 23 **a, b**), see also Figure 2). A search of the PDB database with the GIMAP2 G domain using the DALIlite program [163] recovers the chloroplast-membrane-associated Toc GTPases (e.g. PDB 2je3 and 1h65) as closest GIMAP relatives, and the structures can be superimposed with a root mean square deviation (r.m.s.d.) of 2.8 Å over 186 aligned C_α positions at a sequence identity of 17-18%. Within the core G domain, GIMAP2 displays an additional helix α3* between strand β5 and helix α4 (Figure 23 **b**). Beyond the G domain, the GIMAP2 structure shows a distinct C-terminal extension of two helices α6 and α7 (Figure 23 **b**). The amphipatic helix α7 is connected to α6 and the G domain by a disordered linker of 16 residues and directly contacts the switch II region of the G domain (Figure 23 **b**).

3.2.3 *Structure determination of GDP-bound GIMAP2*

To gain insights into the nucleotide binding mode, it was attempted to crystallize GIMAP2$^{1\text{-}260}$ in the GDP-bound form. Despite extensive screening efforts, it was not possible to obtain crystals of this construct in the presence of Mg and GDP. However, a construct lacking the disordered N-terminus, GIMAP2$^{21\text{-}260}$ (Figure 25 **a**), crystallized in the GDP-bound form using 2-propanol as precipitant

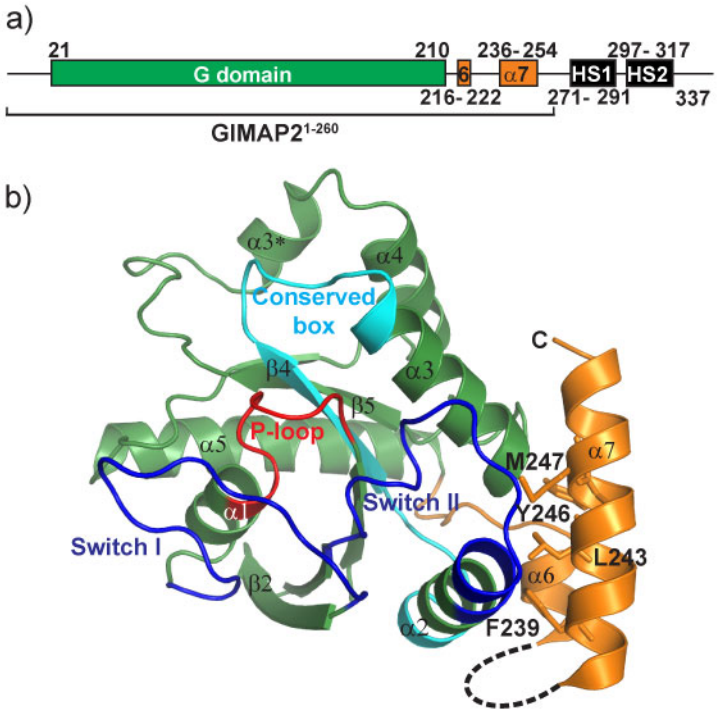

Figure 23: Cartoon representation of the GIMAP2$^{1\text{-}260}$ structure as determined by X-ray crystallography. **a** Schematic representation of the domain structure of GIMAP2, with the amino acid positions indicated. The C-terminal extension is shown in orange and the two hydrophobic segments (HS1, HS2) in black. The crystallized construct is indicated below. **b** Cartoon representation of the nucleotide-free structure of GIMAP2$^{1\text{-}260}$. The G domain is shown in green, the two switch regions in blue, the P-loop in red and the conserved box in cyan. The C-terminal helices α6 and α7 are shown in orange, with the hydrophobic residues indicated as sticks. The disordered loop connecting helices α6 and α7 is indicated by a dashed line.

(2.4.1). The crystals mainly formed clusters of small needles, but single needles could be broken off and were used for data collection (Figure 24).

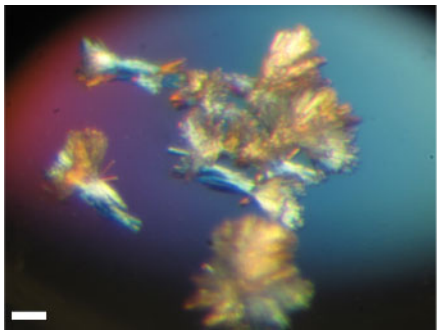

Figure 24: Crystals of GDP-bound GIMAP2$^{21\text{-}260}$. The white bar corresponds to 100 µm

DATA COLLECTION	GIMAP2$^{21\text{-}260}$•GDP NATIVE
Beamline	BESSY 14.2
Wavelength [Å]	0.9184
Space group	$P2_12_12_1$
Cell dimensions	
a [Å]	62.7
b [Å]	76.5
c [Å]	101.6
$\alpha=\beta=\gamma$	90
V_M[†]	2.26
Resolution [Å]	50 (3.07)[‡] - 2.89
No. of observed reflections	45534 (6795)
No. of unique reflections	11194 (1690)
R_{meas} [%][§]	22.0 (62.3)
I/σ(I)	8.5 (3.5)
Completeness [%]	98.2 (95.8)
Overall B-factor (Wilson) [Å^2]	35.0

Table 5: Data collection statistics for crystals of GDP-bound GIMAP2$^{21\text{-}260}$.

[†] According to [166].
[‡] Numbers in parentheses apply for the highest resolution shell.
[§] According to [167].

Crystals diffracted X-rays to a maximal resolution of 2.9 Å and belong to space group $P2_12_12_1$ with cell dimensions a=62.7 Å, b=76.5 Å, c=101.6 Å, $\alpha=\beta=\gamma=90°$. Data were collected from a single needle and the structure was solved by molecular replacement (see 2.4.3, Table 5). The atomic model was completed and refined as described in 2.4.4 (Table 6). The model was validated and deposited in the Protein Data Bank (see 2.4.5). It contains two protein molecules in the asymmetric unit encompassing residues 21-223, 235-255 of chain A and residues 21-223, 235-254 of chain B, with 98% of the residues in the favored region of the Ramachandran plot.

REFINEMENT	GIMAP2$^{21\text{-}260}$•GDP
Resolution [Å]	12 - 2.9
No. of reflections used	11467
R_{work} † / R_{free} ‡	22.9/27.6
No. of atoms	
Protein	3477
Ligand/ion	58
Average B-factors [Å^2]	
Protein	30.8
Ligand/ion	14.0
R.m.s. deviation	
Bond lengths [Å]	0.006
Bond angles [°]	0.980

Table 6: Refinement statistics for GDP-bound GIMAP2$^{21\text{-}260}$

† $R_{work} = \frac{\sum_{h,k,l}||F_{obs}(h,k,l)|-|F_{calc}(h,k,l)||}{\sum_{h,k,l}|F_{obs}(h,k,l)|}$.

‡ R_{free} was calculated with 5% of the data excluded from the refinement.

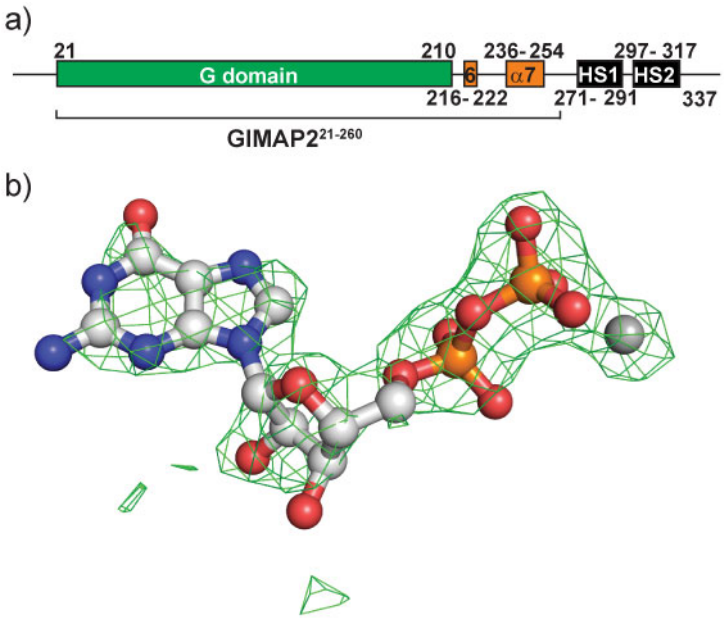

Figure 25: Electron density of GDP bound to GIMAP2$^{21\text{-}260}$. **a** Schematic representation of the domain structure of GIMAP2, with the amino acid positions indicated. The C-terminal extension is shown in orange and the two hydrophobic segments (HS1, HS2) in black. The crystallized GDP-bound construct is indicated below. **b** F_o-F_c electron density was calculated for GIMAP2$^{21\text{-}260}$•GDP without incorporation of the nucleotide in the atomic model. The density is colored in green and contoured at 3 σ with the refined nucleotide model shown as ball-and-sticks and the magnesium ion as grey sphere.

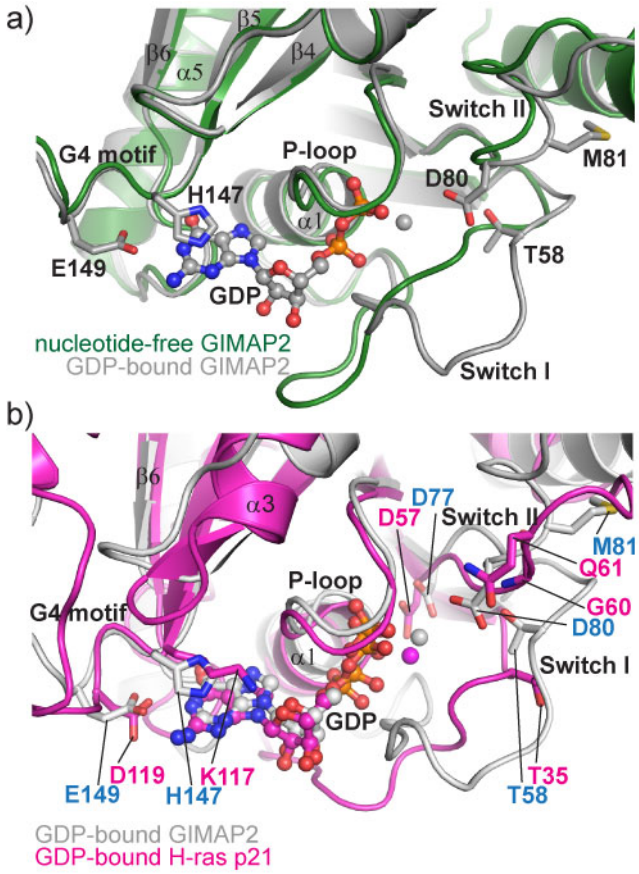

Figure 26: Detailed view of the GDP binding mode of GIMAP2. **a** Details of GDP-binding in the structure of GIMAP2$^{21\text{-}260}$•GDP (shown in grey). Selected residues in the nucleotide binding motifs are shown as sticks. The magnesium ion is shown as gray sphere. Significant structural changes compared to the nucleotide-free structure (green) were observed in switch I. **b** A superposition of GIMAP2$^{21\text{-}260}$•GDP (grey) and H-ras p21•GDP (magenta, PDB 4q21). Elements involved in nucleotide binding are shown in stick representation.

3.2.4 *Insights in the GDP binding mode and comparison to nucleotide-free GIMAP2*

Clear electron density was visible for the GDP molecule in the nucleotide-binding pocket (Figure 25 **b**). The overall structure of GDP-bound GIMAP2$^{21\text{-}260}$ is very similar to the nucleotide-free form, except for significant structural changes observed in the switch I region (Figure 26 **a**). The guanine nucleotide binding motifs G1 - G5 of GIMAP2 show sequence differences compared to the canonical TRAFAC GTPases, but function in a similar manner in nucleotide binding (Figure 26 **b**, see also Figure 3). Interestingly, the side chain of Asp80 in the G3 motif of GIMAP2 points towards the β-phosphate of the nucleotide, whereas Gly60 at the equivalent position in H-ras acts as a sensor for the γ-phosphate, just as in most other TRAFAC class GTPases, including the closely related Tocs and the more distantly related Ras [168]. A glutamine or histidine residue positions the catalytic water molecule in Ras-like small GTPases (Glu60 in H-ras p21), EF1/EF-TU, EF2/EF-G, eIF2, IF2 and SelB (see also 1.1.1). However, in GIMAP2 it is replaced by a hydrophobic residue (Met81), just as in many members of the Toc, septin, dynamin-like, Era

and Eng GTPases. Both GIMAP2 and the Toc GTPase contain a histidine in the second position of the G4 motif, in place of the usual lysine, that recognizes the guanine via a pi-pi stacking interaction between the histidine and guanine rings (Figure 26 **a**).

3.2.5 *Structure determination of GTP-bound GIMAP2*

To characterize the differences between the GDP- and GTP-conformation of GIMAP2, it was attempted to crystallize both GIMAP2$^{1\text{-}260}$ and GIMAP2$^{21\text{-}260}$ in the presence of GTP and non-hydrolyzable GTP-analogs (GMP-PNP, GTP-γ-S). However, neither of these attempts was successful despite numerous screening efforts. Upon closer analysis of the nucleotide-free and GDP-bound GIMAP2 structures, it was noticed that the C-terminal helix α7 had higher temperature (B-) factors compared to the core G domain (Figure 27 **a**), suggesting increased flexibility in this helix, which could hinder crystallization specifically in the GTP-bound state. Therefore, a construct was prepared lacking this helix (GIMAP2$^{1\text{-}234}$, Figure 27 **b**).

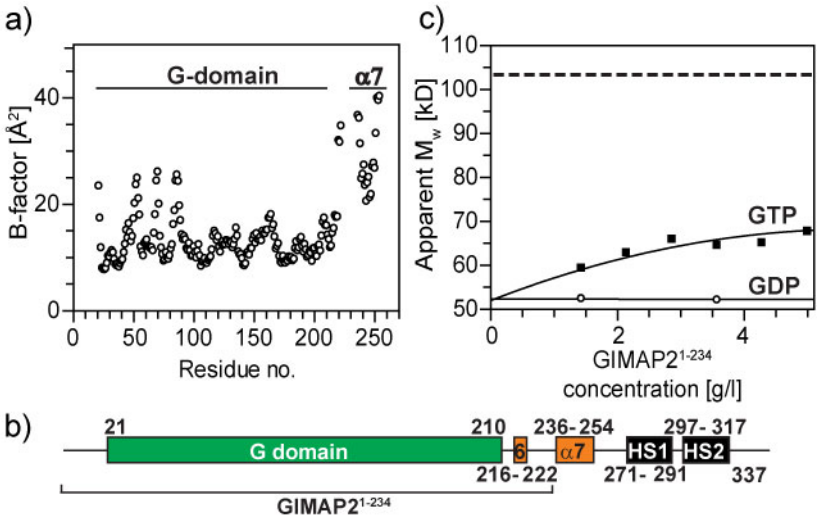

Figure 27: Role of GIMAP2 helix α7 in dimerization. **a** Flexibility of the C-terminal amphipathic helix in GIMAP2. Atomic displacement factors (B-factors) of nucleotide-free GIMAP2$^{1\text{-}260}$ are plotted along the amino acid sequence. The C-terminal amphipathic helices α6 and α7 have higher B-factors than the core G domain suggesting increased flexibility in this region. **b** Schematic representation of the domain structure of GIMAP2, with the amino acid positions indicated. The C-terminal extension is shown in orange and the two hydrophobic segments (HS1, HS2) in black. The dimeric GIMAP2 construct is indicated below. **c** Sedimentation equilibrium ultracentrifugation for GIMAP2$^{1\text{-}234}$ (lacking helix α7), in the presence of 100 µM GDP (○) or GTP (■). In the presence of GTP, a dimer-tetramer equilibrium with a Kd of 310 ± 20 µM was fitted to the data. The dashed line indicates the molecular mass of the GIMAP2 tetramer.

Surprisingly, this construct eluted earlier in the size-exclusion chromatography purification step (see 2.3.8, see also Figure 40 **b**), suggesting a higher hydrodynamic volume of GIMAP2$^{1\text{-}234}$ in solution. Indeed, it was shown by analytical ultracentrifugation (see 2.3.16) that the purified protein forms stable dimers in solution

(Figure 27 **c**). Furthermore, GTP-dependent tetramerization of the construct was observed, with a similar low affinity as GTP-dependent GIMAP2$^{1\text{-}260}$ dimerization (Figure 27 **c**, see also Figure 21 **a**). This already suggests that removal of helix $\alpha 7$ induces stable, nucleotide-independent dimerization in GIMAP2. Additionally, the protein can tetramerize in a GTP-dependent manner via a different molecular interface.

GIMAP2$^{1\text{-}234}$ crystallized in the presence of GTP (Figure 28 **a**) and GDP (Figure 28 **b**, see 2.4.1) using 2-propanol as precipitant. Crystals of the GTP-form diffracted X-rays to a maximal resolution of 1.9 Å and belong to space group $C222_1$ with cell dimensions a=58.0 Å, b=69.2 Å, c=116.6 Å, $\alpha=\beta=\gamma=90°$. Crystals of the GDP-form diffracted X-rays to a maximal resolution of 1.7 Å and belong to space group $P2_12_12_1$ with cell dimensions a=42.9 Å, b=61.8 Å, c=185.3 Å, $\alpha=\beta=\gamma=90°$. Data were collected from single crystals with the data collection statistics shown in Table 7 (see 2.4.2).

The structures of GTP- and GDP-bound GIMAP2$^{1\text{-}234}$ were solved by molecular replacement (see 2.4.3). The models were completed and refined as described in 2.4.4 (Table 8). Final models were validated and deposited in the Protein Data Bank (see 2.4.5). The final model of GIMAP2$^{1\text{-}234}$•GTP contains one protein molecule in the asymmetric unit encompassing residues 21-151, 154-230, and 99% of all residues are in the favored region of the Ramachandran plot. For GIMAP2$^{1\text{-}234}$•GDP, the model contains two protein molecules in the asymmetric unit, with residues 21-227 of chain A and residues 21-50, 58-226 of chain B and 98% of the residues in the favored region of the Ramachandran plot. Clear electron density for the nucleotides was present in both structures (Figure 29) including the γ-phosphate in the GTP-bound structure, indicating that no GTP hydrolysis had occurred in the crystals.

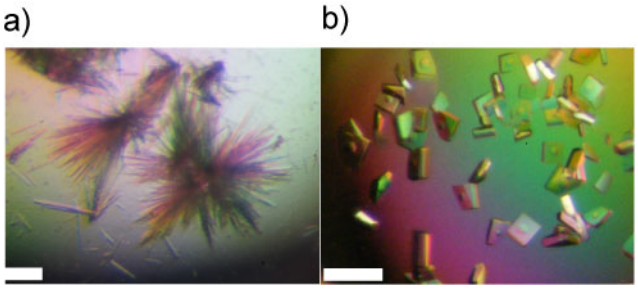

Figure 28: Crystals of GTP- (**a**) and GDP-bound (**b**) GIMAP2$^{1\text{-}234}$. The white bar corresponds to 100 µm

DATA COLLECTION	GIMAP2$^{1\text{-}234}$•GTP	GIMAP2$^{1\text{-}234}$•GDP
Beamline	BESSY 14.1	BESSY 14.2
Wavelength [Å]	0.9184	0.9184
Space group	$C222_1$	$P2_12_12_1$
Cell dimensions		
a [Å]	58.0	42.9
b [Å]	69.2	61.8
c [Å]	116.6	185.3
α=β=γ	90	90
V_M[†]	2.22	2.35
Resolution [Å]	50 (2.00)[‡] - 1.90	50 (1.80) - 1.70
No. of observed reflections	95706 (11945)	224594 (32614)
No. of unique reflections	18848 (2939)	54984 (8607)
R_{meas} [%][§]	6.8 (52.6)	6.6 (57.9)
I/σ(I)	18.1 (3.0)	15.8 (3.0)
Completeness [%]	99.7 (98.8)	99.2 (98.3)
Overall B-factor (Wilson) [Å^2]	32.9	27.1

Table 7: Data collection statistics for crystals GTP-bound and GDP-bound GIMAP2$^{1\text{-}234}$.

[†] According to [166].
[‡] Numbers in parentheses apply for the highest resolution shell.
[§] According to [167].

REFINEMENT	GIMAP2$^{1-234}$•GTP	GIMAP2$^{1-234}$•GDP
Resolution [Å]	50 - 1.9	50 - 2.2
No. of reflections used	17886	52141
R_{work} † / R_{free} ‡	18.5/22.1	18.1/20.2
No. of atoms		
Protein	1596	3134
Ligand/ion	33	58
Water	113	298
Average B-factors [Å²]		
Protein	26.3	23.0
Ligand/ion	20.0	24.0
Water	32.1	21.5
R.m.s. deviation		
Bond lengths [Å]	0.008	0.011
Bond angles [°]	1.410	1.250

Table 8: Refinement statistics for GTP- and GDP-bound GIMAP2$^{1-234}$.
† $R_{work} = \frac{\sum_{h,k,l}||F_{obs}(h,k,l)|-|F_{calc}(h,k,l)||}{\sum_{h,k,l}|F_{obs}(h,k,l)|}$.
‡ R_{free} was calculated with 5% of the data excluded from the refinement.

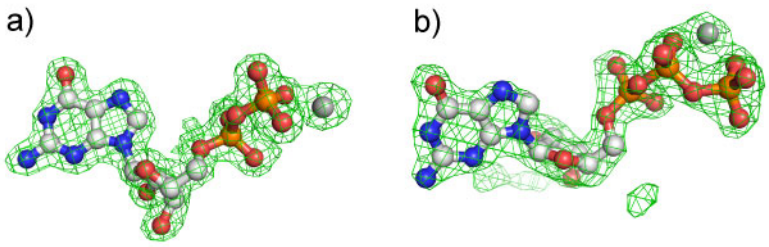

Figure 29: Electron density of nucleotides bound to GIMAP2$^{1-234}$. F_o-F_c electron density was calculated for GIMAP2$^{1-234}$•GTP (**a**) and for GIMAP2$^{1-234}$•GDP (**b**) without incorporation of the nucleotide in the atomic model. The density is colored in green and contoured at 3 σ with the refined nucleotide model shown as ball-and-sticks and the magnesium ion as grey sphere.

3.2.6 *Oligomerization of GTP-bound GIMAP2*

GTP-bound GIMAP2$^{1-234}$ oligomerized via two distinct interfaces in the crystal (Figure 30 **a-d**), with the C-terminal tails of the monomers pointing pairwise in opposite directions. Only in the GTP-, but not in the GDP-bound form of GIMAP2$^{1-234}$, a symmetric interface of 600 Å² was observed across the **G**uanine nucleotide-binding site (the **G**-interface, Figure 30 **b, c**) which involves the conserved box, switch I, the specificity motif G4 and helix α3*; all residues involved

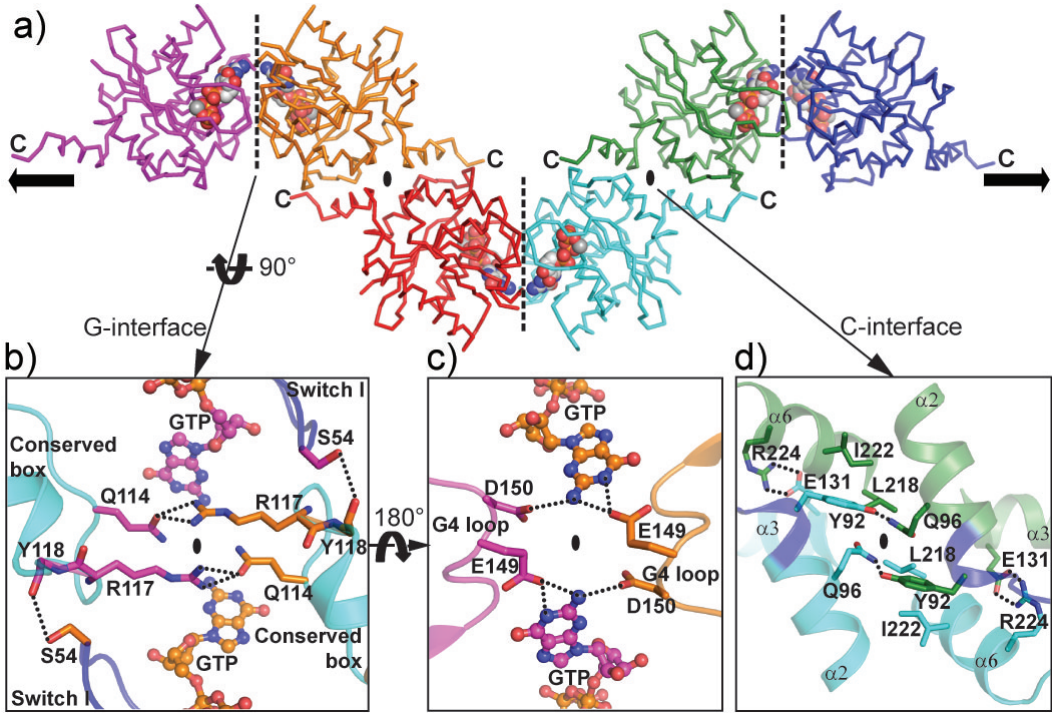

Figure 30: Oligomerization of GIMAP2. **a** Ribbon representation of the GTP-bound GIMAP2$^{1\text{-}234}$ oligomer, with the nucleotides shown as space-filling models. The crystallographic two-fold symmetry axes within the C- (ellipse) and G-interface (dotted line) are indicated. The indicated C-termini point in opposing directions in a pairwise manner. **b** Detailed view of the G-interface with selected residues shown as sticks. The crystallographic two-fold axis is shown as an ellipse. **c** GTP coordination in the oligomer. The exocyclic amino group of the guanine base forms hydrogen bonds to Glu149 *in cis* and to Asp150 *in trans* across the G-interface. The crystallographic two-fold axis is shown as an ellipse. **d** Detailed view of the C-interface. The crystallographic two-fold axis is shown as an ellipse.

in the dimer interface are also indicated in the multiple sequence alignment in Appendix C.

The highly conserved Arg117 from one GIMAP2 monomer forms a hydrogen bond across the G-interface to Gln114 of the opposing monomer (both from the conserved box, Figure 30 **b**). The exocyclic amino group of the guanine base is directly involved in dimerization by forming a hydrogen bond to the highly conserved Asp150 in the G4 loop, directly following the G4 motif (Figure 30 **c**). A strikingly similar interaction across the nucleotide binding site has recently been reported for the dynamin G domain dimer where Asp211 from the G4 loop interacts *in trans* in the same fashion with the nucleotide [27]. GTP-sensing of the G-interface is mediated by switch I. This region is stabilized by hydrogen bonds of Thr58 and a main chain contact of Leu57 to the γ-phosphate which enables Ser54 to form a hydrogen bond to the main chain oxygen of Tyr118 of the opposing molecule (Figures 30 **b**, 31).

A second symmetric, mostly hydrophobic interface of 1100 Å^2, the **C**-interface, was present at the **C**-terminus of both GDP- and GTP-bound GIMAP2$^{1\text{-}234}$ struc-

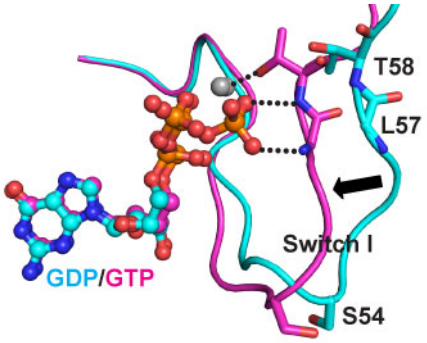

Figure 31: Mechanistic insights into GIMAP oligomerization I. Superposition of GDP-bound GIMAP2$^{21-260}$ (cyan) and GTP-bound GIMAP2$^{1-234}$ (magenta) shows the rearrangement of switch I upon GTP binding, leading to dimerization across the G-interface. The movement of switch I is indicated by the black arrow. Selected residues undergoing major conformational changes are shown as sticks.

tures (Figure 30 **d**). Helices α2 of switch II, α3 and α6 contribute residues to this interface. The C-interface was created by removal of α7, which resulted in stable dimerization of the GIMAP2$^{1-234}$ construct, as already shown by gel filtration and AUC experiments (Figure 27 **c**). This construct further oligomerized with low affinity in the presence of GTP (Figure 27 **c**).

3.2.7 *Switch II rearrangement upon GTP-binding in GIMAP2*

Switch II does not participate in the G-interface but is in direct contact with helix α7 and drastically changes its conformation upon GTP binding (Figure 32 **a**). Asp80 in the GDP-bound form points into the nucleotide-binding pocket, whereas it is expelled from this position in the GTP-bound form by the negatively charged γ-phosphate. Consequently, it flips out and interacts with His87. The resulting rearrangements in switch II induce a repositioning of Glu89 which prevents salt bridge formation to Lys240 in helix α7 (Figure 32 **a**). Our structural analysis therefore suggests that GTP-induced structural changes in switch II disrupt contacts between the G domain and helix α7 and weaken the affinity between these two elements. To exclude that the observed conformational changes in switch II were induced by removal of α7, we compared GDP-bound GIMAP2$^{1-234}$ and GDP-bound GIMAP2$^{21-260}$ and found that they adopt nearly identical conformations (Figure 32 **b**). Accordingly, the structural changes in switch II observed in GTP-bound GIMAP2$^{1-234}$ compared to GDP-bound GIMAP2$^{21-260}$ are solely mediated by the bound nucleotide.

3.3 STRUCTURE OF GIMAP5

3.3.1 *Structure determination of GDP-bound GIMAP5*

For structural comparison of different membrane-anchored GIMAP family members, the cytoplasmic portion of GIMAP5 (GIMAP5$^{1-276}$, Figure 33 **a**) was crystallized in the GDP-bound state (see 2.4.1). Crystals diffracted to a maximal resolution

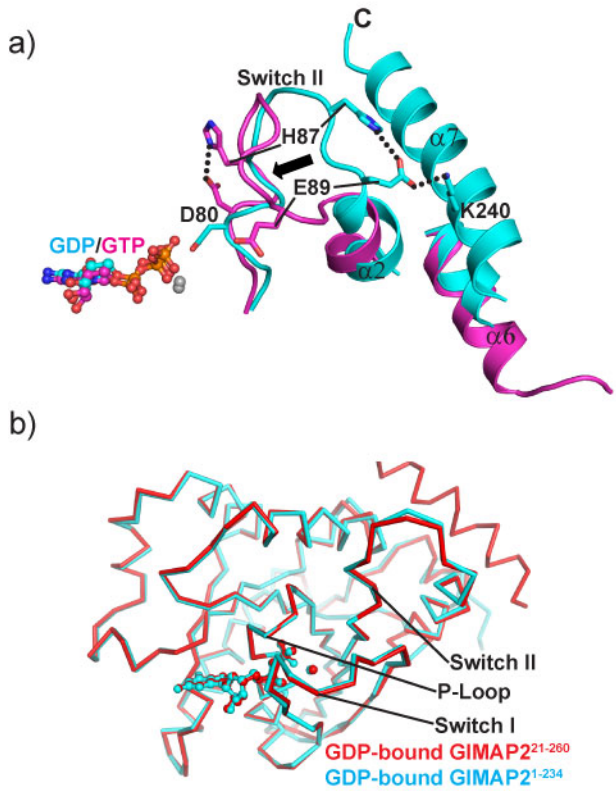

Figure 32: Mechanistic insights into GIMAP oligomerization II. **a** A superposition of GDP-bound GIMAP2$^{21\text{-}260}$ (cyan) and GTP-bound GIMAP2$^{1\text{-}234}$ (magenta) shows the rearrangements of switch II upon GTP binding. The movement of switch II is indicated by a black arrow. Selected residues undergoing major conformational changes are shown as sticks. **b** Removal of helix $\alpha 7$ does not induce major structural changes in switch II. GDP-bound GIMAP2$^{21\text{-}260}$ (red) and GDP-bound GIMAP2$^{1\text{-}234}$ (cyan) were superimposed with an r.m.s.d. of 0.4 Å along 202 aligned residues.

of 2.8 Å and belong to the space group $P2_12_12_1$ with cell dimensions a=41.2 Å, b=57.1 Å, c=106.6 Å, $\alpha=\beta=\gamma=90°$. The data collection statistics (see 2.4.2) from a single crystal are shown in Table 9.

DATA COLLECTION	GIMAP5$^{1\text{-}276}$•GDP NATIVE
Beamline	BESSY 14.1
Wavelength [Å]	0.9184
Space group	$P2_12_12_1$
Cell dimensions	
a [Å]	41.2
b [Å]	57.1
c [Å]	106.6
$\alpha=\beta=\gamma$	90
V_M[†]	2.03
Resolution [Å]	50 (2.95)[‡] - 2.80
No. of observed reflections	31128 (4042)
No. of unique reflections	6623 (964)
R_{meas} [%][§]	18.7 (54)
I/σ(I)	9.37 (3.31)
Completeness [%]	98 (90)
Overall B-factor (Wilson) [Å^2]	33.5

Table 9: Data collection statistics for crystals of GDP-bound GIMAP5$^{1\text{-}276}$.

† According to [166].
‡ Numbers in parentheses apply for the highest resolution shell.
§ According to [167].

The structure of GIMAP5$^{1\text{-}276}$ was solved by molecular replacement (see 2.4.3). A hybrid search model was generated with the program Molrep [155], using the structure of GDP-bound GIMAP2$^{21\text{-}260}$ and an amino acid sequence alignment of GIMAP2 and GIMAP5. Model building and refinement were done as described in 2.4.4 (Table 10). The model was validated and will be submitted to the Protein Data Bank (see 2.4.5). The final model consists of residues 27-263 with 94% of the residues in the favored region of the Ramachandran plot and 0.9% are outliers.

REFINEMENT	GIMAP5$^{1\text{-}276}$•GDP
Resolution [Å]	12 - 2.8
No. of reflections used	6175
R_{work} † / R_{free} ‡	21.9/26.3
No. of atoms	
Protein	1887
Ligand/ion	29
Average B-factors [Å^2]	
Protein	22.9
Ligand/ion	9.2
R.m.s. deviation	
Bond lengths [Å]	0.008
Bond angles [°]	1.102

Table 10: Refinement statistics for GDP-bound GIMAP5$^{1\text{-}276}$.

† $R_{work} = \frac{\sum_{h,k,l}||F_{obs}(h,k,l)|-|F_{calc}(h,k,l)||}{\sum_{h,k,l}|F_{obs}(h,k,l)|}$.

‡ R_{free} was calculated with 5% of the data excluded from the refinement.

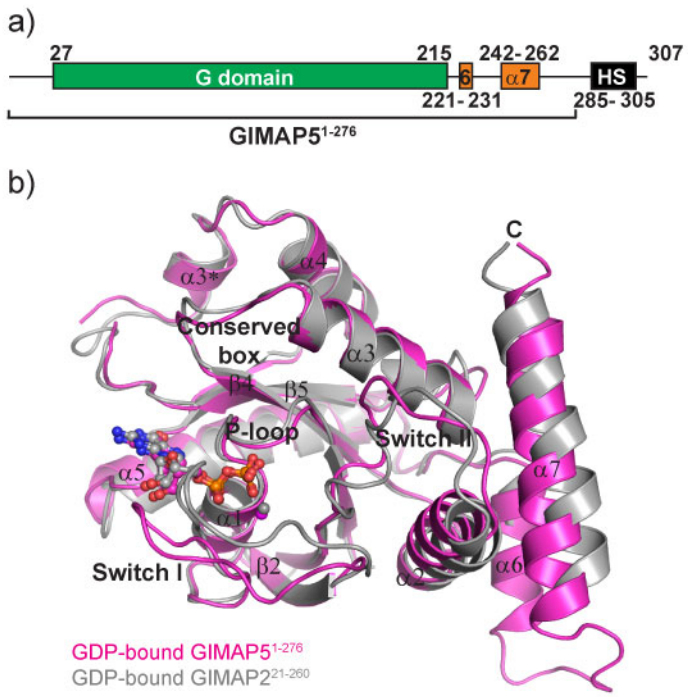

Figure 33: Structural comparison of GDP-bound GIMAP5 and GIMAP2. **a** Schematic representation of the domain structure of GIMAP5, with the amino acid positions indicated. The C-terminal extension is shown in orange and the hydrophobic segment (HS) in black. The crystallized construct is indicated below. **b** Superposition of GDP-bound GIMAP5$^{1\text{-}276}$ (magenta) and GDP-bound GIMAP2$^{21\text{-}260}$ (grey), shown in cartoon representation. GDP is shown as ball-and-sticks.

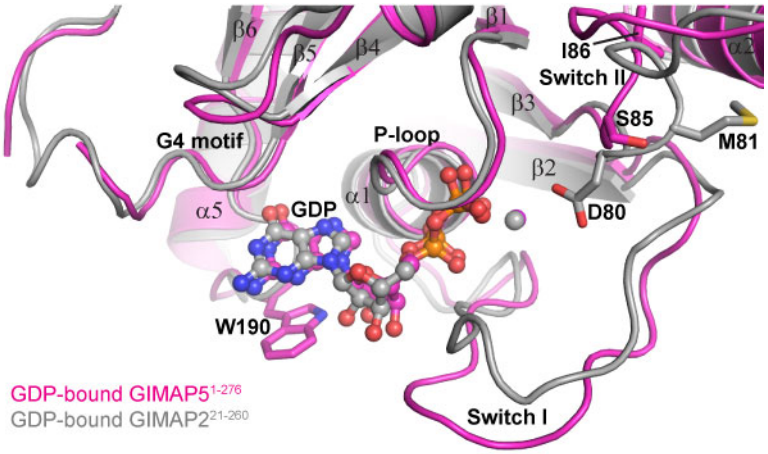

Figure 34: Comparison of the GDP binding modes of GIMAP5 (magenta) and GIMAP2 (grey). Selected residues are shown as sticks. GDP is shown as ball-and-sticks.

3.3.2 *Structural comparison to GDP-bound GIMAP2*

Regarding the amino acid sequence, GIMAP2 and GIMAP5 show 44% sequence identity, 19% strong similarity and 12% weak similarity. The overall architecture of the two proteins is very similar, they can be superposed with an r.m.s.d. of 1.45 Å along 217 aligned residues (Figure 33 **b**). The only significant structural differences occur in the switch regions and in the C-terminal helix α7, which is shifted for approximately half a helical turn. Furthermore, in the case of GIMAP5$^{1\text{-}276}$, contrary to the GIMAP2 constructs, the loop connecting helices α6 and α7 is ordered and resolved in the structure because it is stabilized by crystal contacts.

Additional differences are visible in the nucleotide binding pocket (Figure 34). Trp190 provides an additional stacking interaction to the nucleotide base. Interestingly, the unusual Asp80, which was observed in the G3 motif of GIMAP2 is replaced by Ser85 in GIMAP5, suggesting a different switch II rearrangement upon GTP-binding in GIMAP5. Similar to GIMAP2, the position equivalent to the catalytic Glu61 of Ras is taken by a hydrophobic residue, Ile86.

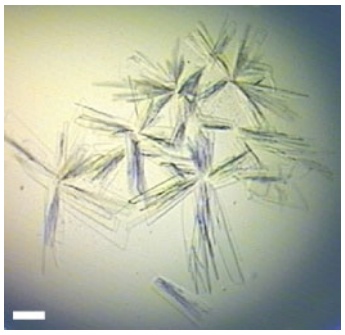

Figure 35: Crystals of GMP-PNP-bound GIMAP7 L100Q. The white bar corresponds to 100 µm

3.4 STRUCTURE OF GIMAP7

3.4.1 *Structure determination of GMP-PNP-bound GIMAP7*

DATA COLLECTION	GIMAP7 L100Q•GMP-PNP NATIVE
Beamline	BESSY 14.1
Wavelength [Å]	0.9184
Space group	P1
Cell dimensions	
a [Å]	45.9
b [Å]	90.9
c [Å]	114.7
α [°]	77.3
β [°]	85.2
γ [°]	89.2
V_M †	2.24
Resolution [Å]	50 (3.28)‡ - 3.1
No. of observed reflections	57768 (31271)
No. of unique reflections	9002 (4925)
R_{meas} [%]§	15.4 (68.8)
I/σ(I)	7.24 (1.58)
Completeness [%]	95.3 (93.2)
Overall B-factor (Wilson) [Å²]	39.2

Table 11: Data collection statistics for crystals of GMP-PNP-bound GIMAP7 L100Q.

† According to [166].
‡ Numbers in parentheses apply for the highest resolution shell.
§ According to [167].

In order to determine the structure of a full length GIMAP family member, the GIMAP7 L100Q variant (the reason for using this variant is explained in 3.1.3) was crystallized in the presence of the non-hydrolyzable GTP analog GMP-PNP employing PEG 3350 as precipitant (see 2.4.1). Representative crystals are shown in Figure 35. Crystals diffracted X-rays to 3.1 Å resolution and belong to the space group P1 with cell dimensions a=45.9 Å, b=90.9 Å, c=114.7 Å, α=77.3°, β=85.2°, γ=89.2°. The data collection statistics (see 2.4.2) are shown in Table 11.

The structure of GIMAP7 was solved by molecular replacement (see 2.4.3) using the structure of GTP-bound GIMAP2$^{1\text{-}234}$ as search model. The model was completed and refined as described in 2.4.4 (Table 12). It was validated and will be submitted to the Protein Data Bank (see 2.4.5). The final model of GIMAP7 contains six protein molecules in the asymmetric unit encompassing residues 8-68, 73-169, 173-286 of chain A, 7-71, 73- 233, 245-287 of chain B, 8-69, 72-102, 104-232, 244-288 of chain C, 9-169, 174-193, 198-219, 258-290 of chain D, 8-169, 173-237, 239-292 of chain E, 8-68, 77-102, 104-138, 141-169, 173-195, 199-238, 243-284 of chain F. 92% of all residues are in the favored region of the Ramachandran plot and 0.4% are outliers.

REFINEMENT	GIMAP7 L100Q•GMP-PNP
Resolution [Å]	32 - 3.15
No. of reflections used	29759
R_{work}†/R_{free}‡	26.2/32.7
No. of atoms	
Protein	10908
Ligand/ion	198
Average B-factors [Å²]	
Protein	51.0
Ligand/ion	34.5
R.m.s. deviation	
Bond lengths [Å]	0.010
Bond angles [°]	1.424

Table 12: Refinement statistics for GMP-PNP-bound GIMAP7 L100Q.

† $R_{work} = \frac{\sum_{h,k,l}||F_{obs}(h,k,l)|-|F_{calc}(h,k,l)||}{\sum_{h,k,l}|F_{obs}(h,k,l)|}$.

‡ R_{free} was calculated with 5% of the data excluded from the refinement.

3.4.2 *The GIMAP7 monomer*

The asymmetric unit of the crystal contains six GIMAP7 monomers. Two pairs of three monomers, respectively, which are arranged side-by-side, face each other via their nucleotide-binding sites. (Figure 36 **a**). In the following, the best resolved monomers A and B are analyzed more closely. Clear electron density for the

nucleotide was visible in the nucleotide binding site for all six GIMAP7 monomers, one example is shown in Figure 36 **b**.

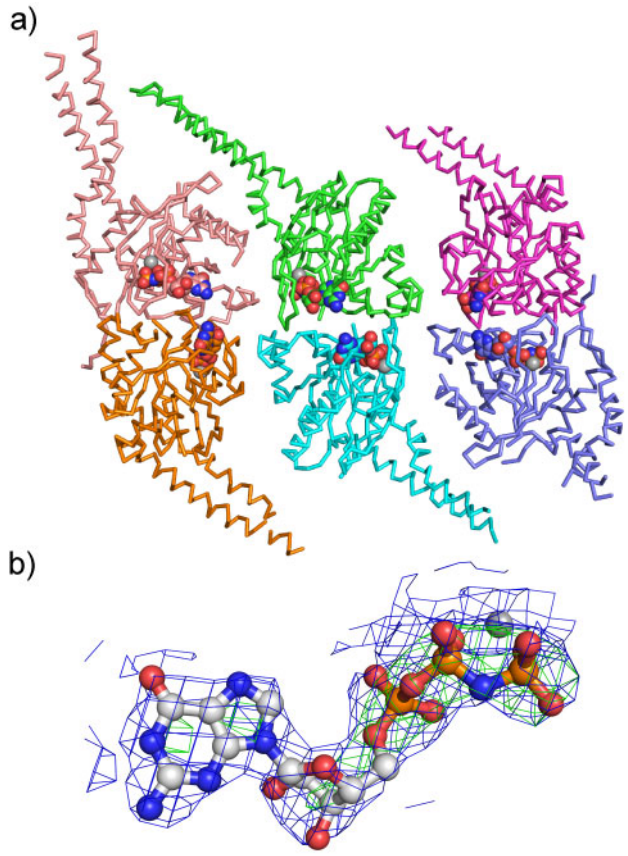

Figure 36: Arrangement of GIMAP7 L100Q molecules in the unit cell. **a** Ribbon representation of the six GIMAP7 monomers in the unit cell of the crystal. GMP-PNP and magnesium are shown as spheres. **b** Electron density for GMP-PNP. F_o-F_c electron density (shown in green and contoured at 3 σ) was calculated for full-length GIMAP7 without incorporation of the nucleotides in the atomic model. Refined $2F_o$-F_c electron density contoured at 1.5 σ is shown in blue. The nucleotide is shown as ball-and-sticks.

The N-terminal 7 residues in GIMAP7 L100Q are disordered. Residues 7-209 build up a Ras-like G-domain with the typical GIMAP-specific helix α3* inserted between strand β5 and helix α4 (Figure 37 **a, b**). The overall G domain structure of GIMAP7 is very similar to the G domain of GIMAP2, they can be superposed with a r.m.s.d. of 1.3 Å along 177 aligned residues. In contrast to GIMAP2, GIMAP7 has a unique C-terminal extension which folds into two elongated helices α6 and α7 constituting a coiled-coil structure of 90 residues (Figure 37 **a, b**). The tip of this helical extension is highly charged (7 glutamates, 1 aspartate and 4 lysines in 14 residues), a feature which is also conserved in the closely related GIMAP4 (see also the multiple sequence alignment in Appendix C). The C-terminal end of helix α7 corresponds to α7 in GIMAP2 and is in contact with switch II via a hydrophobic interaction involving Phe277, Ile280 and Met283 of the extension as well as Phe68, Leu74 and Cys78 of switch II (Figure 37 **c**). The last 10 residues of GIMAP7 are not visible in the electron density.

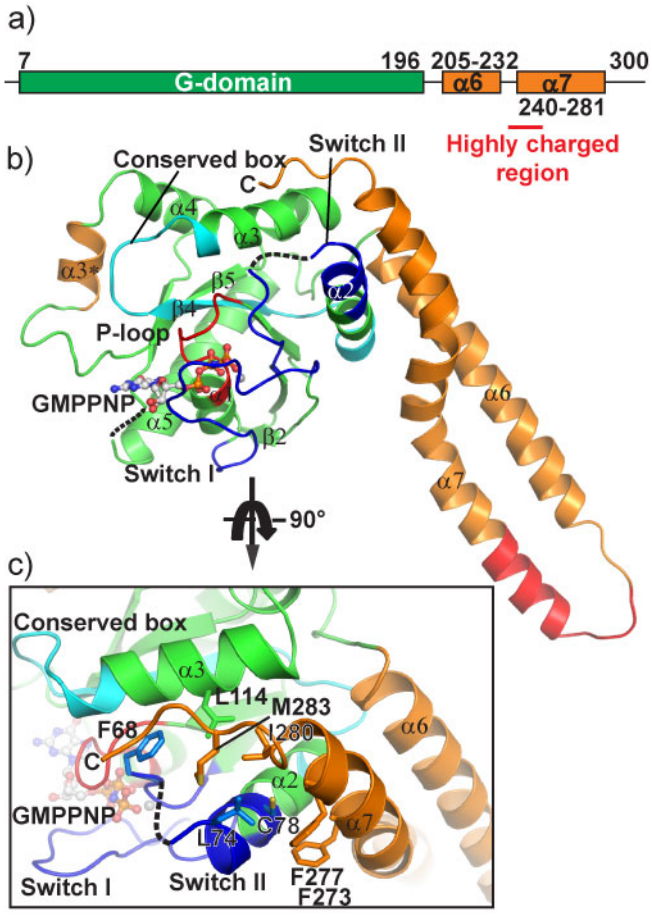

Figure 37: Structure of the GIMAP7 L100Q monomer. **a** Schematic representation of the domain structure of GIMAP7 with amino acid positions indicated. The highly charged region is marked in red. **b** Cartoon representation of the GMP-PNP-bound GIMAP7 monomer. The G-domain is shown in green, switch I and switch II in blue, the P-loop in red and the conserved box in cyan. Secondary structure elements differing from the core G-domain of H-Ras are shown in orange. The highly charged region is colored red. **c** Detailed view of the C-terminal extension and its contact to switch II and the G-domain, with the same color coding as in **a**. Selected residues are shown as sticks.

The nucleotide specificity motifs G1-G5 are involved in a similar fashion in nucleotide binding as in GIMAP2. The most notable difference is observed in the partially disordered switch II, where Gly66 of GIMAP7 is stabilized by the γ-phosphate, in contrast to the corresponding Asp80 of GIMAP2 which becomes displaced by the γ-phosphate (Figure 38). Previously, a function of the GIMAP2 switch II in regulating the release of helix α7 from the G domain was suggested (see 3.2.7). The divergent architecture of switch II in GIMAP7 might indicate a different function of this element.

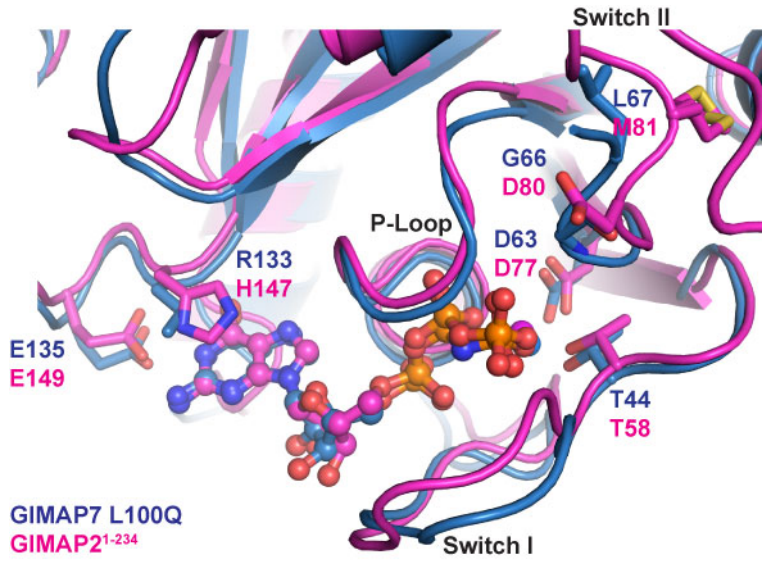

Figure 38: Details of GMP-PNP-binding in GIMAP7 L100Q and comparison to the GTP-binding mode of GIMAP2$^{1-234}$. Shown is a structural superposition of GIMAP7 L100Q •GMPPNP (blue) and GIMAP2$^{1-234}$•GTP (magenta, see 3.2), with emphasis on the nucleotide-binding site. Elements involved in nucleotide-binding are shown in stick representation.

3.4.3 *Dimerization of GMP-PNP-bound GIMAP7*

The six GIMAP7 L100Q monomers in the crystal structure are arranged in three almost identical dimers with an average buried surface area per monomer of 940 Å^2 (Figure 39 **a-c**). Dimerization in GIMAP7 is mediated by switch I and residues in the conserved box, including a double salt bridge of Lys110 to the conserved box residue Glu106 of the opposing monomer (Figure 39 **b**). Further hydrophobic dimerization contacts are provided by residues in switch I, the conserved box, the loop following the G4 specificity motif and helix α3*. All residues involved in dimerization are indicated in the multiple sequence alignment in Appendix C.

GTP-sensing in the dimer is accomplished via a main chain hydrogen bond between Ala40 of switch I and Asp150 at the beginning of helix α4 (Figure 39 **b**). This suggests a similar molecular mechanism of GTP-stimulated GIMAP7 dimerization as found in GIMAP2 (see also Figure 31). Furthermore, the higher affinity of the GIMAP7 dimer compared to the GTP-dependent GIMAP2 dimer (see Figure 21) is caused by more and stronger contacts in the GIMAP7 dimer interface.

The highly conserved GIMAP7 Arg103 corresponds to GIMAP2 Arg117. In GIMAP2, this residue is crucial for GTP-stimulated dimerization (see Figures 30, 31), because it forms a double hydrogen bond across the dimer interface. In GIMAP7, however, the corresponding Arg103 is disordered and not visible in the electron density in four of the six monomers in the unit cell. In two cases, it could be modeled, and in one case it reaches from one monomer over to the nucleotide binding site of the other one and contacts the γ-phosphate of the GMP-PNP indirectly via coordination of a water molecule (Figure 39 **b**).

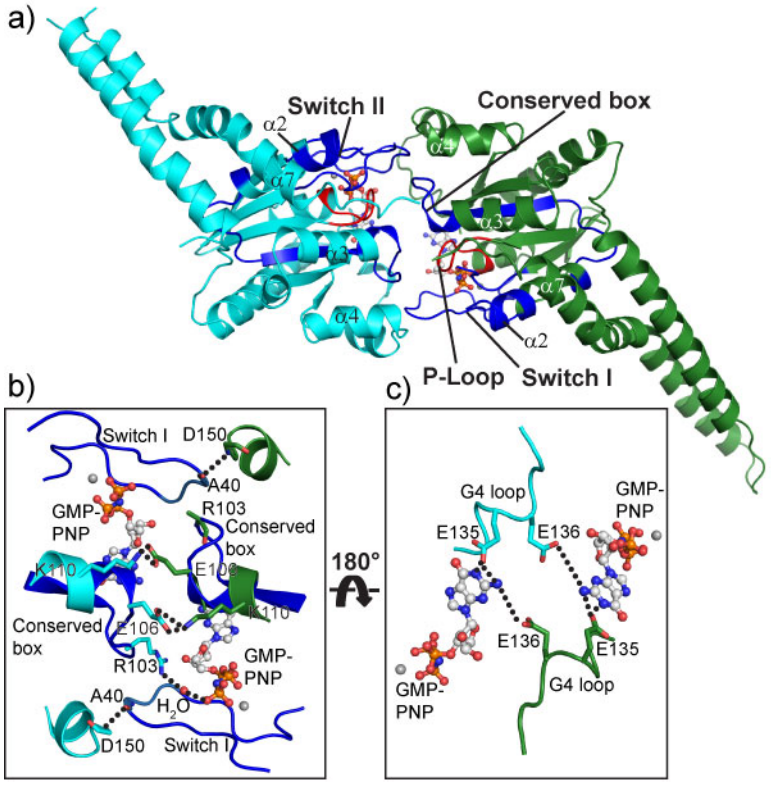

Figure 39: The GIMAP7 L100Q dimer. **a** Cartoon representation of the GIMAP7 dimer formed via the G-interface. The G-domain is colored green or cyan, switch I, switch II and the conserved box in blue and the P-loop in red. **b** Detailed view of the GIMAP7 G-interface, with the same color scheme as in **a**. Selected interacting residues are shown as sticks. **c** GMP-PNP coordination in the dimer. The exocyclic amino group of the guanine base forms hydrogen bonds to Glu135 *in cis* and weak hydrogen bonds to Glu136 *in trans* across the G-interface.

A conserved glutamate residue in the loop directly downstream of the G4 motif forms a weak hydrogen bond to the exocyclic amino group of the nucleotide bound to the opposing monomer (Figure 39 **c**). The same interaction is found in the GIMAP2 G-interface and in dynamin (see 3.2.6). Taken together, the mode of GIMAP7 dimerization is very similar to the arrangement via the G-interface of the GTP-dependent GIMAP2$^{1\text{-}234}$ oligomer (see also 3.2.6), suggesting that the G-interface is a conserved feature in the GIMAP family.

3.5 FUNCTIONAL STUDIES

3.5.1 *Structure-based mutagenesis*

To further study the relevance of the G-interface in solution (see also 3.2.6), the assembly status of GIMAP2 at different protein concentrations was determined by analytical ultracentrifugation (AUC) in the presence of GDP and GTP. As already described above (see Figure 21 **a**), GIMAP2$^{1\text{-}260}$ dimerized with low affinity only in the presence of GTP (Kd = 250 µM). In contrast, mutation of particular amino acid

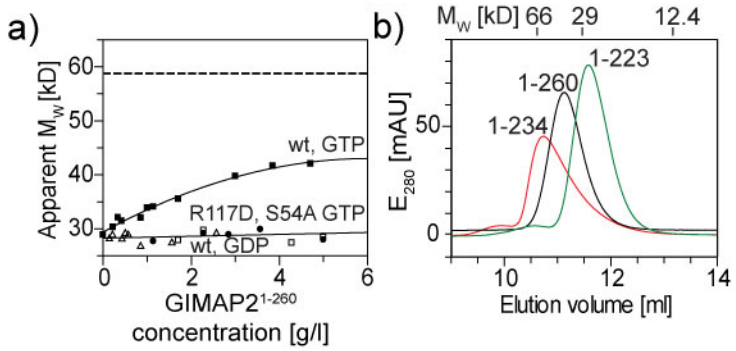

Figure 40: Structure-based mutagenesis in GIMAP2. **a** Probing the G-interface. Sedimentation equilibrium ultracentrifugation experiments for GIMAP2$^{1-260}$ in the presence of 100 µM GTP (■) and GDP (△) and for the GIMAP2$^{1-260}$ mutants R117D (□) and S54A (•) in the presence of 100 µM GTP were carried out to determine apparent molecular masses at different protein concentrations. A monomer-dimer equilibrium was fitted to GIMAP2$^{1-260}$ in the presence of GTP, resulting in K_d=250 ± 20 µM. The dashed line indicates the molecular mass of the GIMAP2 dimer. **b** Analytical gel filtration experiments for GIMAP2$^{1-234}$ (red), GIMAP2$^{1-260}$ (black) and GIMAP2$^{1-223}$ (green) show the involvement of helix α6 in dimerization across the C-interface. Elution volumes of protein standards are indicated on top of the graph.

residues in switch I (S54A) and in the conserved box (R117D) in the G-interface prevented GTP-dependent dimerization (Figure 40 **a**). These results are in line with the findings from the structural analysis of the G-interface.

Furthermore, the involvement of helix α6 in the C-interface, especially residue Arg224, was examined in solution using SEC (see also 2.3.8). As result, further shortening of this helix in the GIMAP2$^{1-223}$ construct resulted again in a monomeric form (Figure 40 **b**).

To explore the role of GIMAP7 dimerization for catalysis, we mutated Glu136 in the centre of the G-interface to tryptophan (see 2.2). Indeed, this mutation did not interfere with nucleotide-binding (Figure 41 **a**), but reduced GTP-promoted dimerization (Figure 41 **b**) and severely slowed down the GTPase reaction (Figure 41 **c**), indicating that dimerization via the G-interface is required for the stimulated GTPase reaction.

The highly conserved Arg103 from the GIMAP7 conserved box is mostly disordered, but its side chain is within reach of the β- and γ-phosphates of the GTP in the opposing molecule (see also 3.4.3). Strikingly, the R103D mutation in GIMAP7 did not interfere with nucleotide binding (Figure 41 **a**) or GTP-dependent dimerization (Figure 41 **b**), but completely blocked the GTPase reaction (Figure 41 **c**). These features are representative for a catalytic residue and indicate that Arg103 in GIMAP7 acts as a catalytic arginine finger which promotes nucleotide hydrolysis in the opposing monomer.

3.5.2 *Subcellular localization studies*

To gain further insights into the function of GIMAP family members in the cell, subcellular localization experiments with GIMAP2 and GIMAP5 N-terminal

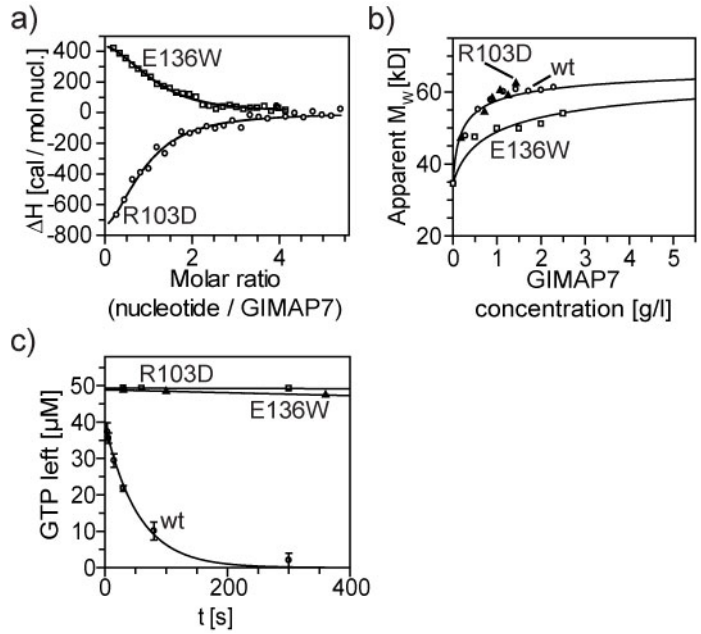

Figure 41: Structure-based mutagenesis in GIMAP7. **a** Nucleotide binding affinities of GIMAP7 mutants to GTP-γ-S were determined using ITC. The following values were obtained from the fittings: R103D (○), Kd=14 ± 4 µM (n=0.8); E136W (□), Kd=19 ± 3 µM (n=1.1). **b** Sedimentation equilibrium ultracentrifugation experiments with GIMAP7 R103D (▲) and E136W (□) in the presence of 200 µM GMP-PNP. The following values for a monomer-dimer equilibrium were obtained from the data fittings: GIMAP7 E136W: Kd=47 ± 6 µM, GIMAP7 R103D Kd=8 ± 1 µM. Data for GIMAP7 wt (○, see Figure 21 **b**) in the presence of 200 µM GMP-PNP are shown for comparison. **c** Nucleotide hydrolysis of the E136W (▲) and R103D (□) mutants of GIMAP7 were measured by HPLC in a single turnover assay. GTP hydrolysis of wt GIMAP7 (○, see Figure 20 a) is shown for comparison. Data points are mean values ± standard deviation of three independent experiments.

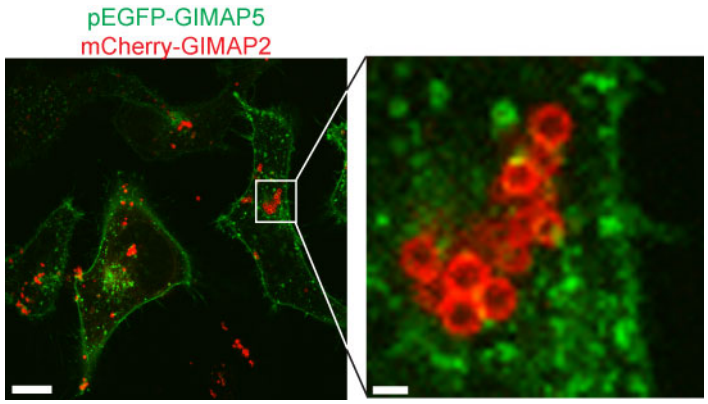

Figure 42: Localization studies in HeLa cells I. Cells were transfected with the indicated constructs, and the living cells were inspected using confocal microscopy. EGFP-tagged GIMAP5 shows green fluorescence, mCherry-tagged GIMAP2 shows red fluorescence. The white bar in the left panel represents 10 µm, the bar in the magnified right panel represents 1 µm.

EGFP-fusion proteins were initiated. For the first trials, adherent HeLa cells were used. HeLa cells were transfected with expression plasmids coding for the fusion proteins and visualized using confocal laser-scanning microscopy 24 hours after the transfection (see 2.5).

In a co-expression experiment, mCherry-tagged GIMAP2 and EGFP-tagged GIMAP5 did not co-localize (Figure 42). GIMAP2 localized to the edges of spherical compartments with a diameter of around 1 µm (Figure 42). In contrast, GIMAP5 localized to smaller, granular compartments of varying size and shape. In approximately 30% of all cells, GIMAP5 also localized to the plasma membrane (Figure 42). In Figure 43 **c, d**, examples of cells without plasma membrane localization are shown.

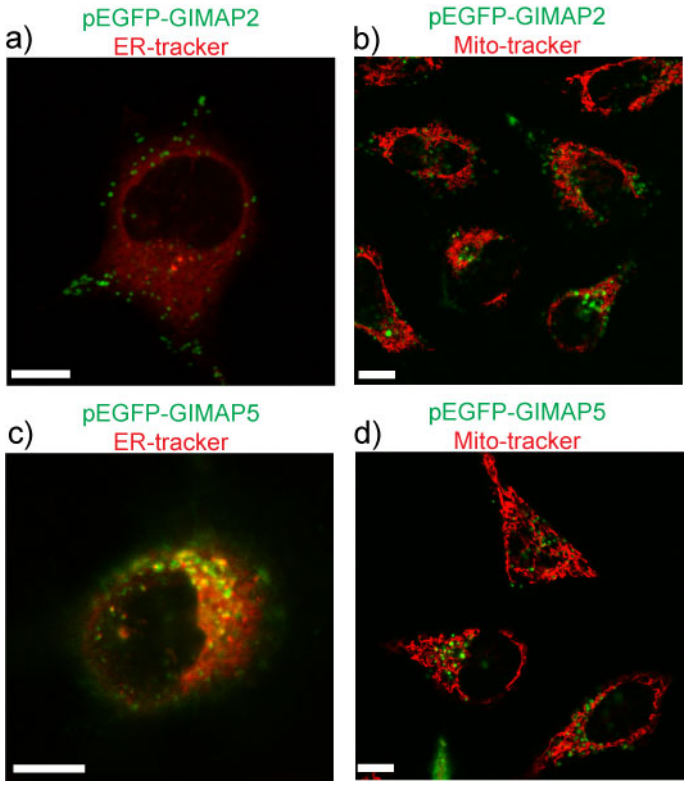

Figure 43: Localization studies in HeLa cells II. Cells were transfected with the indicated constructs and stained with the indicated organelle markers. **a** EGFP-tagged GIMAP2 shows green fluorescence, ER-tracker (BODIPY TR glibenclamide) shows red fluorescence. **b** green: EGFP-GIMAP2, red: MitoTracker Red CM-H_2XRos. **c, d** Same as **a, b**, but employing EGFP-GIMAP5 for transfection. White bars represent 10 µm.

The localization of GIMAP2 and GIMAP5 EGFP-fusion proteins was further explored by co-staining experiments using fluorescent markers for the endoplasmic reticulum (ER) and for mitochondria (see 2.5). The particular spherical fluorescent signal from GIMAP2 did not colocalize with the ER or the mitochondrial marker dye (Figure 43 **a, b**). GIMAP5 showed only very limited colocalization with the ER marker (Figure 43 **c**) and no colocalization with the mitochondrial marker signal (Figure 43 **d**).

GIMAP proteins are mainly expressed in lymphocytes (see 1.3). To explore the cellular localization of GIMAP2 in this particular cell type, over-expression studies in the Jurkat T cell line were performed (see 2.5). mCherry-tagged full-length GIMAP2 localized to the same large spherical structures with a diameter of appoximately 1 µm that were already observed in HeLa cells for mCherry-tagged GIMAP2 (Figures 42, 44 **a**).

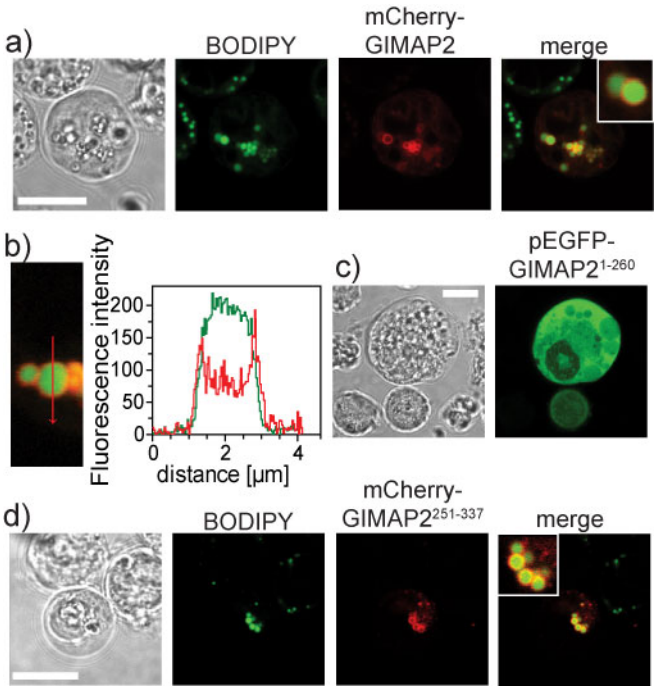

Figure 44: Localization studies in Jurkat cells I. **a** N-terminally mCherry-tagged GIMAP2 (red) was overexpressed in Jurkat cells and lipid droplets (LDs) were stained with BODIPY 493/503 (green). Living cells were analyzed by confocal fluorescence microscopy. All scale bars represent 10 µm. **b** Profile of the fluorescent signals across a LD (right) along the indicated line (left). **c** N-terminally EGFP-tagged GIMAP2$^{1-260}$ lacking the hydrophobic segments was overexpressed in Jurkat cells and analyzed by confocal microscopy. **d** The C-terminal hydrophobic segments of GIMAP2 (residues 251-337) were expressed as N-terminal mCherry fusion in Jurkat cells, co-stained with BODIPY 493/503 (green) and analyzed by confocal microscopy.

Based on a similar staining pattern recently reported for the interferon-induced mouse GTPase Igtp in dendritic cells [169], we tested for co-staining with the lipid droplet (LD) marker BODIPY 493/503, and indeed found co-localization with GIMAP2 (Figure 44 **a, b**). The fluorescent GIMAP2 signal was enriched at the border of LDs (Figure 44 **b**), suggesting that GIMAP2 resides mainly at the phospholipid monolayer surrounding the LD core of neutral lipids, which is stained by BODIPY 493/503. The predicted C-terminal hydrophobic segments of GIMAP2 were necessary and sufficient for the reported localization, since deletion of these segments led to a cytoplasmic staining, and the hydrophobic segments on their own targeted the mCherry fluorescent protein to LDs (Figure 44 **c, d**).

It was furthermore noticed that overexpression of mCherry-tagged full-length GIMAP2 in Jurkat cells induced a significant two-fold increase of LD number per

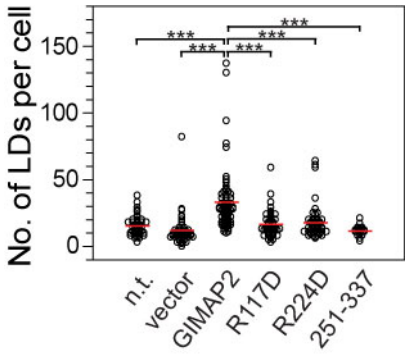

Figure 45: Increase of lipid droplet number upon GIMAP2 over-expression. Jurkat cells were transfected with the indicated GIMAP2 constructs and the number of LDs determined using the BODIPY 493/503 stain in two independent experiments. n.t. - not transfected (n=45), vector - transfected with pmCherry-C (n=48). GIMAP2 - transfected with pmCherry-C-GIMAP2 (n=69). R117D - transfected with pmCherry-C-GIMAP2 R117D (n=48). R224D - transfected with pmCherry-C-GIMAP2 R224D (n=49). 251-337 - transfected with pmCherry-C-GIMAP2251-337 (n=17). Only transfected cells were evaluated, as judged by inspection of the mCherry fluorescence. Red bars indicate the mean number of LDs per cell. Three asterisks represent $P < 0.0001$ according to Wilcoxon-Mann-Whitney test. See also Figure 30, where the role of the mutated amino acid residues Arg117 and Arg224 in GIMAP2 oligomerization is indicated.

cell (average of 33 LDs per cell, Figure 45), compared to non-transfected cells and cells transfected with mCherry only (average of 15 or 12 LDs per cell, respectively, Figure 45). In contrast, over-expressed GIMAP2 point mutants in the G-interface (R117D) or C-interface (R224D) still localized to LDs but did not cause an increase of the LD number (Figure 45), suggesting a function of the GIMAP2 oligomer at the surface of LDs.

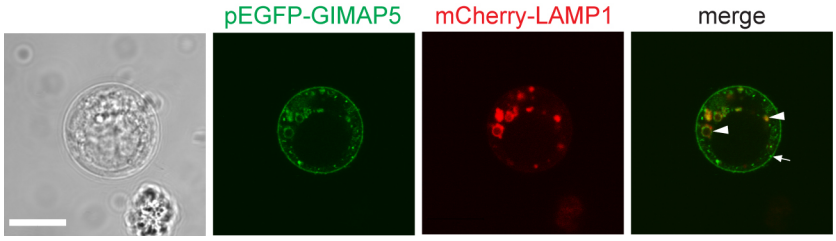

Figure 46: Localization studies in Jurkat cells II. N-terminally EGFP-tagged GIMAP5 (green) was co-expressed with mCherry-tagged LAMP1 (red), a marker protein for late endosomes and lysosomes. Living Jurkat cells were analyzed by confocal fluorescence microscopy. The arrowheads point at spherical, larger intracellular inclusions, where a co-localization of both proteins is visible. The arrow shows smaller, granular structures, unique for EGFP-tagged GIMAP5. The scale bar represents 10 µm.

The localization of GIMAP5 was also in the Jurkat T cell line as well (see 2.5). Expression of EGFP-tagged GIMAP5 at the plasma-membrane membrane was also observed in roughly one third of all inspected cells (one example is shown in Figure 46). The granular intracellular staining which was observed in HeLa cells could also be reproduced in the Jurkat cell line (Figure 46). It was furthermore

demonstrated that at least a spherical form as well as the larger ones of these granules co-localized with mCherry-tagged LAMP1, a protein which resides at the membrane of late endosomes and lysosomes (Figure 46, arrowheads). Smaller granules did not co-stain with mCherry-LAMP1 (Figure 46, arrow).

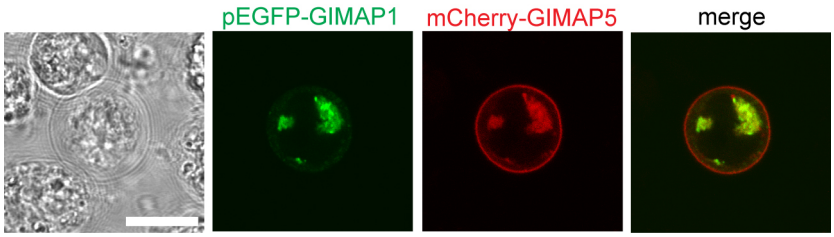

Figure 47: Localization studies in Jurkat cells III. N-terminally EGFP-tagged GIMAP1 (green) was co-expressed with mCherry-tagged GIMAP5 (red). Living Jurkat cells were analyzed by confocal fluorescence microscopy. The scale bar represents 10 µm.

Furthermore, all human GIMAPs except GIMAP6, which could not be cloned (see 3.1.1), were screened for co-localization in Jurkat cells via co-expression of mCherry and EGFP fusion proteins (see 2.5). GIMAP4 and GIMAP8 showed cytoplasmic localization in all co-expression experiments where they were involved (not shown), therefore their co-localization could not be unequivocally proven. EGFP-tagged GIMAP1 and mCherry-tagged GIMAP5 co-localized in two independent experiments in larger intracellular structures. Only the plasma membrane staining of GIMAP5 was unique for this protein and was not observed for GIMAP1 (Figure 47). Interestingly, the smaller granular staining of GIMAP5, which was observed in the co-expression experiment with LAMP1, was lost upon co-expression with GIMAP1.

4 DISCUSSION

4.1 AN ARGININE FINGER WITH DUAL FUNCTION IN THE GIMAP FAMILY

G-proteins generally cycle between an active GTP-bound state and an inactive GDP-bound state (reviewed in [3]), and these states can be inter-converted by nucleotide exchange and GTP hydrolysis (see also 1.1.1). In G-proteins of the Ras superfamily, GTP hydrolysis is stimulated by association with GTPase activating proteins (GAPs) which often supply a catalytic arginine residue *in trans*, the arginine finger, to complement the active site [18]. In a second class of G-proteins, GTPase activity is triggered by nucleotide-dependent dimerization of the G-domains [170]. These proteins include members of the dynamin superfamily [60], the signal recognition particle family [63] and the septin superfamily including septins [44] and Toc proteins [47, 48].

Dimerization often induces rearrangements of catalytic residues *in cis* leading to the observed GTPase stimulation (e.g.[171]). For Toc proteins, however, a conserved arginine residue is supplied *in trans* into the nucleotide binding cleft of the opposing molecule, but its role in catalysis was disputed [47, 48]. His158 at the equivalent position in septin2 was suggested to be involved in catalysis, but the structure of the septin2 dimer as well as site-directed mutagenesis indicated that it does not contact the opposing monomer and is not involved in catalysis [45].

Here we show that the corresponding, highly conserved arginine from the GIMAP conserved box in the G-interface has a dual function. In GIMAP2, it stabilizes dimerization by binding to residues of the opposing monomer and is therefore not available for catalysis (see 3.2.6, 3.5.1). In contrast, it acts as a catalytic arginine finger in GIMAP7 by complementing the active site of the opposing monomer to activate GTP hydrolysis (see 3.4.3, 3.5.1). Thus, depending on the molecular context, the arginine finger controls GIMAP function by promoting self-association in one case or catalyzing GTP hydrolysis and therefore the disassembly of the dimer in the second case.

4.2 MEMBRANE-ANCHORED AND SOLUBLE GIMAPS

Based on their diverging biochemical features it appears that GIMAPs can be subdivided into two groups: membrane-anchored GIMAPs possessing a C-terminal hydrophobic segment and soluble GIMAPs which do not have such a hydrophobic stretch (see also Figure 13). GIMAP2 and also GIMAP5 as members of the membrane-anchored group bind nucleotides with high affinity and do not hydrolyze GTP on their own (see 3.1.3, 3.1.4). In contrast, the soluble GIMAP7 (see 3.1.3, 3.1.4) and GIMAP4 [102] bind guanine nucleotides with lower affinity and catalyze GTP hydrolysis.

Compared to membrane-anchored GIMAP2, GIMAP7 dimerizes with higher affinity in a GTP-dependent fashion (see 3.1.5). This affinity is in a similar range

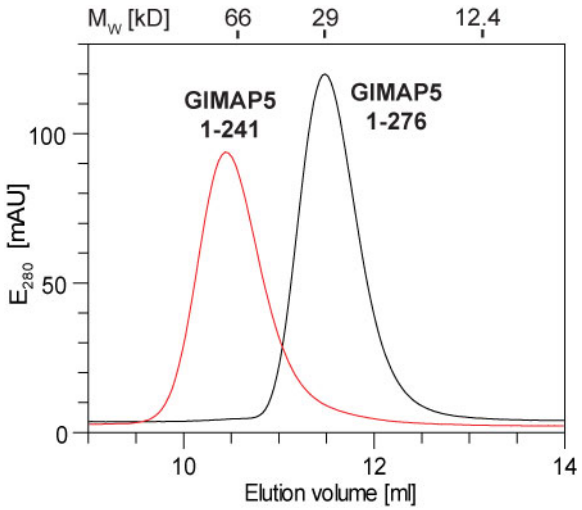

Figure 48: Dimerization of GIMAP5 upon removal of helix α7. Based on a multiple sequence alignment, a GIMAP5 construct was prepared which lacks helix α7 and the predicted TM anchor and encompasses residues 1-241. This construct was subjected to analytic SEC analysis (red trace). The SEC elution profile of GIMAP5$^{1\text{-}276}$, corresponding to the full cytoplasmic portion of GIMAP5 (black trace) is shown for comparison. Elution volumes of protein standards are indicated on top of the graph.

as described for BAR domain containing proteins which are recruited from the cytosol and dimerize at the membrane [172]. We furthermore provided evidence that GTP-binding in GIMAP2 is associated not only with dimerization via the G-interface, but also with oligomerization via the C-interface after displacement of helix α7 (see 3.2.6). Dimerization upon removal of helix α7 was also observed for GIMAP5 (Figure 48), indicating a conservation of the C-interface in membrane-anchored GIMAPs. Together with the findings that GIMAPs interact with Bcl2 family members [104], these data suggest that membrane-anchored GIMAPs form nucleotide-regulated oligomers on the surface of cellular organelles. These might act in a similar way as septin oligomers [44, 43] and organize the assembly of interaction partners. Since GTP is not hydrolyzed within the oligomers, these scaffolds would be intrinsically stable.

In contrast, GTP is hydrolyzed and removal of helix α7 does not lead to higher-order oligomerization in case of GIMAP7 (data not shown), indicating that GIMAP7 as a member of the soluble GIMAPs does not form stable scaffolds on its own. It is tempting to speculate that the soluble GIMAP subgroup controls the nucleotide loading state of membrane-anchored GIMAPs, and thereby their oligomerization status, by induction of nucleotide hydrolysis *in trans* upon hetero-dimerization. A similar scenario was suggested for the IRG resistance GTPases where a specific subgroup controls the assembly of the other subgroup [173].

4.3 OLIGOMERIZATION IN MEMBRANE-ANCHORED GIMAP2

Nucleotide-dependent oligomerization at membrane surfaces is a common feature in many G protein families, e.g. in the dynamins [60], the IRG resistance GTPases

[174] and the septin family [43]. Fitting of non-oligomerized G protein components into low resolution electron microscopy reconstruction of the oligomeric assemblies yielded structural models for helical dynamin [175, 176] and bacterial dynamin-like protein oligomers [61]. Mutagenesis-based modeling was employed to deduce the structure of the ring-like dynamin-related EHD2 oligomer [177]. Only in rare cases, linear oligomers were compatible with crystal formation, e.g. in case of the linear septin oligomer [44] or the stalk of the antiviral MxA GTPase [176].

In the present work, the high-resolution structures of monomeric and oligomerized GIMAP2 constructs are described, which elucidate the mechanism of nucleotide-mediated oligomerization in the GIMAP family. GTP-induced stabilization of switch I leads to low affinity dimerization of GIMAP2 via the G-interface (see 3.2.6). Such low affinity interaction is typical for proteins which are locally concentrated on a membrane surface and thereby restricted in their mobility [178, 179].

Switch II, on the other hand, is not involved in the G-interface (see 3.2.7), unlike in the corresponding G-interfaces of septin2 [44], Toc34 [47, 48] and dynamin1 [27] (Figure 49, see also Appendix D). Our structural analysis suggests that switch II of GIMAP2 instead controls the association of the G domain with helix $\alpha 7$, with Asp80 acting as γ-phosphate sensor. We suggest that in the presence of a suitable acceptor substrate such as membrane or an interaction partner, $\alpha 7$ is released from the G domain in a GTP-dependent fashion and oligomerization proceeds via the C-interface. The same might be true in the case of GIMAP5 (see Figure 48), but the absence of an aspartate residue equivalent to GIMAP2 Asp80 suggest a different mechanism for $\alpha 7$ release. A similar helix-release scenario has been suggested for CHMP proteins involved in multi-vesicular body genesis, where an auto-inhibitory C-terminal amphipathic helix prevents oligomerization on the membrane surface [180]. Furthermore, Arf and Sar GTPases release an N-terminal helix upon GTP-binding which inserts into the membrane and induces membrane remodeling [56, 59]. The amphipathic helix $\alpha 7$ might also interact with binding partners of GIMAPs, e.g. Bcl-2 family members [104], which are known to associate with each other via amphipathic helices that bind into a hydrophobic acceptor groove [181], and this interaction is strongly promoted in the presence of membranes [182]. The C-interface of GIMAPs is unique leading to a different architecture of the oligomer compared to septins [44] and dynamin/MxA [176].

4.4 THE FUNCTION OF GIMAP2 AT LIPID DROPLETS

GIMAP2 is the first described lymphocyte-specific LD component. Targeting of GIMAP2 to LDs is mediated by its two C-terminal hydrophobic segments (see 3.5.2). The presence of two such segments distinguishes GIMAP2 from other human GIMAPs or GIMAP orthologues in mice and rat. Human GIMAP1 and GIMAP5 contain one predicted C-terminal transmembrane helix (see also Figure 13) and have been found at different subcellular compartments, e.g. the Golgi apparatus and lysosomes, respectively (see 1.3.2, 1.3.6). On the other hand, LD targeting of caveolin and other proteins is mediated via long hydrophobic regions which might insert as hairpins into the LD monolayer and which do not share sequence similarity to the hydrophobic segments of GIMAP2 [183]. Furthermore, the overexpression experiments employing wild type and mutant GIMAP2 suggest

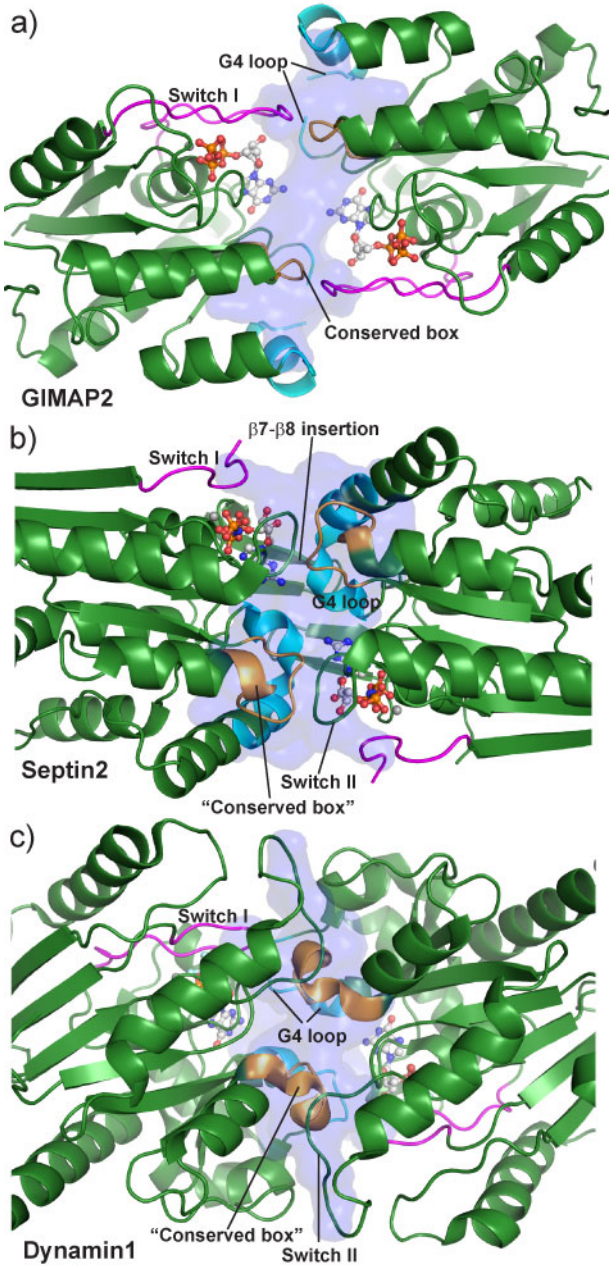

Figure 49: The G-interface in GTP-bound GIMAP2$^{1-234}$ (**a**), GMPPNP-bound septin2 (**b**, PDB 3ftq) and GDP-AlF$_x$-bound dynamin1 (**c**, PDB 2x2f). Switch I is colored in magenta, the region corresponding to the GIMAP conserved box in orange and the G4 loop in cyan. The light blue surfaces correspond to the dimer contact surfaces. Additional dimer interactions in septin and dynamin are indicated. The sequence stretches involved in dimerization are also indicated in the multiple sequence alignment in Appendix D.

a role of the GIMAP2 oligomer in LD formation (see 3.5.2). It is tempting to speculate that the function of the oligomer is related to cross-linking of LDs to each other or to their source membrane. This is supported by the architecture of the GIMAP2 oligomer with its C-terminal tails pointing in opposing directions (see

3.2.6). At the same time, the GIMAP2 oligomer might act as scaffold to assemble interaction partners on the LD membrane.

4.5 THE G-INTERFACE AND HIGHER ORDER EVOLUTIONARY RELATIONSHIPS OF GTPASES

The dimerization mode of GIMAP2 via the G-interface is shared with the dynamin, Toc and septin GTPases, with the associating G domains arranged in a similar head-to-head orientation (Figure 49, see also Appendix D). Corresponding regions of the respective G domains are used to build up the dimer, which are switch I, the GIMAP conserved box (equivalent to the trans stabilizing loop in dynamin 1 [27] and the loop encompassing residues 154-163 in mouse septin 2 [45]) and the G4 loop which in GIMAP2 and dynamin coordinates the nucleotide base *in trans* in a strikingly similar fashion (see also Figure 30). For dynamin and septin G domain dimers, further elements strengthen the G-interface interaction, namely switch II, the dynamin-specific loop or the septin-/Toc specific β7-β8 insertion.

Together with the group of L. Aravind (see also 2.6), the new structural information on GIMAP2 was used to re-analyze higher order evolutionary relationships of GTPases and how versions that operate on the membrane might have emerged from an ancestral TRAFAC class GTPase involved in translation-related functions. Previous sequence-structure analysis suggested that the septins, Tocs and GIMAPs are further related to GTPases of the Era family which bind single stranded 16S rRNA via their C-terminal KH domains and mediate the assembly of the 30S ribosomal subunit [41] (see also 1.1.3). Structures of GIMAP2, along with those of the Tocs, strongly support this relationship despite relatively low sequence similarity.

To systematically assess the higher order relationships between these G proteins, a relationship network was created, connecting pairs of G protein structures by edges representing best hits in DALIlite structure-comparison searches, profile-profile comparisons, best pairwise alignment of dimers, shared unique structural motifs, and specific conserved residue patterns. As result we were able to identify a distinct cluster of TRAFAC GTPases which in addition to the above mentioned proteins also includes the dynamins. Previously, the point of origin of the dynamin-like proteins was not entirely clear - but their dimerization mode, the residues interacting with guanine in the G5 motif (including a characteristic Asn found in several members of the dynamin-like group) and other distinctive structural features (see above) suggest that they belong to the same higher-order clade. Furthermore, this relationship network suggests that Tocs and GIMAPs are the closest sister groups. The septins and dynamin-like proteins are successive sister-groups to this clade, with all of them in turn being related to Era, to the exclusion of other TRAFAC class GTPases (Figure 50).

In terms of phyletic patterns, Era is most broadly distributed and plays an important role in assembly of the translation machinery in bacteria, eukaryotes and some archaea. However, the remaining members of the above-mentioned group show a more sporadic distribution, especially the GIMAPs. Hence, it is conceivable that they emerged later from the more widely distributed regulators of the translation machinery. Further, they are all unified not only by their dimerization mode, but

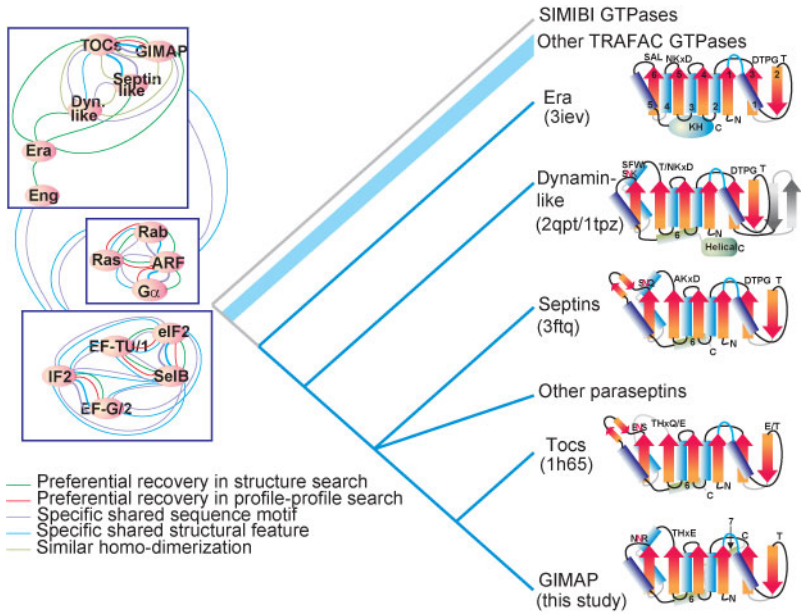

Figure 50: Higher-order relationship analysis of the GIMAP family. The panel to the left indicates the relationship network constructed based on different lines of evidence. The relative thickness of the edges between the nodes in the case of the specific sequence and structure features reflects relative number of such features which are shared. At the higher level the major groups are boxed for simplicity of illustration and the edges between them (i.e. those that define the TRAFAC class of GTPases) are shown. The panel to the right shows the inferred higher order relationships as a cladogram, along with the simplified topologies of representative members of each clade for which structures are available (note PDB id). For the dynamins a reconstructed structure of the ancestral version is depicted based on the two derived versions of the clade typified by EHD2 (2QPT) and IIGP (1TPZ). Also indicated on the topology are the typical forms of the different conserved GTPase motifs in a given group. The P-loop is colored blue. The strands and helices are numbered in the Era structure, with the additional helices indicated in the structures in which they occur. The Figure was kindly provided by L. Aravind, NIH.

also by the fact that they often tend to associate with lipid membranes and perform functions related to it. Hence, it is reasonable to infer that the common ancestor of the GIMAPs, Tocs, septin-like and dynamin-like GTPase evolved a distinctive membrane-binding mode via dimerization.

However, each group appears to have evolved certain distinctive specializations that are reflected in their structure and sequence. In this regard it is interesting to note that both septins and Tocs, which are closer to the GIMAPs, share the unique β7-β8 insertion after the G5 motif. This suggests that the GIMAPs lost this motif, whereas they acquired the α7 helix that is unique to them. This modification probably was critical for the emergence of their GTP-dependent interaction with the membrane or functional partners and subsequent oligomerization.

4.6 GIMAPS AND APOPTOSIS REGULATION IN LYMPHOCYTES

Several studies hint at a role of GIMAP family members in the apoptosis regulation during lymphocyte development and maintenance. Especially the gene targeting studies in mice suggest an anti-apoptotic function of GIMAP1 and GIMAP5, which belong to the membrane-anchored GIMAP subgroup (see also 4.2). Conditional knock out of GIMAP1 in lymphoid tissues leads to massive loss of peripheral B and T cells. Furthermore, in GIMAP5 knock out mice, only peripheral T cells are affected, but upon transplantation of GIMAP5$^{-/-}$ bone marrow in irradiated recipients, the B cell compartment is not reconstituted (see also 1.3.2, 1.3.6).

Our results from live cell microscopy show a partial lysosomal localization of GIMAP5 in the Jurkat T cell line (see 3.5.2). This is substantiated by a recent study which reported a lysosomal localization of GIMAP5 as well in T cells lines using immunostaining with antibodies against endogenous GIMAP5 [119]. Taken together, these data allow a exciting new view on the role of GIMAP5 in apoptotic processes during lymphocyte development and homeostasis. It is well known that lysosomes play a important role in the progression of apoptosis by release of cysteine and aspartate proteases, the so-called cathepsins [184, 185]. Further research in this direction might clarify the exact function of GIMAP5 in lymphocytes.

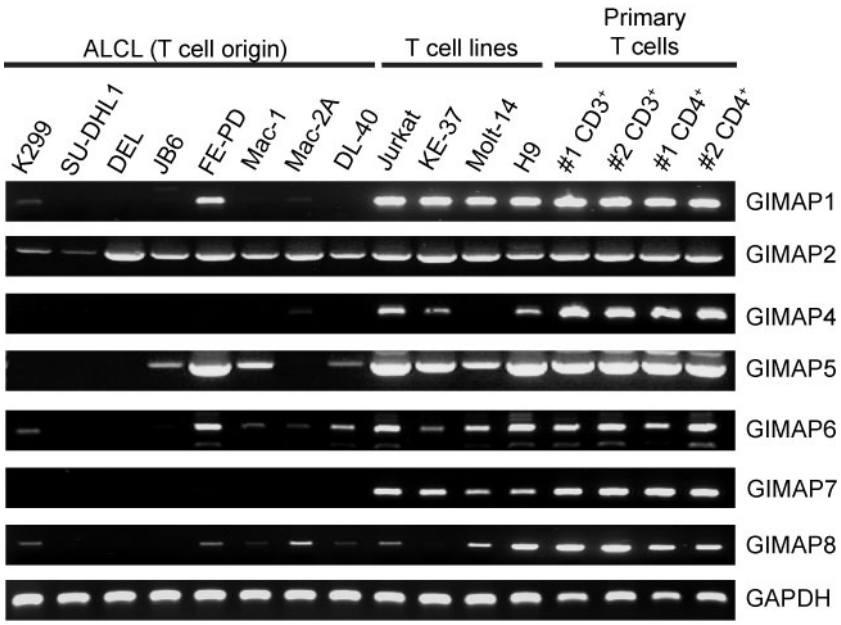

Figure 51: Downregulation of GIMAPs in ALCL cell lines. Expression of GIMAP mRNA in the indicated ALCL cell lines, T cell lines and primary T cells from two individuals were vizualized using RT-PCR. mRNA levels of the GAPDH housekeeping gene are shown as control. The Figure was kindly provided by Karl Köchert, AG Stephan Mathas, MDC Berlin.

How GIMAP1 and GIMAP5 are regulated during lymphocyte development and in which signaling pathway they are integrated is still unknown. However, in a co-expression screen, we showed a co-localization of GIMAP1 and GIMAP5 in the Jurkat T cell line (see 3.5.2). Even if this result is still preliminary and needs to be

corroborated using antibodies against the endogenous proteins in primary T cells, it could indicate the presence of a GIMAP1-GIMAP5 protein complex in the cell. Upon knockout of a single component of this protein complex, its anti-apoptotic function is abolished. This could explain the similar lymphopenic phenotype of the above-mentioned knock-out mouse models.

In contrast, targeting of GIMAP4 in mice lead to a delayed apopotosis phenotype, suggesting a function of GIMAP4 in the acceleration of apoptosis (see also 1.3.5). The somewhat mild phenotype of these mice could probably also be explained by a partial complementation of the GIMAP4 deficiency by GIMAP7. These two proteins are very similar in their primary structure, with 31% sequence identity and 55% similarity (see also Appendix C). Nevertheless, in our own preliminary gene expression studies by RT-PCR, which were perfomed by Karl Köchert from the group of Stephan Mathas at the MDC (see also 2.7), we could show a complete loss of the GIMAP4 and GIMAP7 mRNA in a series of anaplastic large cell lymphoma (ALCL) cell lines, a blood cancer which is derived from the T cell lineage (Figure 51). This result is supported by a recent study which showed down-regulation of GIMAP7 in tumor cell samples derived from ALCL patients [186]. Taken together, these data strongly suggest a pro-apoptotic function of GIMAP4 and GIMAP7 from the soluble subgroup of the GIMAP family.

APPENDIX A

INSTRUMENT	MANUFACTURER
Agarose Gel Electrophoresis System	OLS, Bremen, D
Amicon centrifugal filter devices	Millipore, Billerica, USA
Benchtop Centrifuge 5415 R	Eppendorf, Hamburg, D
Benchtop Centrifuge 5804 R	Eppendorf, Hamburg, D
Binocular Microscope MZ 7.5	Leica, Wetzlar, D
Chromatography column GSTrap HP 1 ml	GE Healthcare, Piscataway, USA
Chromatography column material GSH Sepharose 4B	GE Healthcare, Piscataway, USA
Chromatography columns Superdex 75 16/60, 26/60	GE Healthcare, Piscataway, USA
Chromatography columns Superdex 200 16/60, 26/60	GE Healthcare, Piscataway, USA
Chromatography columns XK 16/20, XK 26/20	GE Healthcare, Piscataway, USA
Confocal Laser Scanning Microscope 510	Zeiss, Göttingen, D
Centrifuge Avanti J-26 XP	Beckman Coulter, Krefeld, D
Electroporation cuvettes, 0.4 cm, red	Invitrogen, Darmstadt, D
Electroporatuion system Gene Pulser Xcell	Bio-Rad, München, D
Fluidizer	Microfluidics, Newton, USA
FPLC Äkta Prime Plus	GE Healthcare, Piscataway, USA
FPLC Äkta Purifier	GE Healthcare, Piscataway, USA
HPLC Ti-Series 1050	Hewlett Packard, Waldbronn, D
Isothermal Titration Calorimeter VP-ITC	GE Healthcare, Piscataway, USA

Table 13 –Continued on Next Page

Table 13 – Continued

INSTRUMENT	MANUFACTURER
Nucleosil 100 C18 HPLC pre-column	Knauer, Berlin, D
PCR Thermocycler	Biometra, Göttingen, D
Peristaltic Pump	Ismatec, Glattbrugg, CH
pH-Meter	Mettler-Toledo, Gießen, D
Reversed-phase ODS-2 hypersil HPLC column	Thermo Scientific, Dreieich, D
Scales	Sartorius, Göttingen, D
SDS PAGE System Xcell Sure Lock	Invitrogen, Darmstadt, D
Shaker Incubator	New Brunswick Scientific, Edison, USA
Ultracentrifuge Optima L-100 K	Beckman Coulter, Krefeld, D
Western Blot Module Xcell II	Invitrogen, Darmstadt, D

Table 13: Instruments used in the present work

ENZYME	MANUFACTURER
DNAse I	Roche, Mannheim, D
Gateway BP clonase enzyme mix	Invitrogen, Darmstadt, D
PreScission Protease	GE Healthcare, Piscataway, USA
Pfu DNA Polymerase	Stratagene, Amsterdam, NL
Restiction Endonucleases	New England Biolabs, Frankfurt am Main, D
T4 DNA Ligase	New England Biolabs, Frankfurt am Main, D

Table 14: Enzymes used in the present work

VECTOR	INSERT	5′ RESTRICTION SITE	3′ RESTRICTION SITE
pGex6P1	hsGIMAP1	BamHI	XhoI
pSkbLNB	hsGIMAP1	BamHI	XhoI
pEGFP-MCS	hsGIMAP1	BamHI	XhoI
pGex6P1	hsGIMAP1 1-275	BamHI	X hoI
pSkbLNB	hsGIMAP1 1-275	BamHI	X hoI

Table 19 –Continued on Next Page

Table 19 – Continued

VECTOR	INSERT	5′ RESTRICTION SITE	3′ RESTRICTION SITE
pGex6P1	hsGIMAP2	BamHI	XhoI
pSkbLNB	hsGIMAP2	BamHI	XhoI
pEGFP-MCS	hsGIMAP2	BamHI	XhoI
pmCherry	hsGIMAP2	XhoI	BamHI
pGex6P1	hsGIMAP2 1-260	BamHI	XhoI
pSkbLNB	hsGIMAP2 1-260	BamHI	XhoI
pGex6P1	hsGIMAP2 1-260 S54A	BamHI	XhoI
pGex6P1	hsGIMAP2 1-260 H87A	BamHI	XhoI
pGex6P1	h sGIMAP2 1-260 Q114A	BamHI	XhoI
pGex6P1	hsGIMAP2 1-260 Q114L	BamHI	XhoI
pGex6P1	hsGIMAP2 1-260 R117D	BamHI	XhoI
pmCherry	hsGIMAP2 R117D	XhoI	BamHI
pEGFP-MCS	hsGIMAP2 R117D	BamHI	XhoI
pGex6P1	hsGIMAP2 1-260 E149A	BamHI	XhoI
pGex6P1	hsGIMAP2 1-260 D150A	BamHI	XhoI
pGex6P1	hsGIMAP2 1-260 D150W	BamHI	XhoI
pmCherry	hsGIMAP2 R224D	XhoI	BamHI
pEGFP-MCS	hsGIMAP2 R224D	BamHI	XhoI
pGex6P1	hsGIMAP2 1-260 F239D	BamHI	XhoI
pGex6P1	hsGIMAP2 1-260 F239D L243D	BamHI	XhoI
pGex6P1	hsGIMAP2 21-260	BamHI	XhoI
pGex6P1	hsGIMAP2 1-260 C-term. 6xHis	BamHI	XhoI

Table 19 –Continued on Next Page

Table 19 – Continued

VECTOR	INSERT	5′ RESTRICTION SITE	3′ RESTRICTION SITE
pGex6P1	hsGIMAP2 231-260	BamHI	XhoI
pEGFP-MCS	hsGIMAP2 Delta223-260	BamHI	XhoI
pEGFP-MCS	hsGIMAP2 Delta234-260	BamHI	XhoI
pmCherry	hsGIMAP2 1-293	XhoI	BamHI
pmCherry	hsGIMAP2 251-337	XhoI	BamHI
pSkbLNB	hsGIMAP4	BamHI	XhoI
pEGFP-MCS	hsGIMAP4	BamHI	XhoI
pmCherry	hsGIMAP4	XhoI	BamHI
pGex6P1	hsGIMAP5	BamHI	XhoI
pSkbLNB	hsGIMAP5	BamHI	XhoI
pEGFP-MCS	hsGIMAP5	BamHI	XhoI
pmCherry	hsGIMAP5	XhoI	BamHI
pGex6P1	hsGIMAP5 1-276	BamHI	XhoI
pEGFP-MCS	hsGIMAP5 1-276	BamHI	XhoI
pGex6P1	hsGIMAP5 1-241	BamHI	XhoI
pGex6P1	hsGIMAP5 229-276	BamHI	XhoI
pmCherry	hsGIMAP5 261-307	XhoI	BamHI
pGex6P1	hsGIMAP7	BamHI	XhoI
pSkbLNB	hsGIMAP7	BamHI	XhoI
pEGFP-MCS	hsGIMAP7	BamHI	XhoI
pmCherry	hsGIMAP7	XhoI	BamHI
pmCherry	hsGIMAP7 1-210	XhoI	BamHI
pmCherry	hsGIMAP7 1-271	XhoI	BamHI
pGex6P1	hsGIMAP7 L100Q	BamHI	XhoI
pGex6P1	hsGIMAP7 L100Q E106K	BamHI	XhoI
pGex6P1	hsGIMAP7 R103D	BamHI	XhoI
pGex6P1	hsGIMAP7 E106K	BamHI	XhoI

Table 19 –Continued on Next Page

Table 19 – Continued

VECTOR	INSERT	5′ RESTRICTION SITE	3′ RESTRICTION SITE
pGex6P1	hsGIMAP7 E136W	BamHI	XhoI
pGex6P1	hsGIMAP8	EcoRI	XhoI
pSkbLNB	hsGIMAP8	EcoRI	XhoI
pEGFP-MCS	hsGIMAP8	EcoRI	XhoI
pSkbLNB	hsBcl2	EcoRI	XhoI
pmCherry	hsBcl2	XhoI	HindIII
pGex6P1	hsBcl2 1-213	EcoRI	XhoI
pGex6P1	hsBcl2L1 (Bcl-xL) 1-209	EcoRI	XhoI
pSkbLNB	hsBcl2L1 (Bcl-xL) 1-209	EcoRI	XhoI
pmCherry	h sBcl2L1 (Bcl-xL)	XhoI	EcoRI

Table 19: Constructs prepared in the present work

KIT	MANUFACTURER
2-Log DNA ladder	New England Biolabs, Frankfurt am Main, D
Additive Screen	Hampton Research, Aliso Viejo, USA
Bradford protein assay	Bio-Rad, München, D
GeneAmp dNTPs	Roche, Roche, Mannheim, D
NuPAGE LDS Sample Buffer (4x)	Invitrogen, Darmstadt, D
NuPAGE MES SDS Buffer Kit	Invitrogen, Darmstadt, D
NuPAGE Novex 4-12% Bis-Tris	Invitrogen, Darmstadt, D
QIAprep Spin Miniprep Kit	Qiagen, Hilden, D
QIAquick PCR Purification Kit	Qiagen, Hilden, D
QIAquick Gel Extraction Kit	Qiagen, Hilden, D
QuickChange	Stratagene, Stratagene, Amsterdam, NL
Roti-Fect	Carl Roth, Karlsruhe, D
The Classics Suite	Qiagen, Hilden, D
The JSCG+ Suite	Qiagen, Hilden, D
The PEGs Suite	Qiagen, Hilden, D
The PEGs II Suite	Qiagen, Hilden, D
The ProComplex Suite	Qiagen, Hilden, D

Table 15: Kits used in the present work

MEDIUM	COMPONENTS
DMEM	ordered from Invitrogen (10370-047)
Luria-Bertani (LB)	5 g/l yeast extract
	10 g/l tryptone
	5 g/l NaCl
M9 minimal medium	6 g/l Na_2HPO_4
	3 g/l KH_2PO_4
	1 g/l NH_4Cl
	0.5 g/l NaCl
	1 mM $MgSO_4$
	0.4% (w/v) glucose
	0.1 g/l riboflavin
	0.1 g/l niacin amide
	0.01 g/l pyridoxine
	0.1 g/l thiamine
Opti-MEM	ordered from Invitrogen (11058-021)
RPMI 1640	ordered from Invitrogen (21875-034)
Terrific broth (TB)	ordered from Roth (HP61.1)

Table 16: Media

BUFFER	COMPONENTS
Elution buffer	50 mM HEPES pH 7.5
	500 mM NaCl
	2.5 mM DTT
	20 mM GSH
GTPase buffer	20 mM HEPES pH 7.5
	150 mM NaCl
	2.5 mM DTT
	5 mM KCl
	5 mM $MgCl_2$
HPLC buffer	100 mM potassium phosphate pH 6.5
	10 mM TBAB
	7.5% (v/v) Acetonitril
ITC buffer	20 mM HEPES pH 7.5
	150 mM NaCl
	2.5 mM DTT
	2 mM $MgCl_2$
Lysis buffer	50 mM HEPES pH 7.5
	500 mM NaCl
	2.5 mM DTT
	0.1 mM Pefabloc SC
	1 µg/ml DNAse I
	1 mM $MgCl_2$
SEC buffer	10 mM HEPES pH 7.5
	150 mM NaCl
	2.5 mM DTT
Wash buffer I	50 mM HEPES pH 7.5
	500 mM NaCl
	2.5 mM DTT
Wash buffer II	50 mM HEPES pH 7.5
	500 mM NaCl
	2.5 mM DTT
	10 mM EDTA

Table 17: Buffers

GENE	IDENTIFIER	SOURCE
hsBax	4578562	Geneservice, Cambridge, UK
hsBcl2	4511027	Geneservice, Cambridge, UK
hsBcl2L1	IRAUp969F0148D	Imagenes, Berlin, D
hsGIMAP1	5220057	Geneservice, Cambridge, UK
hsGIMAP2	3950542	Geneservice, Cambridge, UK
hsGIMAP4	4701647	Geneservice, Cambridge, UK
hsGIMAP5	4337050	Geneservice, Cambridge, UK
hsGIMAP6	30336063	Geneservice, Cambridge, UK
hsGIMAP7	4837773	Geneservice, Cambridge, UK
hsGIMAP8	40001534	Geneservice, Cambridge, UK

Table 18: cDNA clones

B

APPENDIX B

B.1 PROTEIN STRUCTURE DETERMINATION

Here, a short overview of the principles of macromolecular X-ray crystallography is given. However, description of the complete background and derivation of all equations is beyond the scope of this work. For a in-depth description of the theoretical aspect of X-ray crystallography, the reader is referred to the appropriate literature [187], [188].

The smallest building block of a crystal is the asymmetric unit. By application of crystallographic symmetry operations such as inversions, rotations or reflections to the asymmetric unit, the unit cell of the crystal is generated. Translation of the unit cell in three dimensions makes up the macroscopic crystal. The dimensions of the unit cell together with the symmetry operations applied to the asymmetric unit defines the space group of the crystal. Altogether, there are 230 different space groups possible [189], but only 65 are found in protein crystals, since inversions or reflections cannot be applied to chiral molecules.

In a process called elastic or Thomson scattering, the X-ray beam is diffracted by electrons within the crystal. The direction of the diffracted X-ray beams contains information about the unit cell dimensions and the crystallographic symmetry. However, the goal of the crystallographic experiment is the description of the contents of the unit cell, the spatial arrangement of the atoms of the crystallized molecule. The intensities of the diffracted X-ray beams include this information. To be more specific, the intensities contain information about the electron density distribution in the unit cell, since the atom nuclei do not contribute to the scattering process.

The total scattering from a unit cell can be described as sum of the scattering by the individual atoms of the unit cell:

$$\vec{F}(S) = \sum_{j=1}^{n} f_j e^{\left(2\pi i \vec{r}_j \cdot \vec{S}\right)}, \tag{B.1}$$

where j is the number of atoms in the unit cell, $\vec{r}_j$ is the position of the atom j with respect to the origin, f_j is the atomic scattering factor, which can be looked up in tables, and $\vec{S} = \vec{s} - \vec{s_0}$ with $\vec{s}$ as the scattered wave vector and $\vec{s_0}$ as incident wave vector. $\vec{F}(S)$ is also called the structure factor, since it depends on the atomic structure of the unit cell.

A crystal consists of a large number of unit cells: n_1 in direction $\vec{a}$, n_2 in direction $\vec{b}$ and n_3 in direction $\vec{c}$. The position of each unit cell with respect to the

origin can be described as $t \cdot \vec{a} + u \cdot \vec{b} + v \cdot \vec{c}$. The total wave $\vec{K}(\vec{S})$ scattered by the crystal is obtained by summation over all unit cells:

$$\vec{K}(\vec{S}) = \vec{F}(S) \times \sum_{t=0}^{n_1} e^{(2\pi i t \vec{a} \cdot \vec{S})} \times \sum_{u=0}^{n_2} e^{(2\pi i u \vec{b} \cdot \vec{S})} \times \sum_{v=0}^{n_3} e^{(2\pi i v \vec{c} \cdot \vec{S})} \tag{B.2}$$

The value of $\vec{K}(\vec{S})$ is almost always equal to zero, unless $\vec{a} \cdot \vec{S}$ is an integer h, $\vec{b} \cdot \vec{S}$ is an integer k and $\vec{c} \cdot \vec{S}$ is an integer l. These conditions are also known as Laue conditions. Therefore, we see discrete intensity maxima of diffracted X-rays on the detector (the so-called reflections).

Instead of summing up the structure factor over all atoms in the unit cell as in Equation B.1, one can also integrate over all electrons in the unit cell:

$$\vec{F}(\vec{S}) = \int_{cell} \rho(\vec{r}) e^{(2\pi i \vec{r_j} \cdot \vec{S})} dv, \tag{B.3}$$

where $\rho(\vec{r})$ is the electron density at the position $\vec{r}$. With x, y and z as fractional coordinates in the unit cell and V as unit cell volume, dv equals $V \cdot dx\, dy\, dz$, and $\vec{r} \cdot \vec{S} = (\vec{a} \cdot x + \vec{b} \cdot y + \vec{c} \cdot z) \cdot \vec{S} = hx + ky + lz$. Now, $\vec{F}(\vec{S})$ can be written as $\vec{F}(h\,k\,l)$:

$$\vec{F}(h\,k\,l) = V \int_{x=0}^{1} \int_{y=0}^{1} \int_{z=0}^{1} \rho(x\,y\,z) e^{(-2\pi i(hx+ky+lz))} dx\, dy\, dz \tag{B.4}$$

$\vec{F}(h\,k\,l)$ is the Fourier transform of $\rho(x\,y\,z)$, but the reverse is also valid: $\rho(x\,y\,z)$ is the Fourier transform of $\vec{F}(h\,k\,l)$ as well. According to the Laue conditions, scattering occurs only in discrete directions, therefore the integration can be replaced by a summation. With $\vec{F} = |F| e^{i\alpha}$, we obtain

$$\rho(x\,y\,z) = \frac{1}{V} \sum_{h} \sum_{k} \sum_{l} |F(h\,k\,l)|\, e^{-2\pi i(hx+ky+lz)+i\alpha(h\,k\,l)}. \tag{B.5}$$

Now it is theoretically possible to calculate the electron density for every position in the unit cell. However, only the $|F(h\,k\,l)|$ terms are easily experimentally accessible, since they are proportional to the intensities which were measured on the detector. The phase angles $\alpha(h\,k\,l)$ cannot be determined straightforwardly from the diffraction pattern. This challenge is also referred to as the crystallographic phase problem.

Several methods are used to overcome the phase problem [190]. One method, called molecular replacement, requires knowledge of the structure of a homologous protein. This known structure can be used to approximate the phase angles of the crystallized protein and to solve its structure. As rule of thumb, the homologous protein should have at least a sequence identity of >25% to the target protein, and a r.m.s.d. of <2 Å of the C_α positions.

Another method, the isomorphous replacement procedure, implies the attachment of heavy atoms to the crystallized protein. If the crystals of the derivatized

protein are isomorphous to the native protein crystals, differences in the reflection amplitudes can be used as approximation of the heavy atom structure factor amplitudes. The position of the heavy atoms can then be determined using Patterson or direct methods. The protein phase angles can in turn be estimated using the heavy atom phase angles.

Nowadays, the most widely use approach to solve the phase problem, besides molecular replacement, is the utilization of anomalous scattering. If the energy of the incident X-ray photons come close to the absorption edge of an element (in most cases selenium, because selenomethionine-derivatized proteins are easy to produce), differences in reflection pairs $\vec{F}(h\,k\,l)$ and $\vec{F}(-h\,-k\,-l)$ occur, the so-called anomalous differences. These can be used to determine the location of the anomalous scatterers in the crystal (e.g. the selenium positions) and to approximate the phase angles.

APPENDIX C

C.1 STRUCTURE-BASED MULTIPLE SEQUENCE ALIGNMENT OF THE HUMAN GIMAPS

Protein sequences of human (hs) GIMAP1 (UniProt accession code Q8WWP7), GIMAP2 (Q9UG22), GIMAP4 (Q9NUV9), GIMAP5 (Q96F15), GIMAP6 (Q6P9H5), GIMAP7 (Q8NHV1) and GIMAP8 (Q8ND71) were aligned using ClustalW [191]. The three consecutive G domains of GIMAP8 were aligned individually. 100% type-conserved residues are colored in red and residues with at least 60% type-conservation in green. The secondary structure of GIMAP2 is shown on top with α-helices indicated as red barrels, β-strands as green arrows and loop regions as black lines. The flexible loop connecting helices α6 and α7 is shown as dashed line. The G-motifs including switch I and switch II are indicated. Amino acid residues in the G- and C-interface of GIMAP2 are indicated above the alignment by black and red dots, respectively. Residues of the GIMAP7 G-interface are shown as black triangles below the alignment. All GIMAP2 mutants described in this study are indicated. The C-terminal hydrophobic segments of GIMAP1, 2 and 5 are indicated as black boxes.

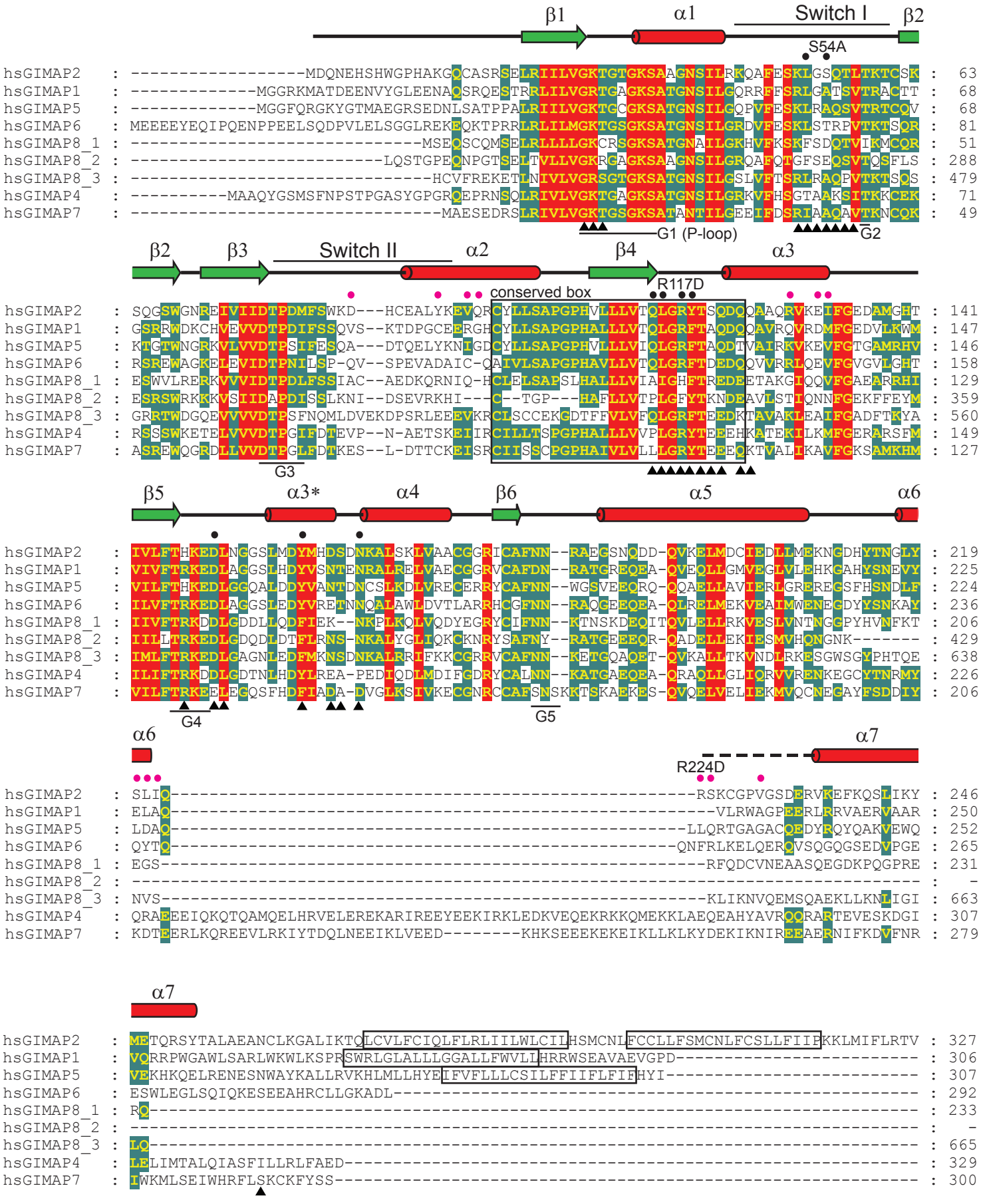
β1
α1
Switch I
β2
S54A
G1 (P-loop)
G2
β2
β3
Switch II
α2
β4
α3
R117D
conserved box
G3
β5
α3*
α4
β6
α5
α6
G4
G5
α6
α7
R224D
α7
hsGIMAP2 : ----------MDQNEHSHWGPHAKGQCASRSELRIILVGKTGTGKSAAGNSILRKQAFESKLGSQTLTKTCSK : 63
hsGIMAP1 : ----------MGGRKMATDEENVYGLEENAQSRQESTRRLILVGRTGAGKSATGNSILGQRRFFSRLGATSVTRACTT : 68
hsGIMAP5 : ----------MGGFQRGKYGTMAEGRSEDNLSATPPALRIILVGKTGCGKSATGNSILGQPVFESKLRAQSVTRTCQV : 68
hsGIMAP6 : MEEEEYEQIPQENPPEELSQDPVLELSGGLREKEQKTPRRLRLILMGKTGSGKSATGNSILGRDVFESKLSTRPVTKTSQR : 81
hsGIMAP8_1 : ----------MSEQSCQMSELRLLLLGKCRSGKSATGNAILGKHVFKSKFSDQTVIKMCQR : 51
hsGIMAP8_2 : ----------LQSTGPEQNPGTSELTVLLVGKRGAGKSAAGNSILGRQAFQTGFSEQSVTQSFLS : 288
hsGIMAP8_3 : ----------HCVFREKETLNIVLVGRSGTGKSATGNSILGSLVFTSRLRAQPVTKTSQS : 479
hsGIMAP4 : ----------MAAQYGSMSFNPSTPGASYGPGRQEPRNSQLRIVLVGKTGAGKSATGNSILGRKVFHSGTAAKSITKKCEK : 71
hsGIMAP7 : ----------MAESEDRSLRIVLVGKTGSGKSATANTILGEEIFDSRIAAQAVTKNCQK : 49
hsGIMAP2 : SQGSWGNREIVIIDTPDMFSWKD---HCEALYKEVQRCYLLSAPGPHVLLLVTQLGRYTSQDQQAAQRVKEIFGEDAMGHT : 141
hsGIMAP1 : GSRRWDKCHVEVVDTPDIFSSQVS--KTDPGCEERGHCYLLSAPGPHALLLVTQLGRFTAQDQQAVRQVRDMFGEDVLKWM : 147
hsGIMAP5 : KTGTWNGRKVLVVDTPSIFESQA---DTQELYKNIGDCYLLSAPGPHVLLLVIQLGRFTAQDTVAIRKVKEVFGTGAMRHV : 146
hsGIMAP6 : RSREWAGKELELVIDTPNILSP-QV--SPEVADAIC-QAIVLSAPGPHAVLLVTQLGRFTDEDQQVVRRLQEVFGVGVLGHT : 158
hsGIMAP8_1 : ESWVLRERKVVVIDTPDLFSSIAC--AEDKQRNIQ-HCLELSAPSLHALLLVIAIGHFTREDEETAKGIQQVFGAEARRHI : 129
hsGIMAP8_2 : ESRSWRKKKVSIIDAPDISSLKNI--DSEVRKHI---C--TGP---HAFLLVTPLGFYTKNDEAVLSTIQNNFGEKFFEYM : 359
hsGIMAP8_3 : GRRTWDGQEVVVVDTPSFNQMLDVEKDPSRLEEEVKRCLSCCEKGDTFFVLVFQLGRFTEEDKTAVAKLEAIFGADFTKYA : 560
hsGIMAP4 : RSSSWKETELVVVDTPGIFDTEVP--N-AETSKEIIRCILLTSPGPHALLLVVPLGRYTEEEHKATEKILKMFGERARSFM : 149
hsGIMAP7 : ASREWQGRDLLVVDTPGLFDTKES--L-DTTCKEISRCIISSCPGPHAIVLVLLLGRYTEEEQKTVALIKAVFGKSAMKHM : 127
hsGIMAP2 : IVLFTHKEDLNGGSLMDYMHDSDNKALSKLVAACGGRICAFNN--RAEGSNQDD-QVKELMDCIEDLLMEKNGDHYTNGLY : 219
hsGIMAP1 : VIVFTRKEDLAGGSLHDYVSNTENRALRELVAECGGRVCAFDN--RATGREQEA-QVEQLLGMVEGLVLEHKGAHYSNEVY : 225
hsGIMAP5 : VILFTHKEDLGGQALDDYVANTDNCSLKDLVRECERRYCAFNN--WGSVEEQRQ-QQAELLAVIERLGREREGSFHSNDLF : 224
hsGIMAP6 : ILVFTRKEDLAGGSLEDYVRETNNQALAWLDVTLARRHCGFNN--RAQGEEQEA-QLRELMEKVEAIMWENEGDYYSNKAY : 236
hsGIMAP8_1 : IIVFTRKDDLGDDLLQDFIEK--NKPLKQLVQDYEGRYCIFNN--KTNSKDEQITQVLELLRKVESLVNTNGGPYHVNFKT : 206
hsGIMAP8_2 : IILLTRKEDLGDQDLDTFLRNS-NKALYGLIQKCKNRYSAFNY--RATGEEEQR-QADELLEKIESMVHQNGNK------- : 429
hsGIMAP8_3 : IMLFTRKEDLGAGNLEDFMKNSDNKALRRIFKKCGRRVCAFNN--KETGQAQET-QVKALLTKVNDLRKESGWSGYPHTQE : 638
hsGIMAP4 : ILIFTRKDDLGDTNLHDYLREA-PEDIQDLMDIFGDRYCALNN--KATGAEQEA-QRAQLLGLIQRVVRENKEGCYTNRMY : 226
hsGIMAP7 : VILFTRKEELEGQSFHDFIADA-DVGLKSIVKECGNRCCAFSNSKKTSKAEKES-QVQELVELIEKMVQCNEGAYFSDDIY : 206
hsGIMAP2 : SLIQ----------RSKCGPVGSDERVKEFKQSLIKY : 246
hsGIMAP1 : ELAQ----------VLRWAGPEERLRRVAERVAAR : 250
hsGIMAP5 : LDAQ----------LLQRTGAGACQEDYRQYQAKVEWQ : 252
hsGIMAP6 : QYTQ----------QNFRLKELQERQVSQGQGSEDVPGE : 265
hsGIMAP8_1 : EGS----------RFQDCVNEAASQEGDKPQGPRE : 231
hsGIMAP8_2 : ---------- : -
hsGIMAP8_3 : NVS----------KLIKNVQEMSQAEKLLKNLIGI : 663
hsGIMAP4 : QRAEEEIQKQTQAMQELHRVELEREKARIREEYEEKIRKLEDKVEQEKRKKQMEKKLAEQEAHYAVRQQRARTEVESKDGI : 307
hsGIMAP7 : KDTEERLKQREEVLRKIYTDQLNEEIKLVEED--------KHKSEEEKEKEIKLLKLKYDEKIKNIREEAERNIFKDVFNR : 279
hsGIMAP2 : METQRSYTALAEANCLKGALIKTQLCVLFCIQLFLRLIILWLCIIHSMCNLFCCLLFSMCNLFCSLLFIIPKKLMIFLRTV : 327
hsGIMAP1 : VQRRPWGAWLSARLWKWLKSPRSWRLGLALLLGGALLFWVLIHRRWSEAVAEVGPD---------- : 306
hsGIMAP5 : VEKHKQELRENESNWAYKALLRVKHLMLLHYEIFVFLLLCSILFFIIFLFIFHYI---------- : 307
hsGIMAP6 : ESWLEGLSQIQKESEEAHRCLLGKADL---------- : 292
hsGIMAP8_1 : RQ---------- : 233
hsGIMAP8_2 : ---------- : -
hsGIMAP8_3 : LQ---------- : 665
hsGIMAP4 : LELIMTALQIASFILLRLFAED---------- : 329
hsGIMAP7 : IWKMLSEIWHRFLSKCKFYSS---------- : 300
hsGIMAP2 : IRLERKTPRL : 337

APPENDIX D

D.1 STRUCTURE-BASED MULTIPLE SEQUENCE ALIGNMENT OF GIMAP2, SEPTIN AND DYNAMINS

Based on a structural superimposition of the G domains, protein sequences of human (hs) GIMAP2 (Uniprot accession code Q9UG22, PDB 2xtn), pea (ps) Toc34 (Q41009, PDB 3bb1), mouse (mm) Septin2 (Q41009, PDB 3ftq), mouse EHD2 (Q8BH64, PDB 2qpt) and human Dynamin1 (Q05193, PDB 2x2f) were manually aligned. 100% type-conserved amino acid residues are shown in red, at least 60% type-conserved residues in green. The secondary structure of GIMAP2 is shown above the alignment with β-strands shown as green arrows, α-helices as red barrels and loops as black lines. Secondary structure elements different from GIMAP2 are shown and annotated below the alignment, and colored in gray. The G motifs involved in nucleotide binding and switch I and II regions are indicated. Regions involved in dimerization which are common in the proteins are highlighted by magenta boxes. Additional dimerization motifs are underlined red. The switch II regions of Toc34, Septin2 and Dynamin all participate in dimerization, but not switch II of GIMAP2. On the other hand, the β6-β7 insertion of Septin2, but not of Toc34, is involved in dimerization.

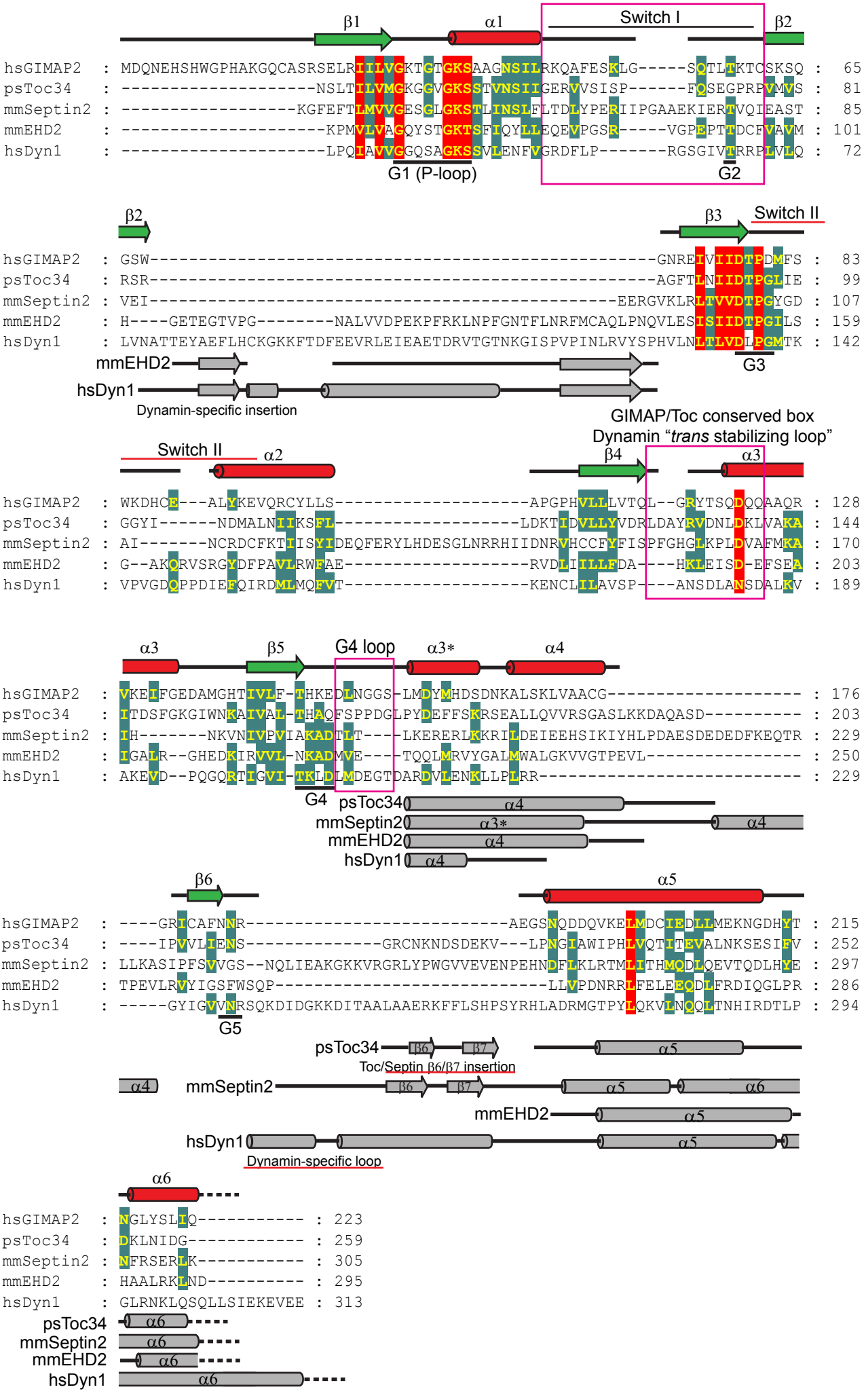
β1
α1
Switch I
β2
G1 (P-loop)
G2
β3
Switch II
G3
mmEHD2
hsDyn1
Dynamin-specific insertion
GIMAP/Toc conserved box
Dynamin "trans stabilizing loop"
α2
β4
α3
α3
β5
G4 loop
α3*
α4
G4
psToc34
mmSeptin2
mmEHD2
hsDyn1
β6
α5
G5
psToc34
β6
β7
Toc/Septin β6/β7 insertion
α5
α4
mmSeptin2
β6
β7
α5
α6
mmEHD2
α5
hsDyn1
α5
Dynamin-specific loop
α6
psToc34
mmSeptin2
mmEHD2
hsDyn1
α6

APPENDIX E

E.1 LIST OF ABBREVIATIONS

ADP	Adenosine-5′-diphosphate
AIRE	Autoimmune regulator
Amp	Ampicillin
AMP-PNP	Adenosine 5′-[β,γ-imido]triphosphate
ATP	Adenosine-5′-triphosphate
Aig1	AvrRpt2-induced gene 1
ALCL	Anaplastic large cell lymphoma
Arf	ADP ribosylation factor
AUC	Analytical ultracentrifugation
BAFF	B cell activating factor belonging to the TNF family
BAR domain	Bin-Amphiphysin-Rvs domain
BBDP	Biobreeding diabetes-prone
BCR	B cell receptor
BESSY	Berliner Elektronenspeicherring-Gesellschaft für Synchrotronstrahlung
BODIPY	Boron-dipyrromethene
C-terminus	Carboxy-terminus
CB	Conserved box
CCD	Charge-coupled device
CCP4	Collaborative Computational Project No. 4
CCR	CC chemokine receptor
CD	Cluster of differentiation
CHMP	Charged multivesicular body protein
CLP	Common lymphoid progenitor
CMP	Common myeloid progenitor
CV	Column volume
CXCL	CXC chemokine ligand
CXCR	CXC chemokine receptor
DC	Dendritic cell
DN	Double negative
DP	Double positive
DTT	Dithiothreitol

Table 20 –Continued on Next Page

Table 20 – Continued

E	Extinction
EBF	Early B cell factor
EDTA	Ethylenediaminetetraacetic acid
EF	Elongation factor
EGFP	Enhanced green fluorescent protein
EH	Epsin-homology
EHD	EH-domain containing
ER	Endoplasmic reticulum
FMP	Leibniz-Institut für Molekulare Pharmakologie Berlin-Buch
FOXP3	Forkhead box P3
G domain	Guanine nucleotide binding domain
G protein	Guanine nucleotide binding protein
GAP	GTPase-activating protein
GDI	Guanine nucleotide dissociation inhibitor
GDP	Guanosine-5′-diphosphate
GEF	Guanine nucleotide exchange factor
GIMAP	GTPase of immunity-associated proteins
GMP	Granulocyte/monocyte precursor
GMP-PNP	Guanosine-5′-[β,γ-imido]triphosphate
GNBP	Guanine nucleotide binding protein
GPCR	G protein coupled receptor
GSH	Reduced glutathione
GST	Glutathione-S-transferase
GTP	Guanosine-5′-triphosphate
GTP-γ-S	Guanosine-5′-O-[γ-thio]triphosphate
HEPES	(4-(2-hydroxyethyl)-1-piperazineethanesulfonic acid
HPLC	High pressure liquid chromatography
HS	Hydrophobic segment
HSC	Hematopoietic stem cell
IAN	Immunity-associated nucleotide binding protein
Ig	Immunoglobulin
IL	Interleukine
IPTG	Isopropyl-β-D-thiogalactopyranosid
ITC	Isothermal titration calorimetry
IRG	Immunity-related GTPases
Kan	Kanamycin
KH	K homology

Table 20 –Continued on Next Page

Table 20 – Continued

LAMP1	Lysosomal-associated membrane protein 1
LB	Lysogeny broth
LD	Lipid droplet
MDC	Max-Delbrück-Centrum für Molekulare Medizin Berlin-Buch
MEM	Minimum essential medium
MEP	Megakaryocyte/erythrocyte progenitor
MHC	Major histocompatibility complex
MOPS	3-(N-morpholino)propanesulfonic acid
MxA	Myxovirus resistance protein A
N-terminus	Amino-terminus
NF-κB	Nuclear factor κB
NK cell	Natural killer cell
NTPase	Nucleoside-5′-triphosphatase
OD	Optical density
P-loop	Phosphate-binding loop
PCR	Polymerase chain reaction
PDB	Protein Data Bank
PEG	Polyethylene glycol
PKN	Protein kinase N
PSGL1	Platelet-selectin glycoprotein ligand 1
Rag	Recombination activating gene
RBD	Ras binding domain
Raf	Rat fibrosarcoma
Ran	Ras-related nuclear protein
Rap	Ras-related protein
Ras	Rat sarcoma
RPMI	Roswell Park Memorial Institute medium
RT-PCR	Reverse transcriptase polymerase chain reaction
Sar1	Secretion-associated and Ras-related protein 1
SDS PAGE	Sodiumdodecylsulfate polyacrylamide gel electrophoresis
SEC	Size-exclusion chromatography
SeMet	Selenomethionine
SIMIBI	Signal recognition/MinD/BioD
SP	Single positive
SRP	Signal recognition particle
STAT	Signal transducer and activator of transcription
T1D	Type 1 diabetes

Table 20 –Continued on Next Page

Table 20 – Continued

TB	Terrific broth
TBC domain	Tre-2/Bub2/Cdc16 domain
TCR	T cell receptor
TEC	Thymic epithelial cell
TGF	Transforming growth factor
TLS	Translation, libration, screw rotation displacement
TNF	Tumor necrosis factor
Toc	Translocon at the outer envelope membrane of chloroplasts
TRAFAC	Translation factor associated
VDJ	Variable, diversity, joining segments

Table 20: List of abbreviations

E.2 AMINO ACID ABBREVIATIONS

For amino acids, the one and three letter code was used: A, Ala: alanine; C, Cys: cysteine; D, Asp: aspartate; E, Glu: glutamate; F, Phe: phenylalanine; G, Gly: glycine; H, His: histidine; I, Ile: isoleucine; K, Lys: lysine; L, Leu: leucine; M, Met: methionine; N, Asn: asparagine; P, Pro: proline; Q, Gln: glutamine; R, Arg: arginine; S, Ser: serine; T, Thr: threonine; V, Val: valine; W, Trp: tryptophane; Y, Tyr: tyrosine; x: any amino acid.

BIBLIOGRAPHY

[1] E. V. Koonin, Y. I. Wolf, and L. Aravind. Protein fold recognition using sequence profiles and its application in structural genomics. *Adv Protein Chem*, 54:245–275, 2000.

[2] H. R. Bourne, D. A. Sanders, and F. McCormick. The gtpase superfamily: a conserved switch for diverse cell functions. *Nature*, 348(6297):125–132, 1990.

[3] I. R. Vetter and A. Wittinghofer. The guanine nucleotide-binding switch in three dimensions. *Science*, 294(5545):1299–1304, 2001.

[4] E. F. Pai, U. Krengel, G. A. Petsko, R. S. Goody, W. Kabsch, and A. Wittinghofer. Refined crystal structure of the triphosphate conformation of h-ras p21 at 1.35 a resolution: implications for the mechanism of gtp hydrolysis. *EMBO J*, 9(8):2351–2359, 1990.

[5] W. Kabsch, W. H. Gast, G. E. Schulz, and R. Leberman. Low resolution structure of partially trypsin-degraded polypeptide elongation factor, ef-tu, from escherichia coli. *J Mol Biol*, 117(4):999–1012, 1977.

[6] J. L. Bos. The ras gene family and human carcinogenesis. *Mutat Res*, 195(3):255–271, 1988.

[7] Alfred Wittinghofer and Herbert Waldmann. Ras - a molecular switch involved in tumor formation. *Angew. Chem. Int. Ed.*, 39:4192–4214, 2000.

[8] S. R. Sprang. G protein mechanisms: insights from structural analysis. *Annu Rev Biochem*, 66:639–678, 1997.

[9] N. Nassar, G. Horn, C. Herrmann, A. Scherer, F. McCormick, and A. Wittinghofer. The 2.2 a crystal structure of the ras-binding domain of the serine/threonine kinase c-raf1 in complex with rap1a and a gtp analogue. *Nature*, 375(6532):554–560, 1995.

[10] M. E. Pacold, S. Suire, O. Perisic, S. Lara-Gonzalez, C. T. Davis, E. H. Walker, P. T. Hawkins, L. Stephens, J. F. Eccleston, and R. L. Williams. Crystal structure and functional analysis of ras binding to its effector phosphoinositide 3-kinase gamma. *Cell*, 103(6):931–943, 2000.

[11] R. Maesaki, K. Ihara, T. Shimizu, S. Kuroda, K. Kaibuchi, and T. Hakoshima. The structural basis of rho effector recognition revealed by the crystal structure of human rhoa complexed with the effector domain of pkn/prk1. *Mol Cell*, 4(5):793–803, 1999.

[12] Alfred Wittinghofer. Phosphoryl transfer in ras proteins, conclusive or elusive? *Trends Biochem Sci*, 31(1):20–23, 2006.

[13] Sushmita D Lahiri, Guofeng Zhang, Debra Dunaway-Mariano, and Karen N Allen. The pentacovalent phosphorus intermediate of a phosphoryl transfer reaction. *Science*, 299(5615):2067–2071, Mar 2003.

[14] G. Michael Blackburn, Nicholas H Williams, Steven J Gamblin, and Stephen J Smerdon. Comment on "the pentacovalent phosphorus intermediate of a phosphoryl transfer reaction". *Science*, 301(5637):1184; author reply 1184, Aug 2003.

[15] J. Feuerstein, R. S. Goody, and M. R. Webb. The mechanism of guanosine nucleotide hydrolysis by p21 c-ha-ras. the stereochemical course of the gtpase reaction. *J Biol Chem*, 264(11):6188–6190, 1989.

[16] K. A. Maegley, S. J. Admiraal, and D. Herschlag. Ras-catalyzed hydrolysis of gtp: a new perspective from model studies. *Proc Natl Acad Sci U S A*, 93(16):8160–8166, 1996.

[17] Guangpu Li and Xuejun C Zhang. Gtp hydrolysis mechanism of ras-like gtpases. *J Mol Biol*, 340(5):921–932, 2004.

[18] Johannes L Bos, Holger Rehmann, and Alfred Wittinghofer. Gefs and gaps: critical elements in the control of small g proteins. *Cell*, 129(5):865–877, 2007.

[19] K. Scheffzek, M. R. Ahmadian, W. Kabsch, L. Wiesmüller, A. Lautwein, F. Schmitz, and A. Wittinghofer. The ras-rasgap complex: structural basis for gtpase activation and its loss in oncogenic ras mutants. *Science*, 277(5324):333–338, 1997.

[20] Astrid Kraemer, Thilo Brinkmann, Ina Plettner, Roger Goody, and Alfred Wittinghofer. Fluorescently labelled guanine nucleotide binding proteins to analyse elementary steps of gap-catalysed reactions. *J Mol Biol*, 324(4):763–774, Dec 2002.

[21] T. Schweins, M. Geyer, K. Scheffzek, A. Warshel, H. R. Kalbitzer, and A. Wittinghofer. Substrate-assisted catalysis as a mechanism for gtp hydrolysis of p21ras and other gtp-binding proteins. *Nat Struct Biol*, 2(1):36–44, 1995.

[22] J. J. Tesmer, D. M. Berman, A. G. Gilman, and S. R. Sprang. Structure of rgs4 bound to alf4–activated g(i alpha1): stabilization of the transition state for gtp hydrolysis. *Cell*, 89(2):251–261, Apr 1997.

[23] Xiaojing Pan, Sudharshan Eathiraj, Mary Munson, and David G Lambright. Tbc-domain gaps for rab gtpases accelerate gtp hydrolysis by a dual-finger mechanism. *Nature*, 442(7100):303–306, 2006.

[24] Michael J Seewald, Carolin Körner, Alfred Wittinghofer, and Ingrid R Vetter. Rangap mediates gtp hydrolysis without an arginine finger. *Nature*, 415(6872):662–666, 2002.

[25] Oliver Daumke, Michael Weyand, Partha P Chakrabarti, Ingrid R Vetter, and Alfred Wittinghofer. The gtpase-activating protein rap1gap uses a catalytic asparagine. *Nature*, 429(6988):197–201, 2004.

[26] Andrea Scrima, Christoph Thomas, Delia Deaconescu, and Alfred Wittinghofer. The rap-rapgap complex: Gtp hydrolysis without catalytic glutamine and arginine residues. *EMBO J*, 27(7):1145–1153, 2008.

[27] Joshua S Chappie, Sharmistha Acharya, Marilyn Leonard, Sandra L Schmid, and Fred Dyda. G domain dimerization controls dynamin's assembly-stimulated gtpase activity. *Nature*, 465(7297):435–440, 2010.

[28] Andrea Scrima and Alfred Wittinghofer. Dimerisation-dependent gtpase reaction of mnme: how potassium acts as gtpase-activating element. *EMBO J*, 25(12):2940–2951, 2006.

[29] J. John, R. Sohmen, J. Feuerstein, R. Linke, A. Wittinghofer, and R. S. Goody. Kinetics of interaction of nucleotides with nucleotide-free h-ras p21. *Biochemistry*, 29(25):6058–6065, 1990.

[30] J. Kleineke, C. Düls, and H. D. Söling. Subcellular compartmentation of guanine nucleotides and functional relationships between the adenine and guanine nucleotide systems in isolated hepatocytes. *FEBS Lett*, 107(1):198–202, Nov 1979.

[31] Detlef D Leipe, Yuri I Wolf, Eugene V Koonin, and L. Aravind. Classification and evolution of p-loop gtpases and related atpases. *J Mol Biol*, 317(1):41–72, 2002.

[32] C. G. Noble and H. Song. Structural studies of elongation and release factors. *Cell Mol Life Sci*, 65(9):1335–1346, 2008.

[33] T. Martin Schmeing, Rebecca M Voorhees, Ann C Kelley, Yong-Gui Gao, Frank V Murphy, John R Weir, and V. Ramakrishnan. The crystal structure of the ribosome bound to ef-tu and aminoacyl-trna. *Science*, 326(5953):688–694, 2009.

[34] Yong-Gui Gao, Maria Selmer, Christine M Dunham, Albert Weixlbaumer, Ann C Kelley, and V. Ramakrishnan. The structure of the ribosome with elongation factor g trapped in the posttranslocational state. *Science*, 326(5953):694–699, 2009.

[35] Katrin Karbstein, Stefanie Jonas, and Jennifer A Doudna. An essential gtpase promotes assembly of preribosomal rna processing complexes. *Mol Cell*, 20(4):633–643, 2005.

[36] David J Comartin and Eric D Brown. Non-ribosomal factors in ribosome subunit assembly are emerging targets for new antibacterial drugs. *Curr Opin Pharmacol*, 6(5):453–458, 2006.

[37] John Buglino, Vincent Shen, Payam Hakimian, and Christopher D Lima. Structural and biochemical analysis of the obg gtp binding protein. *Structure*, 10(11):1581–1592, 2002.

[38] Bo Huang, Hao Wu, Ning Hao, Fabian Blombach, John van der Oost, Xuemei Li, Xuejun C Zhang, and Zihe Rao. Functional study on gtp hydrolysis by

the gtp-binding protein from sulfolobus solfataricus, a member of the hflx family. *J Biochem*, 148(1):103–113, 2010.

[39] Hao Wu, Lei Sun, Fabian Blombach, Stan J J Brouns, Ambrosius P L Snijders, Kristina Lorenzen, Robert H H van den Heuvel, Albert J R Heck, Sheng Fu, Xuemei Li, Xuejun C Zhang, Zihe Rao, and John van der Oost. Structure of the ribosome associating gtpase hflx. *Proteins*, 78(3):705–713, 2010.

[40] Catherine E Caldon and Paul E March. Function of the universally conserved bacterial gtpases. *Curr Opin Microbiol*, 6(2):135–139, 2003.

[41] Chao Tu, Xiaomei Zhou, Joseph E Tropea, Brian P Austin, David S Waugh, Donald L Court, and Xinhua Ji. Structure of era in complex with the 3' end of 16s rrna: implications for ribosome biogenesis. *Proc Natl Acad Sci U S A*, 106(35):14843–14848, 2009.

[42] Victoria L Robinson, Jihwan Hwang, Eileen Fox, Masayori Inouye, and Ann M Stock. Domain arrangement of der, a switch protein containing two gtpase domains. *Structure*, 10(12):1649–1658, 2002.

[43] Christine S Weirich, Jan P Erzberger, and Yves Barral. The septin family of gtpases: architecture and dynamics. *Nat Rev Mol Cell Biol*, 9(6):478–489, 2008.

[44] M. Sirajuddin, M. Farkasovsky, F. Hauer, D. Kuhlmann, I.G. Macara, M. Weyand, H. Stark, and A. Wittinghofer. Structural insight into filament formation by mammalian septins. *Nature*, 449(7160):311–315, 2007.

[45] Minhajuddin Sirajuddin, Marian Farkasovsky, Eldar Zent, and Alfred Wittinghofer. Gtp-induced conformational changes in septins and implications for function. *Proc Natl Acad Sci U S A*, 106(39):16592–16597, 2009.

[46] Mislav Oreb, Ivo Tews, and Enrico Schleiff. Policing tic 'n' toc, the doorway to chloroplasts. *Trends Cell Biol*, 18(1):19–27, 2008.

[47] Yuh-Ju Sun, Farhad Forouhar, Hsou min Li Hm, Shuh-Long Tu, Yi-Hong Yeh, Sen Kao, Hui-Lin Shr, Chia-Cheng Chou, Chinpan Chen, and Chwan-Deng Hsiao. Crystal structure of pea toc34, a novel gtpase of the chloroplast protein translocon. *Nat Struct Biol*, 9(2):95–100, 2002.

[48] Patrick Koenig, Mislav Oreb, Anja Höfle, Sabine Kaltofen, Karsten Rippe, Irmgard Sinning, Enrico Schleiff, and Ivo Tews. The gtpase cycle of the chloroplast import receptors toc33/toc34: implications from monomeric and dimeric structures. *Structure*, 16(4):585–596, 2008.

[49] T. L. Reuber and F. M. Ausubel. Isolation of arabidopsis genes that differentiate between resistance responses mediated by the rps2 and rpm1 disease resistance genes. *Plant Cell*, 8(2):241–249, 1996.

[50] Laura Biller, Paul H Davis, Manuela Tillack, Jenny Matthiesen, Hannelore Lotter, Samuel L Stanley, Egbert Tannich, and Iris Bruchhaus. Differences in the transcriptome signatures of two genetically related entamoeba histolytica cell lines derived from the same isolate with different pathogenic properties. *BMC Genomics*, 11:63, 2010.

[51] Meng-Tse Gabe Lee, Ashwini Mishra, and David G Lambright. Structural mechanisms for regulation of membrane traffic by rab gtpases. *Traffic*, 10(10):1377–1389, 2009.

[52] Sarah J Heasman and Anne J Ridley. Mammalian rho gtpases: new insights into their functions from in vivo studies. *Nat Rev Mol Cell Biol*, 9(9):690–701, 2008.

[53] Stephen R Sprang, Zhe Chen, and Xinlin Du. Structural basis of effector regulation and signal termination in heterotrimeric galpha proteins. *Adv Protein Chem*, 74:1–65, 2007.

[54] John J G Tesmer. The quest to understand heterotrimeric g protein signaling. *Nat Struct Mol Biol*, 17(6):650–652, 2010.

[55] Alison K Gillingham and Sean Munro. The small g proteins of the arf family and their regulators. *Annu Rev Cell Dev Biol*, 23:579–611, 2007.

[56] Marcus C S Lee, Lelio Orci, Susan Hamamoto, Eugene Futai, Mariella Ravazzola, and Randy Schekman. Sar1p n-terminal helix initiates membrane curvature and completes the fission of a copii vesicle. *Cell*, 122(4):605–617, 2005.

[57] A. Marx, J. Müller, and E. Mandelkow. The structure of microtubule motor proteins. *Adv Protein Chem*, 71:299–344, 2005.

[58] H. Lee Sweeney and Anne Houdusse. Structural and functional insights into the myosin motor mechanism. *Annu Rev Biophys*, 39:539–557, 2010.

[59] Thomas J Pucadyil and Sandra L Schmid. Conserved functions of membrane active gtpases in coated vesicle formation. *Science*, 325(5945):1217–1220, 2009.

[60] Gerrit J K Praefcke and Harvey T McMahon. The dynamin superfamily: universal membrane tubulation and fission molecules? *Nat Rev Mol Cell Biol*, 5(2):133–147, 2004.

[61] Harry H Low, Carsten Sachse, Linda A Amos, and Jan Löwe. Structure of a bacterial dynamin-like protein lipid tube provides a mechanism for assembly and membrane curving. *Cell*, 139(7):1342–1352, 2009.

[62] Pascal F Egea, Robert M Stroud, and Peter Walter. Targeting proteins to membranes: structure of the signal recognition particle. *Curr Opin Struct Biol*, 15(2):213–220, 2005.

[63] Pascal F Egea, Shu-Ou Shan, Johanna Napetschnig, David F Savage, Peter Walter, and Robert M Stroud. Substrate twinning activates the signal recognition particle and its receptor. *Nature*, 427(6971):215–221, 2004.

[64] I. Hayashi, T. Oyama, and K. Morikawa. Structural and functional studies of mind atpase: implications for the molecular recognition of the bacterial cell division apparatus. *EMBO J*, 20(8):1819–1828, 2001.

[65] Martin F Flajnik and Masanori Kasahara. Origin and evolution of the adaptive immune system: genetic events and selective pressures. *Nat Rev Genet*, 11(1):47–59, 2010.

[66] Kenneth M. Murphy, Paul Travers, and Mark Walport. *Janeways Immunobiology*. Garland Science, 7th edition, 2007.

[67] Gary W Litman, Jonathan P Rast, and Sebastian D Fugmann. The origins of vertebrate adaptive immunity. *Nat Rev Immunol*, 10(8):543–553, 2010.

[68] Bianca Blom and Hergen Spits. Development of human lymphoid cells. *Annu Rev Immunol*, 24:287–320, 2006.

[69] F. M. Burnet. *The Clonal Selection Theory of Acquired Immunity*. Cambridge University Press, 1959.

[70] Martin Gellert. V(d)j recombination: Rag proteins, repair factors, and regulation. *Annu Rev Biochem*, 71:101–132, 2002.

[71] S. Tonegawa. Somatic generation of antibody diversity. *Nature*, 302(5909):575–581, 1983.

[72] Sue J Sohn, Arvind Rajpal, and Astar Winoto. Apoptosis during lymphoid development. *Curr Opin Immunol*, 15(2):209–216, 2003.

[73] Takashi Nagasawa. Microenvironmental niches in the bone marrow required for b-cell development. *Nat Rev Immunol*, 6(2):107–116, 2006.

[74] Colin H Martin, Iannis Aifantis, M. Lucila Scimone, Ulrich H von Andrian, Boris Reizis, Harald von Boehmer, and Fotini Gounari. Efficient thymic immigration of b220+ lymphoid-restricted bone marrow cells with t precursor potential. *Nat Immunol*, 4(9):866–873, 2003.

[75] A. G. Rolink, C. Schaniel, J. Andersson, and F. Melchers. Selection events operating at various stages in b cell development. *Curr Opin Immunol*, 13(2):202–207, 2001.

[76] Tomohiro Kurosaki, Hisaaki Shinohara, and Yoshihiro Baba. B cell signaling and fate decision. *Annu Rev Immunol*, 28:21–55, 2010.

[77] Harald von Boehmer and Fritz Melchers. Checkpoints in lymphocyte development and autoimmune disease. *Nat Immunol*, 11(1):14–20, 2010.

[78] S. L. Tiegs, D. M. Russell, and D. Nemazee. Receptor editing in self-reactive bone marrow b cells. *J Exp Med*, 177(4):1009–1020, 1993.

[79] Scott N Mueller and Ronald N Germain. Stromal cell contributions to the homeostasis and functionality of the immune system. *Nat Rev Immunol*, 9(9):618–629, 2009.

[80] Yousuke Takahama. Journey through the thymus: stromal guides for t-cell development and selection. *Nat Rev Immunol*, 6(2):127–135, 2006.

[81] Ivan Maillard, Terry Fang, and Warren S Pear. Regulation of lymphoid development, differentiation, and function by the notch pathway. *Annu Rev Immunol*, 23:945–974, 2005.

[82] Andrea C Carpenter and Rémy Bosselut. Decision checkpoints in the thymus. *Nat Immunol*, 11(8):666–673, 2010.

[83] Timothy K Starr, Stephen C Jameson, and Kristin A Hogquist. Positive and negative selection of t cells. *Annu Rev Immunol*, 21:139–176, 2003.

[84] Sue J Sohn, Jennifer Thompson, and Astar Winoto. Apoptosis during negative selection of autoreactive thymocytes. *Curr Opin Immunol*, 19(5):510–515, 2007.

[85] Ed Palmer. Negative selection–clearing out the bad apples from the t-cell repertoire. *Nat Rev Immunol*, 3(5):383–391, 2003.

[86] Bruno Kyewski and Jens Derbinski. Self-representation in the thymus: an extended view. *Nat Rev Immunol*, 4(9):688–698, 2004.

[87] Mark S Anderson, Emily S Venanzi, Zhibin Chen, Stuart P Berzins, Christophe Benoist, and Diane Mathis. The cellular mechanism of aire control of t cell tolerance. *Immunity*, 23(2):227–239, 2005.

[88] Jason D Fontenot and Alexander Y Rudensky. A well adapted regulatory contrivance: regulatory t cell development and the forkhead family transcription factor foxp3. *Nat Immunol*, 6(4):331–337, 2005.

[89] Kensuke Takada and Stephen C Jameson. Naive t cell homeostasis: from awareness of space to a sense of place. *Nat Rev Immunol*, 9(12):823–832, 2009.

[90] G. M. Poirier, G. Anderson, A. Huvar, P. C. Wagaman, J. Shuttleworth, E. Jenkinson, M. R. Jackson, P. A. Peterson, and M. G. Erlander. Immune-associated nucleotide-1 (ian-1) is a thymic selection marker and defines a novel gene family conserved in plants. *J Immunol*, 163(9):4960–4969, 1999.

[91] Jürgen Krücken, Regina M U Schroetel, Inga U Müller, Nadia Saïdani, Predrag Marinovski, W. Peter M Benten, Olaf Stamm, and Frank Wunderlich. Comparative analysis of the human gimap gene cluster encoding a novel gtpase family. *Gene*, 341:291–304, 2004.

[92] T. Nitta and Y. Takahama. The lymphocyte guard-ians: regulation of lymphocyte survival by ian/gimap family proteins. *Trends Immunol.*, 28(2):58–65, 2007.

[93] J. Krücken, H. P. Schmitt-Wrede, U. Markmann-Mulisch, and F. Wunderlich. Novel gene expressed in spleen cells mediating acquired testosterone-resistant immunity to plasmodium chabaudi malaria. *Biochem Biophys Res Commun*, 230(1):167–170, 1997.

[94] J. Krücken, O. Stamm, H. P. Schmitt-Wrede, A. Mincheva, P. Lichter, and F. Wunderlich. Spleen-specific expression of the malaria-inducible intronless mouse gene imap38. *J Biol Chem*, 274(34):24383–24391, 1999.

[95] Armand J MacMurray, Daniel H Moralejo, Anne E Kwitek, Elizabeth A Rutledge, Brian Van Yserloo, Paul Gohlke, Sara J Speros, Ben Snyder, Jonathan Schaefer, Sabine Bieg, Jianjie Jiang, Ruth A Ettinger, Jessica Fuller, Terri L Daniels, Anna Pettersson, Kimberly Orlebeke, Bruce Birren, Howard J Jacob, Eric S Lander, and Ake Lernmark. Lymphopenia in the bb rat model of type 1 diabetes is due to a mutation in a novel immune-associated nucleotide (ian)-related gene. *Genome Res*, 12(7):1029–1039, 2002.

[96] O. Stamm, J. Krucken, H.P. Schmitt-Wrede, W.P. Benten, and F. Wunderlich. Human ortholog to mouse gene imap38 encoding an er-localizable g-protein belongs to a gene family clustered on chromosome 7q32-36. *Gene*, 282(1-2):159–167, 2002.

[97] Julie A Lang, Douglas Kominski, Donald Bellgrau, and Robert I Scheinman. Partial activation precedes apoptotic death in t cells harboring an ian gene mutation. *Eur J Immunol*, 34(9):2396–2406, 2004.

[98] M. Pandarpurkar, L. Wilson-Fritch, S. Corvera, H. Markholst, L. Hornum, D.L. Greiner, J.P. Mordes, A.A. Rossini, and R. Bortell. Ian4 is required for mitochondrial integrity and t cell survival. *Proc.Natl.Acad.Sci.U.S.A*, 100(18):10382–10387, 2003.

[99] Lars Hornum, John Rømer, and Helle Markholst. The diabetes-prone bb rat carries a frameshift mutation in ian4, a positional candidate of iddm1. *Diabetes*, 51(6):1972–1979, 2002.

[100] Ulla Nøhr Andersen, Helle Markholst, and Lars Hornum. The antiapoptotic gene ian4l1 in the rat: genomic organization and promoter characterization. *Gene*, 341:141–148, 2004.

[101] Tone Sandal, Linda Aumo, Lars Hedin, Bjørn T Gjertsen, and Stein O Døskeland. Irod/ian5: an inhibitor of gamma-radiation- and okadaic acid-induced apoptosis. *Mol Biol Cell*, 14(8):3292–3304, 2003.

[102] Marie Cambot, Sandra Aresta, Brigitte Kahn-Perlès, Jean de Gunzburg, and Paul-Henri Roméo. Human immune associated nucleotide 1: a member of a new guanosine triphosphatase family expressed in resting t and b cells. *Blood*, 99(9):3293–3301, 2002.

[103] Carine Dion, Christine Carter, Lucy Hepburn, W. John Coadwell, Geoff Morgan, Margaret Graham, Nicholas Pugh, Graham Anderson, Geoffrey W Butcher, and J. Ross Miller. Expression of the ian family of putative gtpases during t cell development and description of an ian with three sets of gtp/gdp-binding motifs. *Int Immunol*, 17(9):1257–1268, 2005.

[104] Takeshi Nitta, Mariam Nasreen, Takafumi Seike, Atsushi Goji, Izumi Ohigashi, Tadaaki Miyazaki, Tsutomu Ohta, Masamoto Kanno, and Yousuke Takahama. Ian family critically regulates survival and development of t lymphocytes. *PLoS Biol*, 4(4):e103, 2006.

[105] Amy Saunders, Tracey Lamb, John Pascall, Amanda Hutchings, Carine Dion, Christine Carter, Lucy Hepburn, Jean Langhorne, and Geoffrey W Butcher. Expression of gimap1, a gtpase of the immunity-associated protein family, is not up-regulated in malaria. *Malar J*, 8:53, 2009.

[106] Jan-Jonas Filén, Sanna Filén, Robert Moulder, Soile Tuomela, Helena Ahlfors, Anne West, Petri Kouvonen, Suvi Kantola, Mari Björkman, Mikko Katajamaa, Omid Rasool, Tuula A Nyman, and Riitta Lahesmaa. Quantitative proteomics reveals gimap family proteins 1 and 4 to be differentially regulated during human t helper cell differentiation. *Mol Cell Proteomics*, 8(1):32–44, 2009.

[107] M. H. Kaplan, U. Schindler, S. T. Smiley, and M. J. Grusby. Stat6 is required for mediating responses to il-4 and for development of th2 cells. *Immunity*, 4(3):313–319, 1996.

[108] Amy Saunders, Louise M C Webb, Michelle L Janas, Amanda Hutchings, John Pascall, Christine Carter, Nicholas Pugh, Geoff Morgan, Martin Turner, and Geoffrey W Butcher. Putative gtpase gimap1 is critical for the development of mature b and t lymphocytes. *Blood*, 115(16):3249–3257, 2010.

[109] L. Dahéron, T. Zenz, L. D. Siracusa, C. Brenner, and B. Calabretta. Molecular cloning of ian4: a bcr/abl-induced gene that encodes an outer membrane mitochondrial protein with gtp-binding activity. *Nucleic Acids Res*, 29(6):1308–1316, 2001.

[110] C. Combet, C. Blanchet, C. Geourjon, and G. Deléage. Nps@: network protein sequence analysis. *Trends Biochem Sci*, 25(3):147–150, 2000.

[111] Kevin Howe, Alex Bateman, and Richard Durbin. Quicktree: building huge neighbour-joining trees of protein sequences. *Bioinformatics*, 18(11):1546–1547, 2002.

[112] Silke Schnell, Corinne Démollière, Paul van den Berk, and Heinz Jacobs. Gimap4 accelerates t-cell death. *Blood*, 108(2):591–599, 2006.

[113] Christine Carter, Carine Dion, Silke Schnell, W. John Coadwell, Margaret Graham, Lucy Hepburn, Geoffrey Morgan, Amanda Hutchings, John C Pascall, Heinz Jacobs, J. Ross Miller, and Geoffrey W Butcher. A natural hypomorphic variant of the apoptosis regulator gimap4/ian1. *J Immunol*, 179(3):1784–1795, 2007.

[114] Troy A Baldwin and Kristin A Hogquist. Transcriptional analysis of clonal deletion in vivo. *J Immunol*, 179(2):837–844, 2007.

[115] Adrian Liston, Kristine Hardy, Yvonne Pittelkow, Susan R Wilson, Lydia E Makaroff, Aude M Fahrer, and Christopher C Goodnow. Impairment of organ-specific t cell negative selection by diabetes susceptibility genes: genomic analysis by mrna profiling. *Genome Biol*, 8(1):R12, 2007.

[116] Kia A Duthie, Lisa C Osborne, Leonard J Foster, and Ninan Abraham. Proteomics analysis of interleukin (il)-7-induced signaling effectors shows

selective changes in il-7ralpha449f knock-in t cell progenitors. *Mol Cell Proteomics*, 6(10):1700–1710, 2007.

[117] Nusrat Rahman, Graeme Stewart, and Graham Jones. A role for the atopy-associated gene phf11 in t-cell activation and viability. *Immunol Cell Biol*, 2010.

[118] T. Zenz, A. Roessner, A. Thomas, S. Frohling, H. Dohner, B. Calabretta, and L. Daheron. hian5: the human ortholog to the rat ian4/iddm1/lyp is a new member of the ian family that is overexpressed in b-cell lymphoid malignancies. *Genes Immun.*, 5(2):109–116, 2004.

[119] V. W. Y. Wong, A. E. Saunders, A. Hutchings, J. C. Pascall, C. Carter, N. A. Bright, S.A. Walker, N. T. Ktistakis, and G.W. Butcher. The autoimmunity-related gimap5 gtpase is a lysosome-associated protein. *Self/Nonself*, 1, 2010.

[120] A. F. Nakhooda, A. A. Like, C. I. Chappel, C. N. Wei, and E. B. Marliss. The spontaneously diabetic wistar rat (the "bb" rat). studies prior to and during development of the overt syndrome. *Diabetologia*, 14(3):199–207, 1978.

[121] A. Naji, W. K. Silvers, H. Kimura, D. Bellgrau, J. F. Markmann, and C. F. Barker. Analytical and functional studies on the t cells of untreated and immunologically tolerant diabetes-prone bb rats. *J Immunol*, 130(5):2168–2172, 1983.

[122] G. Hernández-Hoyos, S. Joseph, N. G. Miller, and G. W. Butcher. The lymphopenia mutation of the bb rat causes inappropriate apoptosis of mature thymocytes. *Eur J Immunol*, 29(6):1832–1841, 1999.

[123] C. G. Jung, T. Kamiyama, and T. Agui. Elevated apoptosis of peripheral t lymphocytes in diabetic bb rats. *Immunology*, 98(4):590–594, 1999.

[124] M. Michalkiewicz, T. Michalkiewicz, R.A. Ettinger, E.A. Rutledge, J.M. Fuller, D.H. Moralejo, Yserloo B. Van, A.J. Macmurray, A.E. Kwitek, H.J. Jacob, E.S. Lander, and A. Lernmark. Transgenic rescue demonstrates involvement of the ian5 gene in t cell development in the rat. *Physiol Genomics*, 19(2):228–232, 2004.

[125] Tyson Hawkins, Jessica Fuller, Kara Olson, Sara Speros, and Ake Lernmark. Dr.lyp/lyp bone marrow maintains lymphopenia and promotes diabetes in lyp/lyp but not in +/+ recipient dr.lyp bb rats. *J Autoimmun*, 25(4):251–257, 2005.

[126] Robert H Wallis, KeSheng Wang, Leili Marandi, Eugene Hsieh, Terri Ning, Gary Y C Chao, Janice Sarmiento, Andrew D Paterson, and Philippe Poussier. Type 1 diabetes in the bb rat: a polygenic disease. *Diabetes*, 58(4):1007–1017, 2009.

[127] Jens van den Brandt, Henrike J Fischer, Lutz Walter, Thomas Hünig, Ingrid Klöting, and Holger M Reichardt. Type 1 diabetes in biobreeding rats is critically linked to an imbalance between th17 and regulatory t cells and an altered tcr repertoire. *J Immunol*, 185(4):2285–2294, 2010.

[128] Lesley Cousins, Margaret Graham, Reuben Tooze, Christine Carter, J. Ross Miller, Fiona M Powrie, Gordon G Macpherson, and Geoffrey W Butcher. Eosinophilic bowel disease controlled by the bb rat-derived lymphopenia/gimap5 gene. *Gastroenterology*, 131(5):1475–1485, 2006.

[129] Parthav Jailwala, Jill Waukau, Sanja Glisic, Srikanta Jana, Sarah Ehlenbach, Martin Hessner, Ramin Alemzadeh, Shigemi Matsuyama, Purushottam Laud, Xujing Wang, and Soumitra Ghosh. Apoptosis of cd4+ cd25(high) t cells in type 1 diabetes may be partially mediated by il-2 deprivation. *PLoS One*, 4(8):e6527, 2009.

[130] J-H. Shin, M. Janer, B. McNeney, S. Blay, K. Deutsch, C. B. Sanjeevi, I. Kockum, A. Lernmark, J. Graham, Swedish Childhood Diabetes Study Group, Diabetes Incidence in Sweden Study Group, Hans Arnqvist, Elizabeth Björck, Jan Eriksson, Lennarth Nyström, Lars Olof Ohlson, Bengt Scherstén, Jan Ostman, M. Aili, L. E. Bååth, E. Carlsson, H. Edenwall, G. Forsander, B. W. Granström, I. Gustavsson, R. Hanås, L. Hellenberg, H. Hellgren, E. Holmberg, H. Hörnell, Sten-A. Ivarsson, C. Johansson, G. Jonsell, K. Kockum, B. Lindblad, A. Lindh, J. Ludvigsson, U. Myrdal, J. Neiderud, K. Segnestam, S. Sjöblad, L. Skogsberg, L. Strömberg, U. Ståhle, B. Thalme, K. Tullus, T. Tuvemo, M. Wallensteen, O. Westphal, and J. Aman. Ia-2 autoantibodies in incident type i diabetes patients are associated with a polyadenylation signal polymorphism in gimap5. *Genes Immun*, 8(6):503–512, 2007.

[131] Anna Hellquist, Marco Zucchelli, Katja Kivinen, Ulpu Saarialho-Kere, Sari Koskenmies, Elisabeth Widen, Heikki Julkunen, Andrew Wong, Marja-Liisa Karjalainen-Lindsberg, Tiina Skoog, Johanna Vendelin, Deborah S Cunninghame-Graham, Timothy J Vyse, Juha Kere, and Cecilia M Lindgren. The human gimap5 gene has a common polyadenylation polymorphism increasing risk to systemic lupus erythematosus. *J Med Genet*, 44(5):314–321, 2007.

[132] M. K. Lim, D. H. Sheen, S. A. Kim, S. K. Won, S-S. Lee, S-C. Chae, H-T. Chung, and S. C. Shim. Ian5 polymorphisms are associated with systemic lupus erythematosus. *Lupus*, 18(12):1045–1052, 2009.

[133] Ryan D Schulteis, Haiyan Chu, Xuezhi Dai, Yuhong Chen, Brandon Edwards, Dipica Haribhai, Calvin B Williams, Subramaniam Malarkannan, Martin J Hessner, Sanja Glisic-Milosavljevic, Srikanta Jana, Edward J Kerschen, Soumitra Ghosh, Demin Wang, Anne E Kwitek, Ake Lernmark, Jack Gorski, and Hartmut Weiler. Impaired survival of peripheral t cells, disrupted nk/nkt cell development, and liver failure in mice lacking gimap5. *Blood*, 112(13):4905–4914, 2008.

[134] Michael J Barnes, Halil Aksoylar, Philippe Krebs, Tristan Bourdeau, Carrie N Arnold, Yu Xia, Kevin Khovananth, Isaac Engel, Sosathya Sovath, Kristin Lampe, Eleana Laws, Amy Saunders, Geoffrey W Butcher, Mitchell Kronenberg, Kris Steinbrecher, David Hildeman, H. Leighton Grimes, Bruce Beutler, and Kasper Hoebe. Loss of t cell and b cell quiescence precedes the onset of

microbial flora-dependent wasting disease and intestinal inflammation in gimap5-deficient mice. *J Immunol*, 184(7):3743–3754, 2010.

[135] Mamadou Keita, Chantal Leblanc, David Andrews, and Sheela Ramanathan. Gimap5 regulates mitochondrial integrity from a distinct subcellular compartment. *Biochem Biophys Res Commun*, 361(2):481–486, 2007.

[136] Nicholas Chadwick, Leo Zeef, Virginia Portillo, Carl Fennesy, Fiona Warrander, Sarah Hoyle, and Anne-Marie Buckle. Identification of novel notch target genes in t cell leukaemia. *Mol Cancer*, 8(1):35, 2009.

[137] Steven C Pino, Bryan O'Sullivan-Murphy, Erich A Lidstone, Chaoxing Yang, Kathryn L Lipson, Agata Jurczyk, Philip diIorio, Michael A Brehm, John P Mordes, Dale L Greiner, Aldo A Rossini, and Rita Bortell. Chop mediates endoplasmic reticulum stress-induced apoptosis in gimap5-deficient t cells. *PLoS ONE*, 4(5):e5468, 2009.

[138] Yu-Ming Shiao, Ya-Hui Chang, Yen-Ming Liu, Jian-Chiuan Li, Jih-Shyun Su, Ko-Jiunn Liu, Yu-Fen Liu, Ming-Wei Lin, and Shih-Feng Tsai. Dysregulation of gimap genes in non-small cell lung cancer. *Lung Cancer*, 62(3):287–294, 2008.

[139] Jürgen Krücken, Markus Epe, W. Peter M Benten, Nina Falkenroth, and Frank Wunderlich. Malaria-suppressible expression of the anti-apoptotic triple gtpase mgimap8. *J Cell Biochem*, 96(2):339–348, 2005.

[140] W. F. Scherer, J. T. Syverton, and G. O. Gey. Studies on the propagation in vitro of poliomyelitis viruses. iv. viral multiplication in a stable strain of human malignant epithelial cells (strain hela) derived from an epidermoid carcinoma of the cervix. *J Exp Med*, 97(5):695–710, 1953.

[141] U. Schneider, H. U. Schwenk, and G. Bornkamm. Characterization of ebv-genome negative "null" and "t" cell lines derived from children with acute lymphoblastic leukemia and leukemic transformed non-hodgkin lymphoma. *Int J Cancer*, 19(5):621–626, 1977.

[142] J. Sambrook, Fritsch E. F., and Maniatis T. *Molecular Cloning: A Laboratory Manual*. Cold Spring Harbor Laboratory Press, 1989.

[143] C. T. Chung, S. L. Niemela, and R. H. Miller. One-step preparation of competent escherichia coli: transformation and storage of bacterial cells in the same solution. *Proc Natl Acad Sci U S A*, 86(7):2172–2175, 1989.

[144] S. Doublie. Preparation of selenomethionyl proteins for phase determination. *Methods Enzymol.*, 276:523–530, 1997.

[145] M. M. Bradford. A rapid and sensitive method for the quantitation of microgram quantities of protein utilizing the principle of protein-dye binding. *Anal Biochem*, 72:248–254, 1976.

[146] E. Gasteiger, C. Hoogland, A. Gattiker, S. Duvaud, M. R. Wilkins, R. D. Appel, and A. Bairoch. *The Proteomics Protocols Handbook*. Humana Press, 2005.

[147] C. Lenzen, R.H. Cool, and A. Wittinghofer. Analysis of intrinsic and cdc25-stimulated guanine nucleotide exchange of p21ras-nucleotide complexes by fluorescence measurements. *Methods Enzymol.*, 255:95–109, 1995.

[148] G. J. Praefcke, M. Geyer, M. Schwemmle, H. Robert Kalbitzer, and C. Herrmann. Nucleotide-binding characteristics of human guanylate-binding protein 1 (hgbp1) and identification of the third gtp-binding motif. *J Mol Biol*, 292(2):321–332, 1999.

[149] J. Behlke, O. Ristau, and H. J. Schönfeld. Nucleotide-dependent complex formation between the escherichia coli chaperonins groel and groes studied under equilibrium conditions. *Biochemistry*, 36(17):5149–5156, 1997.

[150] A.G. Leslie. The integration of macromolecular diffraction data. *Acta Crystallogr.D.Biol.Crystallogr.*, 62(Pt 1):48–57, 2006.

[151] W. Kabsch. Automatic processing of rotation diffraction data from crystals of initially unknown symmetry and cell constants. *J.Appl.Cryst.*, 26:795–800, 1993.

[152] C. Vonrhein, E. Blanc, P. Roversi, and G. Bricogne. Automated structure solution with autosharp. *Methods Mol.Biol.*, 364:215–230, 2007.

[153] G.M. Sheldrick. A short history of shelx. *Acta Crystallogr.A*, 64(Pt 1):112–122, 2008.

[154] Paul D Adams, Pavel V Afonine, Gábor Bunkóczi, Vincent B Chen, Ian W Davis, Nathaniel Echols, Jeffrey J Headd, Li-Wei Hung, Gary J Kapral, Ralf W Grosse-Kunstleve, Airlie J McCoy, Nigel W Moriarty, Robert Oeffner, Randy J Read, David C Richardson, Jane S Richardson, Thomas C Terwilliger, and Peter H Zwart. Phenix: a comprehensive python-based system for macromolecular structure solution. *Acta Crystallogr D Biol Crystallogr*, 66(Pt 2):213–221, 2010.

[155] A. Vagin and A. Teplyakov. Molrep: an automated program for molecular replacement. *J.Appl.Cryst.*, 30:1022–1025, 1997.

[156] P. Emsley, B. Lohkamp, W. G. Scott, and K. Cowtan. Features and development of coot. *Acta Crystallogr D Biol Crystallogr*, 66(Pt 4):486–501, 2010.

[157] G.N. Murshudov, A.A. Vagin, and E.J. Dodson. Refinement of macromolecular structures by the maximum-likelihood method. *Acta Crystallogr.D.Biol.Crystallogr.*, 53(Pt 3):240–255, 1997.

[158] Number 4 Collaborative Computational Project. The ccp4 suite: programs for protein crystallography. *Acta Crystallogr.D.Biol.Crystallogr.*, 50(Pt 5):760–763, 1994.

[159] M. D. Winn, M. N. Isupov, and G. N. Murshudov. Use of tls parameters to model anisotropic displacements in macromolecular refinement. *Acta Crystallogr D Biol Crystallogr*, 57(Pt 1):122–133, 2001.

[160] A. T. Brünger. Free r value: cross-validation in crystallography. *Methods Enzymol*, 277:366–396, 1997.

[161] I.W. Davis, A. Leaver-Fay, V.B. Chen, J.N. Block, G.J. Kapral, X. Wang, L.W. Murray, III Arendall, W.B., J. Snoeyink, J.S. Richardson, and D.C. Richardson. Molprobity: all-atom contacts and structure validation for proteins and nucleic acids. *Nucleic Acids Res.*, 35(Web Server issue):W375–W383, 2007.

[162] P. M. Gocze and D. A. Freeman. Factors underlying the variability of lipid droplet fluorescence in ma-10 leydig tumor cells. *Cytometry*, 17(2):151–158, 1994.

[163] L. Holm, S. Kääriäinen, P. Rosenström, and A. Schenkel. Searching protein structure databases with dalilite v.3. *Bioinformatics*, 24(23):2780–2781, 2008.

[164] Arun S Konagurthu, James C Whisstock, Peter J Stuckey, and Arthur M Lesk. Mustang: a multiple structural alignment algorithm. *Proteins*, 64(3):559–574, 2006.

[165] Johannes Söding, Andreas Biegert, and Andrei N Lupas. The hhpred interactive server for protein homology detection and structure prediction. *Nucleic Acids Res*, 33(Web Server issue):W244–W248, 2005.

[166] B.W. Matthews. Solvent content of protein crystals. *J.Mol.Biol.*, 33(2):491–497, 1968.

[167] K. Diederichs and P.A. Karplus. Improved r-factors for diffraction data analysis in macromolecular crystallography. *Nat.Struct.Biol.*, 4(4):269–275, 1997.

[168] A. Wittinghofer and E.F. Pai. The structure of ras protein: a model for a universal molecular switch. *Trends Biochem.Sci.*, 16(10):382–387, 1991.

[169] Laurence Bougnères, Julie Helft, Sangeeta Tiwari, Pablo Vargas, Benny Hung-Junn Chang, Lawrence Chan, Laura Campisi, Gregoire Lauvau, Stephanie Hugues, Pradeep Kumar, Alice O Kamphorst, Ana-Maria Lennon Dumenil, Michel Nussenzweig, John D MacMicking, Sebastian Amigorena, and Pierre Guermonprez. A role for lipid bodies in the cross-presentation of phagocytosed antigens by mhc class i in dendritic cells. *Immunity*, 31(2):232–244, 2009.

[170] Raphael Gasper, Simon Meyer, Katja Gotthardt, Minhajuddin Sirajuddin, and Alfred Wittinghofer. It takes two to tango: regulation of g proteins by dimerization. *Nat Rev Mol Cell Biol*, 2009.

[171] Agnidipta Ghosh, Gerrit J K Praefcke, Louis Renault, Alfred Wittinghofer, and Christian Herrmann. How guanylate-binding proteins achieve assembly-stimulated processive cleavage of gtp to gmp. *Nature*, 440(7080):101–104, 2006.

[172] Brian J Peter, Helen M Kent, Ian G Mills, Yvonne Vallis, P. Jonathan G Butler, Philip R Evans, and Harvey T McMahon. Bar domains as sensors of

membrane curvature: the amphiphysin bar structure. *Science*, 303(5657):495–499, 2004.

[173] Julia P Hunn, Stephanie Koenen-Waisman, Natasa Papic, Nina Schroeder, Nikolaus Pawlowski, Rita Lange, Frank Kaiser, Jens Zerrahn, Sascha Martens, and Jonathan C Howard. Regulatory interactions between irg resistance gtpases in the cellular response to toxoplasma gondii. *EMBO J*, 27(19):2495–2509, 2008.

[174] Cemalettin Bekpen, Julia P Hunn, Christoph Rohde, Iana Parvanova, Libby Guethlein, Diane M Dunn, Eva Glowalla, Maria Leptin, and Jonathan C Howard. The interferon-inducible p47 (irg) gtpases in vertebrates: loss of the cell autonomous resistance mechanism in the human lineage. *Genome Biol*, 6(11):R92, 2005.

[175] Jason A Mears, Pampa Ray, and Jenny E Hinshaw. A corkscrew model for dynamin constriction. *Structure*, 15(10):1190–1202, 2007.

[176] Song Gao, Alexander von der Malsburg, Susann Paeschke, Joachim Behlke, Otto Haller, Georg Kochs, and Oliver Daumke. Structural basis of oligomerization in the stalk region of dynamin-like mxa. *Nature*, 465(7297):502–506, 2010.

[177] Oliver Daumke, Richard Lundmark, Yvonne Vallis, Sascha Martens, P. Jonathan G Butler, and Harvey T McMahon. Architectural and mechanistic insights into an ehd atpase involved in membrane remodelling. *Nature*, 449(7164):923–927, 2007.

[178] P. Katsamba, K. Carroll, G. Ahlsen, F. Bahna, J. Vendome, S. Posy, M. Rajebhosale, S. Price, T. M. Jessell, A. Ben-Shaul, L. Shapiro, and Barry H Honig. Linking molecular affinity and cellular specificity in cadherin-mediated adhesion. *Proc Natl Acad Sci U S A*, 106(28):11594–11599, 2009.

[179] Eva M Schmid and Harvey T McMahon. Integrating molecular and network biology to decode endocytosis. *Nature*, 448(7156):883–888, 2007.

[180] Tadeusz Muziol, Estela Pineda-Molina, Raimond B Ravelli, Alessia Zamborlini, Yoshiko Usami, Heinrich Göttlinger, and Winfried Weissenhorn. Structural basis for budding by the escrt-iii factor chmp3. *Dev Cell*, 10(6):821–830, 2006.

[181] Andrew M Petros, Edward T Olejniczak, and Stephen W Fesik. Structural biology of the bcl-2 family of proteins. *Biochim Biophys Acta*, 1644(2-3):83–94, 2004.

[182] Ana J García-Sáez, Jonas Ries, Mar Orzáez, Enrique Pérez-Payà, and Petra Schwille. Membrane promotes tbid interaction with bcl(xl). *Nat Struct Mol Biol*, 16(11):1178–1185, 2009.

[183] Ellen Umlauf, Edina Csaszar, Manuel Moertelmaier, Gerhard J Schuetz, Robert G Parton, and Rainer Prohaska. Association of stomatin with lipid bodies. *J Biol Chem*, 279(22):23699–23709, 2004.

[184] Ann-Charlotte Johansson, Hanna Appelqvist, Cathrine Nilsson, Katarina Kågedal, Karin Roberg, and Karin Ollinger. Regulation of apoptosis-associated lysosomal membrane permeabilization. *Apoptosis*, 15(5):527–540, 2010.

[185] K. F. Ferri and G. Kroemer. Organelle-specific initiation of cell death pathways. *Nat Cell Biol*, 3(11):E255–E263, 2001.

[186] S. Eckerle, V. Brune, C. Döring, E. Tiacci, V. Bohle, C. Sundström, R. Kodet, M. Paulli, B. Falini, W. Klapper, A. B. Chaubert, K. Willenbrock, D. Metzler, A. Bräuninger, R. Küppers, and M-L. Hansmann. Gene expression profiling of isolated tumour cells from anaplastic large cell lymphomas: insights into its cellular origin, pathogenesis and relation to hodgkin lymphoma. *Leukemia*, 2009.

[187] Jan Drenth. *Principles of Protein X-Ray Crystallography*. Springer Science and Business Media LLC, 3rd edition, 2007.

[188] A. Messerschmidt. *X-Ray Crystallography of Biomacromolecules - A Practical Guide*. Wiley-VCH, 1st edition, 2006.

[189] T. Hahn. *International Tables for Crystallography Volume A: Space-group symmetry*. Springer Science+Business Media, 2002.

[190] Garry Taylor. The phase problem. *Acta Crystallogr D Biol Crystallogr*, 59(Pt 11):1881–1890, Nov 2003.

[191] J. D. Thompson, D. G. Higgins, and T. J. Gibson. Clustal w: improving the sensitivity of progressive multiple sequence alignment through sequence weighting, position-specific gap penalties and weight matrix choice. *Nucleic Acids Res*, 22(22):4673–4680, 1994.

ABSTRACT

GTPases of Immunity-Associated Proteins (GIMAPs) are a distinctive family of GTPases, which control apoptosis in lymphocytes and play a central role in lymphocyte maturation and lymphocyte-associated diseases. To explore their function and mechanism, we determined crystal structures of several GIMAP family members in different nucleotide-loading and oligomerization states.

Nucleotide-free and GDP-bound GIMAP2 were monomeric and revealed a guanine nucleotide binding domain (G domain) of the TRAFAC (Translation Factor associated) GTPase superclass with a unique amphipathic helix $\alpha 7$ packing against the switch II region of the G domain. In the absence of $\alpha 7$ and presence of GTP, GIMAP2 oligomerized via two distinct interfaces in the crystal. GTP-induced stabilization of switch I mediates dimerization across the nucleotide binding site which also involves the GIMAP conserved box, which is a sequence stretch downstream of the G3 motif, and the nucleotide base. Structural rearrangements in switch II appear to induce the release of $\alpha 7$ allowing oligomerization to proceed via a second interface. The unique architecture of the linear oligomer was confirmed by mutagenesis. Furthermore, we showed a function for the GIMAP2 oligomer at the surface of lipid droplets.

The structure of the GDP-bound GIMAP5 monomer was very similar to GDP-bound GIMAP2, suggesting the conservation of the fold within the GIMAPs. The protein was shown to partially co-localize with the lysosomal compartment in a T cell line. In the crystal structure of GMPPNP-bound GIMAP7, a dimeric arrangement of the protein was observed. The dimer interface proved to be identical to one of the GIMAP2 oligomerization interfaces. We termed this binding interface G-interface, since it involves the Guanin-nucleotide binding site and the bound nucleotide. Using site-directed mutagenesis, we identified a conserved arginine residue within the G-interface, which stimulates the GTPase reaction in the opposing protomer within the GIMAP7 dimer. In GIMAP2, the corresponding arginine plays a structural role in the dimerization process and is not involved in catalysis, since GIMAP2 does not show any GTP-hydrolytic activity.

While earlier studies indicated that GIMAPs are related to the septins, the current structure also revealed a strikingly similar nucleotide coordination and dimerization mode as in the dynamin GTPase. Based on this, we re-examined the relationships of the septin- and dynamin-like GTPases and demonstrate that these are likely to have emerged from a common membrane-associated dimerizing ancestor. This ancestral property appears to be critical for the role of GIMAPs as nucleotide-regulated scaffolds on intracellular membranes.

ZUSAMMENFASSUNG

Die GTPasen der immun-assoziierten Proteine (GIMAPs) sind eine spezielle GTPase-Familie, die Apoptosevorgänge in Lymphozyten kontrollieren und eine zentrale Rolle in der Lymphozytenentwicklung und in Lymphozyten-Erkrankungen spielen. Um ihre Funktion und ihre Mechanismen zu verstehen, wurden mehrere Kristallstrukturen von verschiedenen Familienmitgliedern gelöst, in verschiedenen Nukleotidbeladungs- und Oligomerisierungsstadien.

Nukleotidfreies, monomeres GIMAP2 besteht aus einer Guaninnukleotidbindedomäne (G-Domäne) der translationsfaktor-assoziierten (TRAFAC) Klasse und einer besonderen amphipatischen Helix $\alpha 7$, die gegen die switch II Region der G-Domäne faltet. Ohne diese Helix $\alpha 7$ und in GTP-gebundenem Zustand oligomerisiert GIMAP2 über zwei verschiedende Kontaktflächen. GTP-induzierte Stabilisierung der switch I Region ermöglicht die GTP-spezifische Dimerisierung über die GTP-Bindestelle hinweg, wobei auch die GIMAP-spezifische konservierte Box beteiligt ist, ein Aminosäure-Sequenzabschnitt direkt nach dem G3-Motiv. Die Nukleotidbase selbst spielt auch eine Rolle in der Dimerisierung. GTP-induzierte Strukturveränderungen in der switch II Region könnten zur Ablösung von $\alpha 7$ führen und eine weitere Oligomerisierung über eine zweite Kontaktfläche hervorrufen. Die einzigartige Architektur des Oligomers wurde durch Mutagenese einzelner Aminosäuren und weiterfürende Studien bestätigt. Weiterhin konnten wir in einer T-Zellline die Lokalisierung von GIMAP2 an der Hülle von intrazellulären Lipidtröpfchen zeigen.

Die Struktur des GDP-gebundenen, monomeren GIMAP5-Proteins erwies sich der Struktur des GDP-gebundenen GIMAP2 als sehr ähnlich, daher könnte die festgestellte Faltung stellvertretend für die ganze Proteinfamilie gelten. In einer T-Zelllinie wurde eine teilweise Kolokalisierung des Proteins mit Lysosomen festgestellt. In der Kristallstruktur von GMP-PNP-gebundenem GIMAP7 lag das Protein als Dimer vor. Die Dimer-Kontaktfläche ist äquivalent zu der, die in GTP-gebundenem GIMAP2 beobachtet wurde. Durch Mutagenesestudien konnte ein konservierter Arginin-Aminosäurerest identifiziert werden, der die GTP-Hydrolyse im gegenüberliegenden Protomer des GIMAP7 Dimers stimuliert. Der entsprechende Argininrest im GTP-abhängigen GIMAP2 Dimer ist hingegen nur ein struktureller Rest, der an der Dimerisierung beteiligt ist. GIMAP2 besitzt auch keinerlei GTP-Hydrolyseaktivität.

Frühere Studien zeigten, dass die GIMAP-Familie mit den Septin-Proteinen verwandt ist. Der GTP-abhängige Dimer, der in dieser Arbeit gefunden wurde, zeigt jedoch einen Dimerisierungsmodus, der auch im Dynamin G-Domänendimer vorliegt, dessen Struktur kürzlich ermittelt wurde. Unter diesem Gesichtspunkt wurden die phylogenetischen Beziehungen zwischen Septin- und Dynamin-ähnlichen GTPasen erneut untersucht, und es wurde gezeigt, dass diese einen gemeinsamen membran-assoziierten Vorfahren besitzen, der als Dimer vorliegt. Diese Ureigenschaft scheint auch wichtig zu sein für die Funktion von GIMAPs als nukleotid-gesteuerte Gerüstproteine an intrazellulären Membranen.

PUBLICATIONS

Schwefel D, Fröhlich C, Daumke O (2010) Purification, crystallization and preliminary X-ray analysis of human GIMAP2. *Acta Cryst* F66:725-9

Schwefel D, Fröhlich C, Eichhorst J, Wiesner B, Behlke J, Aravind L, Daumke O (2010) Structural basis for oligomerization in the septin-like GTPase of immunity-associated proteins 2 (GIMAP2). *Proc Natl Acad Sci U S A* 107(47):20299-304

Schwefel D, Daumke O. (2011) GTP-dependent scaffold formation in the GTPase of Immunity Associated Protein family. *Small GTPases* 2(1):27-30

ACKNOWLEDGMENTS

Many thanks to Oli Daumke and the whole group, Joachim Behlke, L Aravind, Udo Heinemann and the whole group, Uwe Müller and the BESSY team, Erich Wanker, Pablo Porras Millan, Matthias Selbach, Florian Paul, Hans-Peter Rahn, Burkhard Wiesner, Jenny Eichhorst, Diana Rüthnick, my parents and Annegret Brandau.